EXPLORING THE SUSTAINABILITY OF FORESTRY RESOURCES AT THE NEXUS OF CHANGING LAND USE AND CLIMATE: A CASE STUDY FROM THE GULF COAST OF THE PANHANDLE FLORIDA

by

SYED MOHAMMAD ASIFUL ALAM

(Under the Direction of Puneet Dwivedi)

ABSTRACT

The Intergovernmental Panel on Climate Change (IPCC) summarizes that human activities are the primary cause of global warming, leading to an increase in global surface temperature of 1.1°C above the pre-industrial period (1850-1900) between 2011 and 2020. Human-induced climate change already affects numerous extreme weather events and climate patterns worldwide. Consequently, since 2000, the Atlantic Ocean, the Caribbean, and the US Gulf Coast have witnessed an increase in tropical storm and hurricane activity attributed to global warming. In this context, this research is organized into three papers, each addressing distinct facets of widespread negative consequences to the environment and human populations in light of rising hurricane risks in the US Gulf Coast. In the first paper, I estimate the damage to urban vegetation, identify hotspots, and track changes in land cover resulting from significant hurricanes along the US Gulf Coast. Findings reveal that canopy loss and the presence of water vapor during these catastrophic hurricanes are key factors magnifying potential hotspots. The second paper delves into the comparison of aboveground carbon in different components of trees (sapling, bole, stump, top, and foliage) before (2001-2003) and after (2005-2007) Hurricane Ivan. This analysis demonstrates that hurricanes can render a substantial loss of aboveground carbon, with tree biophysical characteristics playing a pivotal role in the recovery of aboveground carbon. The third paper focuses on predicting land use changes in 2050 by taking into account the frequency of hurricanes and monitoring carbon dynamics along the Gulf Coast. Our projections indicate that, despite an anticipated increase in the frequency of hurricanes, urban and forestlands are expected to expand.

Furthermore, changes in land use are set to contribute to an overall increase in carbon storage, mainly through enhanced forestland conservation efforts. The outcomes of this research provide valuable information for relevant stakeholder groups, aiding them in decision-making processes related to future land use, conservation initiatives, and the promotion of forest resiliency, ultimately contributing to the long-term sustainability of ecosystem services.

Index Keywords: Optimized Hotspot and Outlier Analysis, Land Cover, Log-linear Model, Forest Inventory Database (FIA), Multi-Layer Perceptron (MLP) Model, InVEST Model, Ecosystem Services, Aboveground Carbon

EXPLORING THE SUSTAINABILITY OF FORESTRY RESOURCES AT THE NEXUS OF CHANGING LAND USE AND CLIMATE: A CASE STUDY FROM THE GULF COAST OF THE PANHANDLE FLORIDA

By

SYED MOHAMMAD ASIFUL ALAM

B.U.R.P., Chittagong University of Engineering & Technology, 2014

M.S., University of Georgia, 2019

A Dissertation Submitted to the Graduate Faculty of the University of Georgia in Partial Fulfillment of the Requirements for the Degree

DOCTOR OF PHILOSOPHY

ATHENS, GEORGIA

2024

EXPLORING THE SUSTAINABILITY OF FORESTRY RESOURCES AT THE NEXUS OF CHANGING LAND USE AND CLIMATE: A CASE STUDY FROM THE GULF COAST OF THE PANHANDLE FLORIDA

by

SYED MOHAMMAD ASIFUL ALAM

Major Professor:	Puneet Dwivedi
Committee:	James Marshall Shepherd Alicia Peduzzi Deepak Mishra

Electronic Version Approved:

Ron Walcott
Dean of the Graduate School
The University of Georgia
May 2024

ACKNOWLEDGMENTS

My profound gratitude goes to Dr. Puneet Dwivedi, my major advisor, for his continuous guidance, support, and suggestions throughout the research. I would also like to thank my committee members, Drs. James Marshall Shepherd, Alicia Peduzzi, and Deepak Mishra, for their constant support, constructive comments, and inspiring advice.

My deepest indebtedness goes to Thomas Brandeis and Andres Baeza-Castro from the United States Forest Service for their timely responses and continuous guidance on the FIA data preparation for my research. My heartfelt gratitude also goes to Dr. Parag Kadam, one of my research lab mates at the University of Georgia Warnell School of Forestry and Natural Resources, for his endless support of my research. I also received support from other lab mates: Dr. Carolina Berget, Dr. Kai Huang, Dr. Farhad Hussain Masum, Hosne Ara Akter, Kanchana Chinnannan Balasubramanian, Manuja Aparekke, Lalita Dhal, Sabyasachi Kar, Catie Cooper, Chambers English and Jacqueline Miner especially for their critical reviews and encouragement on my research. I found my research lab, Dwivedi Forest Sustainability Lab, very helpful and felt lucky to have a positive and cheerful team environment, which helped me discuss my research problems and needs. I am also indebted to Kate DeDufour, Warnell School's Graduate Program Coordinator, for taking care of all administrative work.

My parents have always sacrificed their own needs over ours and embraced my passion for higher education. Thank you for being excited to hear about my work every time I spoke to you both about it. I would also like to thank my wife, Nashid Mumtaz, for her sacrifices to make my dreams come true. Your partnership, support, encouragement, and presence have helped me move forward to complete my doctoral studies at the University of Georgia. Additionally, I would also like to thank the Bangladeshi student community, whose presence, gathering, and support made missing home a bit easier.

Finally, this research would not have been possible without the grant, facility, and resources of Warnell School of Forestry and Natural Resources, University of Georgia.

Contents

List of Tables

List of Figures

Supplementary Tables

Supplementary Figures

CHAPTER 1

INTRODUCTION

The Intergovernmental Panel on Climate Change (IPCC) climate change 2023 synthesis report AR6 summarizes that human activities are the primary cause of global warming, leading to an increase in global surface temperature of 1.1°C above the pre-industrial period (1850-1900) between 2011 and 2020 (IPCC, 2023a). Human-induced climate change already impacts numerous extreme weather events and climate patterns worldwide (IPCC, 2015). Due to global warming, tropical storms and hurricane activity in the Atlantic Ocean, the Caribbean, and the US Gulf of Mexico has increased since 2000 (NASA, 2022; US EPA, 2022). About 6 to 7 hurricanes have formed in the North Atlantic every year since 1878, and roughly 2 per year land on the coast of the United States (NOAA, 2021a, 2021b). Several measures of historical Atlantic hurricane activity, including annual numbers of tropical storms, hurricanes, and major hurricanes, as well as hurricane intensities, power dissipation index (PDI), and rapid intensification occurrence, all show pronounced increases since around 1980 (NOAA, 2023). According to the total annual Accumulated Cyclone Energy (ACE) Index, hurricane intensity has risen noticeably over the past 20 years, and 8 of the 10 most active years since 1950 have occurred since the mid-1990s (US EPA, 2022). This suggests at least the possibility of a large anthropogenic influence on Atlantic hurricanes. The relationship between tropical Atlantic SSTs (sea surface temperature) and hurricane activity infers future changes in Atlantic hurricane activity will be accompanied by substantial increases in hurricane destructive potential–roughly a 300% increase in the PDI by 2100 (Vecchi et al., 2008). However, the number of tropical storms and hurricanes may decrease by around 15% over the Atlantic Ocean, Caribbean Sea, and Gulf of Mexico for a 2^0C global warming scenario with large uncertainty. These projections were based on the metrics and models available in published studies across many modeling groups in the Geophysical Fluid Dynamics Laboratory of the National Oceanic and Atmospheric Administration (Hsieh et al., 2020).

Damage from tropical storms and hurricanes in the United States and elsewhere around the Atlantic basin is expected to continue to double every generation because of the increasing

population and infrastructure along the coast (IPCC, 2014; US Global Change Research Program, 2017). Economic damage from hurricanes in the United States has increased remarkably since 1900, and the dominant driver of the increase has been the historical rise in the amount and economic value of built infrastructure and wealth along the coast of the nation (GFDL, 2023). Since 1980, about 32 catastrophic hurricanes and tropical cyclones hit the US South and Gulf Coast. The approximate cost of damages from these tropical cyclones and hurricanes was $1.3 trillion (NCEI, 2022; NOAA, 2021c). The year 2017 was the deadliest in terms of cumulative costs; 16 separate billion-dollar weather events cost $306.2 billion, breaking the previous cost record of $214.8 billion in 2005.

Apart from economic damage, hurricanes cause adverse impacts on forest structure and composition (Zhang et al., 2016) and have major influences on the recovery of the coastal forests (Murdiyarso et al., 2015). About 320 million large trees were severely damaged by Hurricane Katrina (Chambers et al., 2007; NASA, 2007a), and Hurricane Laura destroyed 3,642 km^2 of forested land along the US Gulf Coast (USDA, 2020). Loss of trees and forestlands compounded with carbon stock loss following a catastrophic hurricane is enormous (NASA, 2007a). Since 1851, tropical cyclones and hurricanes have damaged an estimated 97 million trees annually in the continental United States, resulting in an average yearly carbon loss of 26.5 million metric tons (Zeng et al., 2009). The study showed about 43.9±8.4 million metric tons and 37.9 ± 6.4 million metric tons of carbon lost due to Hurricanes Katrina and Rita in 2005, respectively (Negrón-Juárez et al., 2010). Aboveground carbon decreased by 4.6 metric tons/km^2 due to Hurricane Maria (2017) in Puerto Rico, and it is estimated that it will take 15 years for forests to recover their pre-hurricane carbon stock (Chevalier et al., 2022a). Hurricane Charley (2004) damaged 0.61 km^2 of mangrove forest land in southwest Florida, and the estimated carbon loss ranges from 427 metric tons to 3,599 metric tons of carbon (Peneva-Reed et al., 2021a).

Due to different methodologies or insufficient evaluation of carbon pools following a major cyclone, the quantification of forest carbon is typically accompanied by a high degree of uncertainty (Houghton et al., 2012; Peneva-Reed et al., 2021b). Researchers are developing models to predict the probability of hurricanes and the amount of damage inflicted by them to support overall decision-making and mitigate these catastrophic effects on forests (Blennow and Sallnäs,

2004; Peltola et al., 1999; Schmidt et al., 2016). Some models are used for quantifying damage at the single tree level (Schmidt et al., 2010), while others are used for stand-level projections (Hanewinkel et al., 2014) or regional-level assessment (Talkkari et al., 2000). Research on physiological changes in aboveground carbon, particularly those involving saplings, boles, stumps, tops, and leaves, is scarce. With an impact on carbon sequestration, forest health, resilience, biodiversity, and ecosystem functioning, aboveground carbon at the whole physiological level of trees needs to be monitored closely.

Establishing sustainable land use practices and assessing land use change in natural ecosystems requires an understanding of the intricate link between carbon dynamics and hurricanes. Even though there are disastrous hurricanes almost every year, the amount of urban land in the southern states and along the Gulf Coast is growing. About 5% of the Gulf of Mexico region is covered by urban land cover, which is a comparatively modest portion of the total land cover (NOAA, 2022a). Since 2001, the annual rate of urban expansion from New Orleans to Austin has ranged from 0.66% to 4.57% (MRLC, 2023). While the region benefits greatly from this urban expansion, several areas saw it happen far faster. Areas of change were most prevalent in the counties further away from the coast and marginally more numerous between Houston, Texas, and Orlando, Florida. Metropolitan land utilization along the Gulf Coast rose by more than 15%, including open space in urban areas, according to the 2017 Ecosystem Status Report update for the Gulf of Mexico (Karnauskas et al., 2017; NOAA, 2017a). From 1996 to 2010, the amount of developed area increased in the Gulf of Mexico by 3,978 square kilometers, which represents a 17% rate of growth. During the 14-year period, new development spread across the Gulf of Mexico in areas that had previously been classified as agricultural (31%), upland forest (25%), marshes (17%), shrub (14%), and grass (9%). An additional 3% came from barren land and water features (NOAA, 2017a). Development intensity increased on 456 km^2 of already developed land; this type of change is commonly associated with increasing density of housing or infill development within city limits (NOAA, 2017b).

Concurrently, forestland decreased in cities and surrounding watersheds by 0.23% to 2.21% every year since 2001. The Gulf of Mexico Regional Land Cover Change Report (1996-2010) estimated about 34,252 km^2 of forestland changed to other land cover types. About 22,548 km^2 of forestland

was lost between 1996 and 2010 (Homer et al., 2020; Mendoza-González et al., 2012). Most of the forestland losses in the land cover consisted of changes from forest to grassland and shrub. Approximately 1,513 km^2 of forest was lost to development/urban land during the study period, accounting for 4% of the net losses. Of these losses, 1,028 km^2 were upland forests, and 484 km^2 were wetland forests (NOAA, 2017b). In addition, about 2,578 km^2 of wetlands decreased between 1996 and 2010 and were primarily lost to water (48%) (NOAA, 2017a).

In the dissertation, I aim to address the subsequent impact of hurricanes on the Gulf Coast Forest resources using a mix of advanced geospatial and statistical techniques. In Chapter 2, I utilize the land cover change techniques and calculate possible hotspots while considering the existence of water bodies and greenness following a catastrophic storm event. Using geospatial computing methods, I estimate the urban vegetation damage and land cover change caused by a significant hurricane along the Gulf Coast. In Chapter 3, I aim to compare aboveground carbon in saplings, bole, stump, top, and foliage between pre (2001-2003) and post (2005-2007) Hurricane Ivan (2004) periods and assess the changes of aboveground carbon in different physiological levels of trees after Hurricane Ivan and the relevance of different tree characteristics using statistical modeling. Chapter 4 aims to develop a land use scenario-based prediction model for 2050 and estimate the overall carbon storage in different carbon pools. This chapter allows me not only to forecast future land use changes but also to evaluate the corresponding shifts in carbon storage expected by 2050 in the Gulf Coast region.

Results of Chapter 2 suggest that canopy loss and the presence of water vapor during the catastrophic hurricane are evident to magnify the potential hotspots. Chapter 3 suggests a hurricane can cause a significant amount of aboveground carbon loss, and the biophysical characteristics of trees play a pivotal role in recovering aboveground carbon. Finally, Chapter 4 suggests urban land and forest land will increase despite more frequent hurricanes in the coming decades. The change in land use accounts for an increase in overall carbon storage upon more significant forestland conservation. The results of my study equip relevant stakeholder groups with valuable information for decision-making processes to facilitate future land use, conservation efforts, and forest resiliency toward long-term sustainable ecosystem services.

CHAPTER 2

SPATIOTEMPORAL CHARACTERIZATION OF THE IMPACT OF HURRICANE MICHAEL ON URBAN VEGETATION COVER IN PANAMA CITY AND PANAMA CITY BEACH, FLORIDA*

* Alam A., Mishra D. & Dwivedi P. To be submitted to [Jounral of Urban Forestry and Urban Greening]

Abstract

The impacts of major climatic events on urban vegetation cover are not well understood. We used Landsat 8 ETM+ derived land cover in Google Earth Engine (GEE) to determine damage to urban vegetation and Optimized Hotspot and Outlier Analyses to identify significant spatial clusters of hotspots and cold spots from Hurricane Michael in Panama City and Panama City Beach, Florida. We used two indices (Normalized Difference Water Index-NDWI and Enhanced Vegetation Index-EVI) to assess the impact of Hurricane Michael on urban vegetation cover. Results show that more than 30.07% of the land cover changed after two months of the hurricane's landfall, including a rapid increase of 19.64% in water bodies. Overall, we observed a 4.91% decrease in vegetation cover, out of which 34.44% were coastal woody wetlands. Our analysis showed a rapid increase in water content in the study area due to intense precipitation, coastal storm surge, and vegetation loss by strong sustained winds. The spatial cluster ($\geq$ 95% confidence, $z \geq 1.96$) of water content increased to 76.11% from 61.02%, whereas the vegetation cluster decreased from 65.46% to 56.29%. This estimate suggests that vegetation cover changed into bare land or open space and reflects a pattern of the random spatial process. Panama City Beach, Southport, and Youngstown CCD (census county division) were identified as hotspots of vegetation loss, with a noticeable increase in water content after the hurricane. Our findings demonstrate the benefits of applying spatial statistical techniques to characterize the spatiotemporal status of the urban vegetation along the Gulf Coast to assist in creating plans for mitigating natural hazards and risk reduction strategies.

2.1 Introduction

Hurricanes are major natural threats to the Gulf Coast states (The Atlantic, 2017). In their 2022 Atlantic Hurricane Season Outlook, the National Hurricane Center (NHC) anticipates a likely range of 14 to 21 storms, of which 6 to 10 could develop into hurricanes (winds of 74 mph or higher), including 3 to 6 significant hurricanes (category 3, 4 or 5; with winds of 111 mph or higher) (NOAA, 2022a). The approximate cost of damages from tropical cyclones and hurricanes on the Gulf Coast from 1980 to 2020 has been about $790 billion (NCEI, 2022; NOAA, 2021a). In addition to the economic loss, hurricanes take several lives every year. Hurricanes have claimed about 3,163 lives since 1980, and the devastating hurricane Katrina alone in 2005 left more than 2,000 people dead along the Gulf Coast (Figure 2.1).

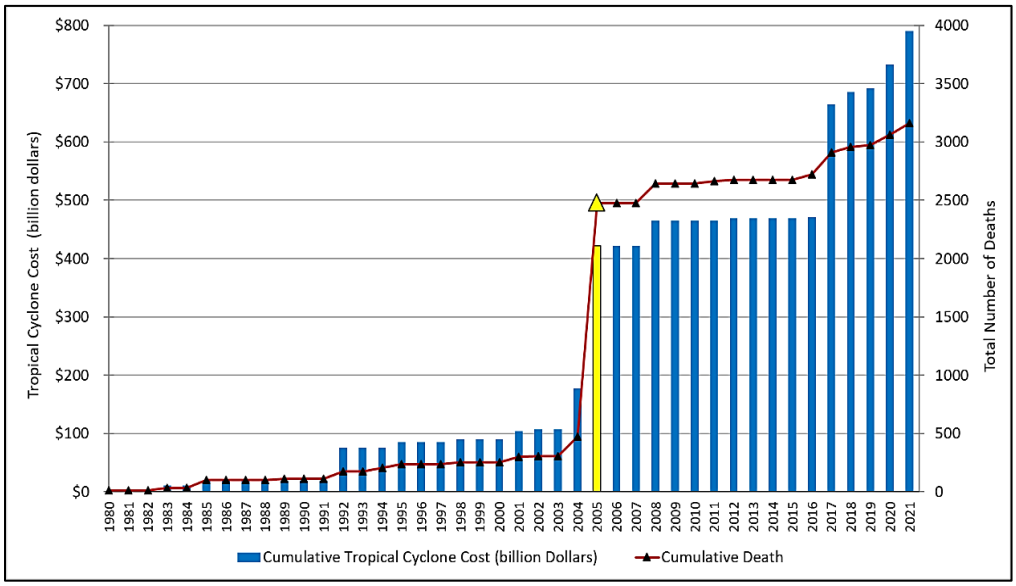

Figure 2.1: Death and damage costs by tropical cyclones in the Gulf states from 1980 to 2021 (NCEI, 2022). The yellow bar in 2005 represents the catastrophic Hurricane Katrina.

In addition to devastating casualties and financial losses, hurricanes also seriously harm the coastal ecology, changing the land cover (NOAA, 2021b, 2020, 2018). For example, about 320 million large trees were severely damaged by Hurricane Katrina (Chambers et al., 2007; NASA, 2007b), and Hurricane Laura destroyed 3,642 km^2 of forested land along the Gulf Coast, resulting in an overall $63 million in economic loss (USDA, 2020). Hurricane Ike (2008) resulted in the removal of 4.3% of all trees measured in Houston, Texas. Approximately 2,590 km^2 of coastal woody wetland were lost or changed to other land cover types between 1996 and 2010 due to catastrophic

hurricanes and tropical cyclones on the Gulf Coast (NOAA, 2018). Louisiana alone lost more than 414 km^2 of wetland area to water after Hurricane Katrina (NOAA, 2021b, 2005).

Some studies have quantified the effects of hurricanes on forest ecosystems using advanced geospatial techniques. Ramsey Ill et al. (1997) used AVHRR 250m multi-temporal images to analyze the effects of 1992 Hurricane Andrew on forests. They found that regional averaged NDVI (Normalized Difference Vegetation Index) change followed damage severity but did not provide a quantitative relationship between NDVI change and damage severity. Ayala-Silva and Twumasi, (2004) used the standardized change of NDVI produced from AVHRR data to assess forest damage brought on by Hurricane Georges in 1998. They inferred the linear relationship between regional averaged NDVI and the length of the hurricane track. Using local scale data from the Advanced Spaceborne Thermal Emission and Reflection Radiometer (ASTER) satellite, Aosier et al. (2007) investigated the effects of 2004 Typhoon Songda on vegetation cover. They discovered that the change in adjusted NDII (Normalized Difference Infrared Index) was smaller than the change in NDVI (Normalized Difference Vegetation Index) for damaged trees. Their results were at odds with earlier research, which found that NIR-SWIR (Near Infrared-Short wave Infrared)-based vegetation indices were more effective in detecting vegetation alterations than NIR-Red-based vegetation indices (Wilson and Sader, 2002).

The majority of existing studies to date have used passive optical remote sensing, in which the change or standardized change of different vegetation indices are adopted as damage indicators with little effort to assess their quantitative relationship with forest damage at the pixel level and with little comparative analysis on the performance of these vegetation indices (Hanssen et al., 2021; Lacerda et al., 2021; Landry et al., 2021; Moody et al., 2021). Due to the data volume of pixel-based analysis and continuous Earth observation, studies require continuous time series data with highly configured computer platforms and storage (Gorelick et al., 2017; Kumar and Mutanga, 2018; Salcedo-Sanz et al., 2020). For instance, to create a global land cover map for any time point, almost 10,000 Landsat scenes or 3 TBs of storage are needed (Giri et al., 2013). High-performance cloud computing platforms have made it possible to store, process, and analyze geographic data at a massive scale on the cloud at a low cost and effectively (Giri et al., 2013; Hansen et al., 2013). In 2010, Google introduced the Google Earth Engine (GEE) platform with

more than forty years of satellite imagery at no cost (Dong et al., 2016; USGS, 2014). Amazon Web Service (AWS) also now provides access to the Landsat data archive, enabling analysis of this dataset on the cloud (Amazon, 2015; USGS, 2015). Recently, NASA (National Aeronautics and Space Administration) launched the NASA Earth Exchange Program (NEX), which allows the processing and analysis of NASA Earth observation data (NASA, 2021).

With the aid of cloud computing, in this study, we aim to bridge the gap left by earlier research utilizing the land cover change technique and calculate possible hotspots while considering the existence of water bodies and greenness following a catastrophic storm event. Using geospatial computing methods, we estimate the urban vegetation damage and land cover change caused by a significant hurricane along the Gulf Coast. The specific objectives of this study are to estimate land cover changes after a major hurricane landfall on the Gulf Coast and identify hotspots for rapid post-hurricane urban vegetation assessment.

2.2 Materials and Methods

Study area

The Gulf Coast has a history of experiencing hurricanes and tropical storms landfall in the Summer-Fall season. Since 1900, the Gulf Coast has been devastated by 46 hurricanes, and since 1990, the frequency of hurricanes in this area has grown by 70% (NOAA, 2020). Recent years (since 2017) show an early start of hurricane season and NOAA's Climate Prediction Center (CPC) alarms of no respite in terms of a significant decrease in Categories 3, 4, and 5 hurricanes in the Gulf Coast (NOAA, 2021c, 2021b). Panama City and Panama City Beach are in the southeastern United States in the area of northwest Florida known as the Panhandle, which was greatly affected by Hurricane Michael in 2018 (Figure 2.2). More than 3 million tourists visit Panama City every year, and this number is likely to increase to more than 5 million by the end of 2050. Around 0.90 million people live in the surrounding census county divisions (CCD), and it is estimated that there will be more than 1.6 million by 2050 (US Census Bureau, 2020). Panama City and Panama City Beach are dominated by forestland (21.14%) and woody wetlands (35.54%), which are significantly affected by catastrophic hurricanes. However, urban lands (5.30%) comprise a small portion of the total land use in Panama City and Panama City Beach (MRLC, 2017).

Image Preprocessing

Figure 2.3 shows the overall methodology of our study. We used LANDSAT-derived multi-spectral data products on the open-source GEE Platform. Considering the track of Hurricane Michael with landfall time (October 10, 2018), we selected Landsat 8 cloud-free satellite images, including vegetation indices on GEE, within 90 days before the landfall date (Table 2.1). To find the ideal cloud-free (<10%) image on the event day, we employed the object-based "CFmask" technique in GEE. “CFmask” is a C programming-based function of mask, which is a translation of “Fmask” developed by USGS Earth Resources Observation and Science (EROS) (Foga et al., 2017; Zhu et al., 2015; Zhu and Woodcock, 2012). After employing “CFmask”, cloud-masked photos were saved in GEE Assets via "Asset Manager" for eventual replication.

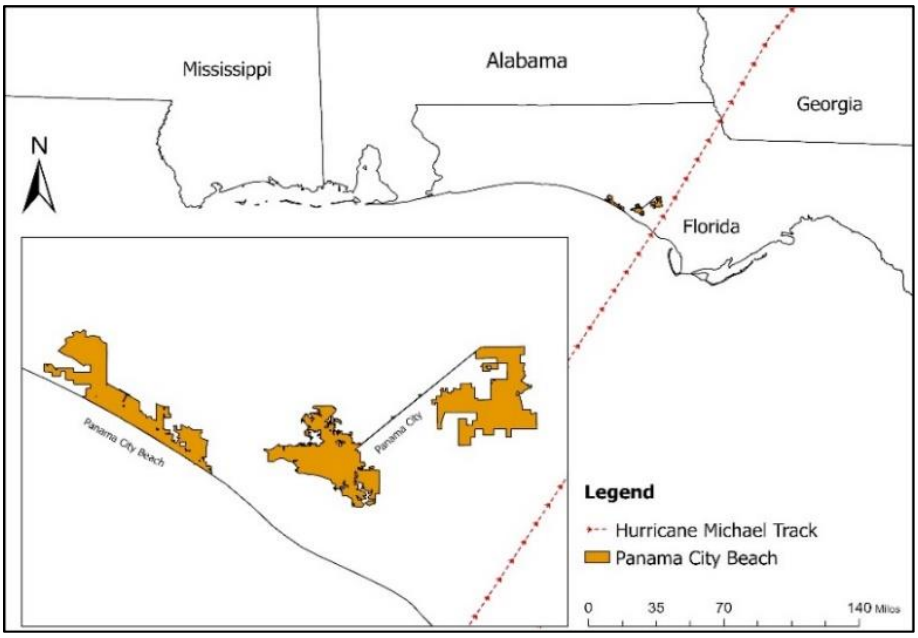

Figure 2.2: Track of Hurricane Michael (October 10, 2018; 0735 CDT) over Panama City and Panama City Beach, Florida (red dotted line). Key map shows the geographic location of the landfall near Panama City and Panama City Beach (Panama City Beach, 2022)

Table 2.1: Description of spatial data requirements for land use change analysis.

Data Layer	Source	Scale/Spatial Resolution	Date/Year
Panama City Boundary	Bay County, Florida Website	Scale 1:12880 (meter)	2017
Hurricane Michael (AL142018)	National Hurricane Center (NHC), Florida	Scale 1:12880 (meter)	October 10, 2018; 0735 Central Daylight Time
Landsat 8 Surface Reflectance (SR)	Google earth engine (GEE) data provided by U.S. Geological Survey (USGS)	30	Pre: May 1, 2018 Post: January 28, 2019
National Agriculture Imagery Program (NAIP)	Google earth engine (GEE) data provided by U.S. Department of Agriculture (USDA)	1	2019
Digital Elevation Model (DEM)	Google earth engine (GEE) data provided by NASA/USGS/Jet Propulsion Laboratory-Caltech	30	2000
Enhanced Vegetation Index (EVI)	Google earth engine (GEE) data provided by U.S. Geological Survey (USGS)	30	Pre: May 1, 2018 Post: January 28, 2019
Normalized Difference Water Index (NDWI)	Google earth engine (GEE) data provided by U.S. Geological Survey (USGS)	30	Pre: May 1, 2018 Post: January 28, 2019

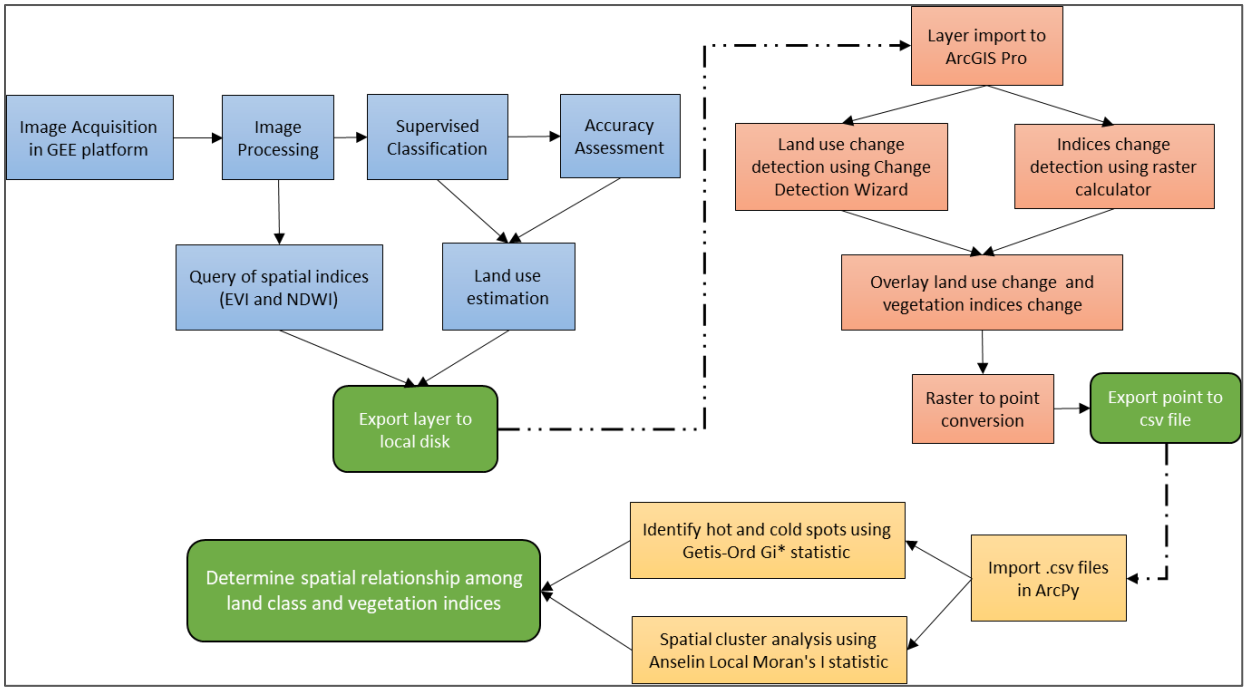

Figure 2.3: Methodological flowchart of land use change analysis and impact assessment on urban vegetation after a major hurricane.

Land cover categories and reference data

Along with the requirements of image processing, the land cover analysis also needs reference datasets, land cover classification, indices evaluation, and statistical analysis for pre- and post-hurricane events. Land cover change detection technique applied and evaluated on GEE platform using Random Forest (RF) classifier algorithm. The RF classifier has been widely used in land cover change studies over the years (Oliphant et al., 2019; Pelletier et al., 2016; Pimple et al., 2018; Qu et al., 2021; Rwanga and Ndambuki, 2017). The RF classifier has been effective in retaining classification accuracy when applied to analyze data with stronger noise (Breiman, 2001; Schmidt et al., 2016; Tian et al., 2016). The RF is an ensemble classification approach that creates an ensemble of classification (using multiple decision trees) by employing bootstrap aggregating, or "bagging," where each tree trains on a different subset of the whole training data (Breiman, 2001; Waske and Braun, 2009).

Classifying heterogeneous land cover from satellite images is a challenging task (Sidhu et al., 2018; Zurqani et al., 2018). Considering the size and scale, we identified four major land covers for Panama City: 1) vegetation, 2) impervious layer, 3) water body, and 4) barren land. For the accuracy assessment of the land cover classification, the reference dataset is an essential element (Rodriguez-Galiano et al., 2012; Zurqani et al., 2018). We delineated 305 reference points on NAIP images (2019) by visual inspection in the GEE platform randomly using equation (1) adopted from (Cochran, 1977).

$$n = \frac{(\sum W_i S_i)^2}{\left[S\left(\hat{O}\right)\right]^2 + (1/N)\sum W_i S_i^2} \approx \left(\frac{\sum W_i S_i}{S\left(\hat{O}\right)}\right)^2 \quad (1)$$

where N = number of units in the study area, S(O) is the standard error of the estimated overall accuracy that we would like to achieve, W_i is the mapped proportion of the area of class i, and S_i is the standard deviation of stratum i, S_i is the standard deviation of the stratum I, $S_i = \sqrt{(U_i(1-U_i)}$ (Cochran, 1977).

A training dataset that consisted of 70% randomly selected observations were created; the remaining 30% of the observations were used in the validation data set (Olofsson et al., 2014). The

training dataset was used to improve the supervised classifier algorithm, while the validation dataset was used in the accuracy assessment of the produced land cover classification maps.

Accuracy assessments and change detection

The purpose of accuracy assessment is to estimate the error and uncertainty of the output classification, to either choose the most appropriate mapping procedure or to inform the interpretation of the output (Lyons et al., 2018; Olofsson et al., 2014). The produced land cover maps were validated using field-verified GPS point data in Panama City and Panama City Beach. One-third (~100) of field locations were verified using handheld precision GPS, Google Spreadsheet using mobile hotspots, and Google Maps. Finally, a confusion matrix of land cover maps was calculated to evaluate the accuracy of the outputs using the producer's accuracy, user's accuracy, and kappa statistics.

Change detection of land cover is the final step to demonstrate change analysis that designates differences between images of the same scene at different times (ESRI, 2022; You et al., 2017). The mosaic plot method of GEE was used to represent the gain and loss of the land cover change. The mosaic plot provides a statistical summary of losses and gains over time (Google Earth Engine, 2019). Our study used the Change Detection Technique in ArcGIS Pro and the Image Difference Technique in GEE to see the difference between the two different images taken before and after the hurricane event.

To produce the greenness and wetness of the components for validating land cover change, we used EVI and NDWI for each image scene (before and after the hurricane) using at-sensor reflectance values and stacked them for later classification. We used EVI instead of NDVI because of its additional correction capability for some atmospheric and canopy background noise, and EVI is also more sensitive in areas with dense vegetation (USGS, 2016; Vermote et al., 2016). On the other hand, NDWI is used to highlight open water features in a satellite image, allowing a water body to "stand out" against the soil and vegetation (EOS, 2019; Oliphant et al., 2019). We used EVI and NDWI in the GEE platform to process the normalized index values for greenness and wetness in Panama City and Panama City Beach after the hurricane event. GEE JavaScript for this analysis is available in Appendix 1.

Optimized Hot Spot Analysis and Optimized Outlier Analysis

We used the Optimized Hot Spot Analysis (Getis-Ord Gi*) tool in the ArcGIS Pro platform to determine the observed hotspots and coldspots using indices (EVI and NDWI) derived from our input data and equation (2). The resultant z-scores and p-values indicate where features with either high or low values cluster spatially. This tool looks at each feature within the context of neighboring features (Getis and Ord, 1992; Hakim et al., 2021; Xiao et al., 2016). A feature with a high value is interesting but may not be a statistically significant hotspot. To be a statistically significant hotspot, a feature will have to have a high value and be surrounded by other features with high values as well.

$$G_i^* = \frac{\sum_{j=1}^{n} w_{ij}x_j - \bar{x}\sum_{j=1}^{n} w_{ij}}{S\sqrt{\frac{n\sum_{j=1}^{n} w_{ij}^2 - \left(\sum_{j=1}^{n} w_{ij}\right)^2}{n-1}}} \quad (2)$$

where x_i is the attribute value for feature j, w_{ij} is the spatial weight between feature i and $_j$, n is equal to the total number of features.

We used optimized outlier analysis to evaluate the characteristics of the input NDWI and EVI values. This analysis interrogates input data to determine settings that will produce optimal cluster and outlier analysis results. The tool calculates a local Moran's I value, a z-score, a pseudo p-value, and a code representing the cluster type for each statistically significant feature. The z-scores and pseudo p-values represent the statistical significance of the computed index values and are measures of statistical significance that tell us whether to reject the null hypothesis, pixel by pixel (Anselin, 1995; ESRI, 2019a). The Local Moran's I statistic of spatial association is given as:

$$I_i = \frac{x_i - \bar{X}}{S_i^2} \sum_{j=1, j\neq i}^{n} w_{i,j}(x_j - \bar{X}) \quad (3)$$

where x_i is an attribute for feature i, X is the mean of the corresponding attribute, $w_{i,j}$ is the spatial weight between feature i and j.

The cluster/outlier type (COType) field in the output table distinguishes between a statistically significant cluster of high values (HH), a cluster of low values (LL), an outlier in which a high value is surrounded primarily by low values (HL), and an outlier in which a low value is surrounded primarily by high values (LH). A high positive z-score (++ quadrants) for pixels indicates that the surrounding pixels have similar values (either high values or low values), and a low negative z-score (-- quadrants) for pixels indicates a statistically significant spatial data outlier. Statistical significance is set at the 95% confidence level. When no FDR (False Discovery Rate) correction is applied, features with p-values smaller than 0.05 are considered statistically significant (Columbia Public Health, 2019; ESRI, 2019b). The FDR correction reduces this p-value threshold from 0.05 to a value that better reflects the 95% confidence level given multiple testing (ESRI, 2019c).

2.3 Results

Land use change and distribution

Figure 2.4 shows the significant land cover transition before and after Hurricane Michael in the southwestern part of Panama City Beach. Table 2.2 shows the land cover transition matrix before and after the hurricane. Over the study period for pre- and post-hurricane, 69.93% of the total study area remained unchanged, while 30.07% changed. The barren land area declined by 20.50% after the hurricane. The abrupt change from barren land to impervious layer and vegetation cover shows how our supervised classification correctly detected this type of land cover transition. Since the post-hurricane image was taken in January 2019, some regeneration was identified in the southwestern part of Panama City Beach. Inland water inundation after the hurricane increased by 19.64%, which infers heavy rainfall and flooding on the shoreline and inland of Panama City and Panama City Beach during the event. The overall accuracies of the supervised images (Table 2.3) were 81.44% (pre-hurricane) and 80.01% (post-hurricane), respectively. It is likely that classification accuracy was reduced by the variation in the availability of high-resolution imagery from the NAIP that was not always available for the same period as the Landsat scenes.

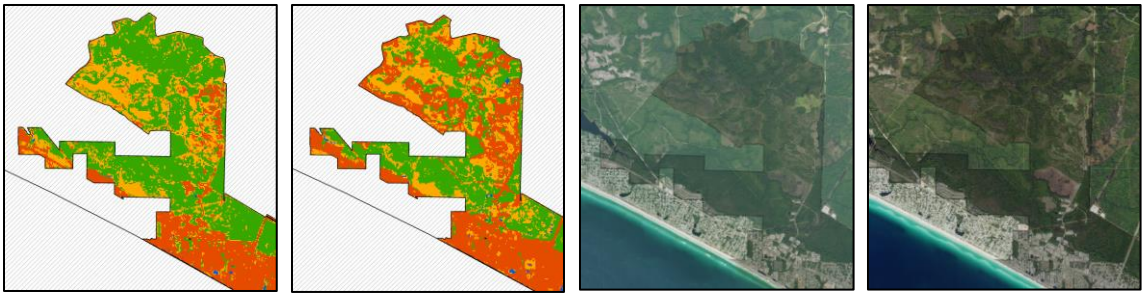

Figure 2.4: Land cover transition before and after Hurricane Michael. (a) supervised land cover on May 1, 2018 (b) supervised land cover on January 1, 2019 (c) NAIP DOQQ, 2015 (d) NAIP DOQQ, 2019.

After land cover consolidation (Table 2.4), i.e., vegetation and non-vegetation, intensive rainfall (122 mm ~ 6 hours), and wind speed (252 km/h) on the landfall day (National Weather Service, 2018) resulted in vegetation loss of 4.91%. As the hurricane track passed through Panama City Beach, our study found coastal vegetation and woody wetlands loss was about 34.44% of the total vegetation loss (Supplementary Figures S2.1 & S2.2).

Table 2.2: Land cover transition matrix of Panama City and Panama City Beach. Units are in km^2.

		Post-Michael			
	Land Class	**Barren Land**	**Impervious Layer**	**Vegetation**	**Water Body**
Pre-Michael	**Barren Land**	0.00	5.30	7.01	0.90
	Impervious Layer	3.14	0.00	1.98	0.36
	Vegetation	6.77	4.41	0.00	0.59
	Water Body	0.71	0.42	0.42	0.00

Figure 2.5 illustrates the standard error of the land cover classes before and after the hurricane event. Error bars provide the accuracy of the land cover classification by measuring the pixel as sample variability. Data are more variable for the impervious layer, and our analysis shows that the standard error for water bodies is negligible before and after the event, even though more areas were inundated by the hurricane-induced storm surge.

Table 2.3: Accuracy assessment of land cover transition after Hurricane Michael.

	Pre-Michael	**Post-Michael**
Training Accuracy	99.23%	99.85%
Validation Accuracy	81.44%	80.01%
Producers Accuracy	78.29%	81.57%
Kappa coefficient	0.69	0.72

Table 2.4: Vegetation cover change (in km^2) after Hurricane Michael. The percentage in parentheses shows the share of total land use of vegetation and non-vegetation.

	Pre-Michael	Post-Michael	Relative Change
Vegetation	377.53 (24.63%)	359.87 (23.48%)	-4.91%
Non-vegetation	1155.43 (75.37%)	1173.09 (76.52%)	1.51%

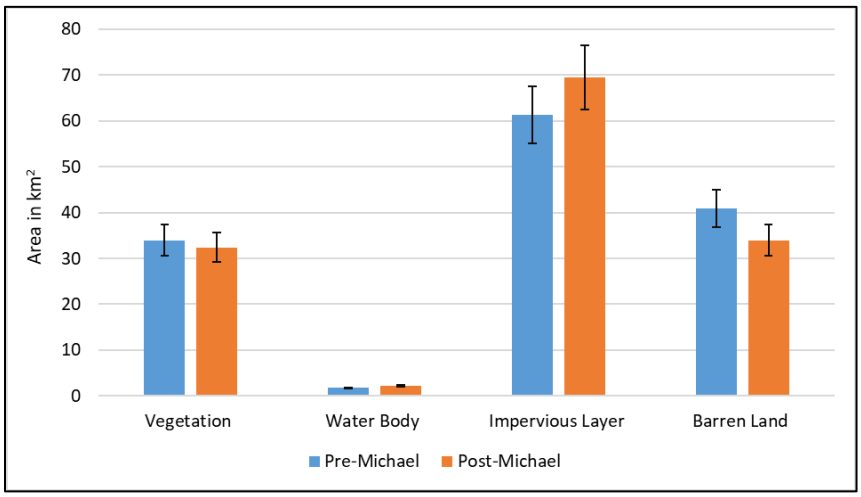

Figure 2.5: Standard error of land cover classes before and after the hurricane event. Error bars before and after the event overlap, indicating that there is no statistically significant difference between the two-time series.

NDWI and EVI change detection

NDWI positive threshold has been increased in the southwestern part of Panama City Beach and the northeastern part of Panama City after the hurricane event. While limiting the low reflectance of water characteristics, the near-infrared wavelengths maximize the high reflectivity of terrestrial vegetation and soil components. Water and moisture contents (> 0.2) are identified after Hurricane Michael, reflecting the intensity of heavy rainfall during the event (Figure 2.6). The loss of green foliage, which should be directly connected with a fall in EVI and indirectly correlated with a reduction in total chlorophyll and water content at the canopy level, is the most recognizable aspect of sudden canopy alteration that can be detected by optical remote sensing. The hurricane impact identified by EVI than NDWI was consistent with damage severity assessed by the USDA Forest Service, Forest Inventory and Analysis (Brandeis et al., 2022). The impacted area detected by NDWI was smaller (<11%) than EVI, while NDWI underestimated the impacted area and did not differentiate the damage level as well as EVI. Based on the analysis, we discovered that, to a certain extent, both NDWI and EVI could identify post-hurricane vegetation damage. Therefore, we further analyzed only the statistical properties of pixel-based NDWI and EVI hotspot analysis.

The Southwestern part of Panama City Beach and the northeastern part of Panama City were identified with more green cover loss than the surrounding inland area. Figures 6 and 7 show mixed characteristics after the hurricane since the image was taken in January – analysis found 6.7% of the canopy regeneration and 1.6% of wetland regeneration in the affected area. The histogram distribution (Supplementary Figures S2.3 & S2.4) shows the increment mean shift after the hurricane, reflecting the water intrusion in the study area during the hurricane. More water content (>7.6%) was found in the affected area by the NDWI analysis, which reflects the non-seasonality effect of hurricane season. However, EVI shows different scenarios than NDWI as the overall mean values (Supplementary Figures S2.5 and S2.6) for EVI increased after the hurricane event. The restoration of the green canopies and green grasslands following the incident was one factor in the increase in EVI values. The histogram of the EVI values shows the regeneration of the green canopies in Panama City and Panama City Beach. Average values of EVI in the previous years during hurricane season (June-October) were 9.31% higher than that of 2018.

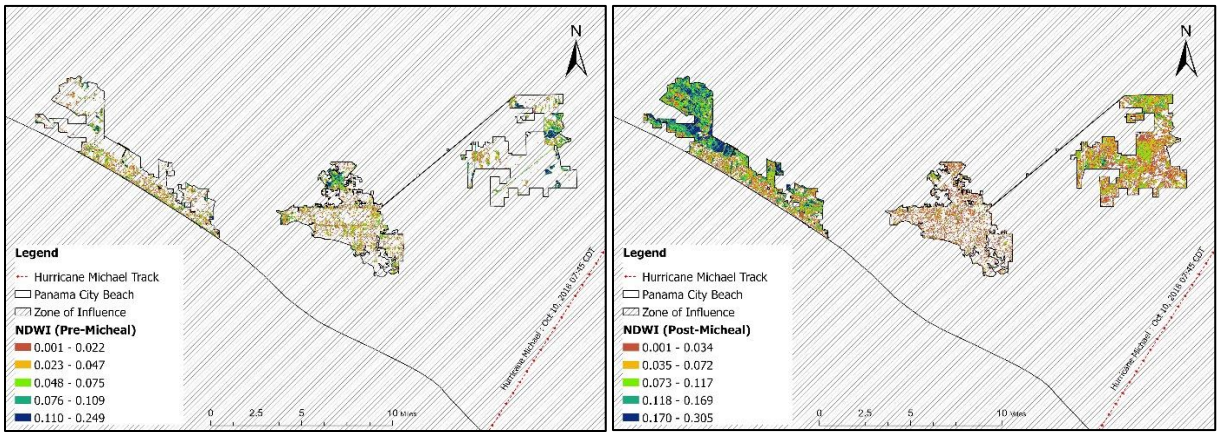

Figure 2.6: Change of NDWI after Hurricane Michael. Higher values approaching +1 usually appear blue and correspond to either a high-water content or a water surface, while lower values all the way to 0 are the tell-tale signs of drought conditions unless the area of interest is a non-aqueous surface.

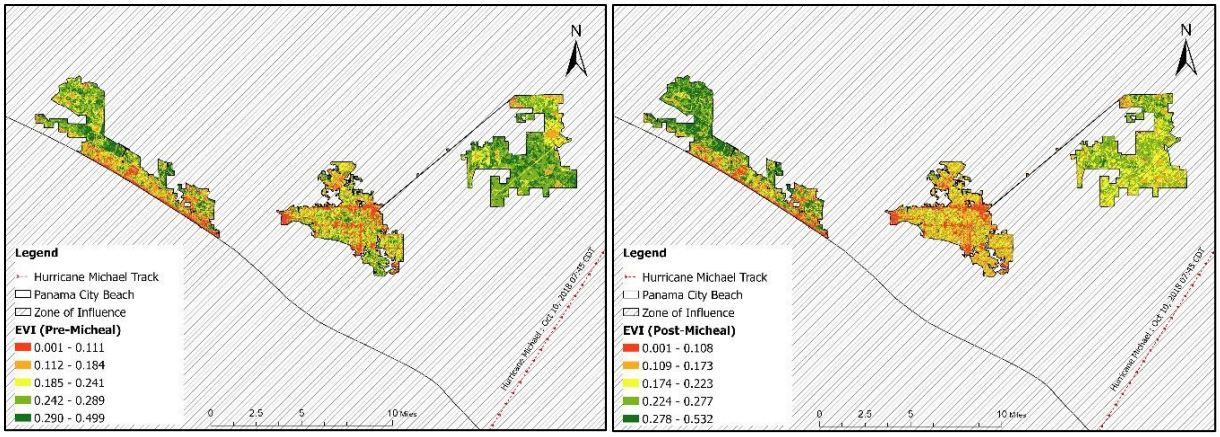

Figure 2.7: Change of EVI after Hurricane Michael. Negative values are omitted because they correspond to areas with water surfaces, manmade structures, rocks, clouds, and snow; bare soil usually falls within 0.1- 0.2 range; and plants will always have positive values between 0.2 and 1. Healthy, dense vegetation canopy should be above 0.5, and sparse vegetation will most likely fall within 0.2 to 0.5.

Optimized hotspot and outlier analysis

Using the Getis-Ord Gi* statistic (Equation 2), optimized hotspot (OHS) analysis evaluated the characteristics of the input feature class (EVI and NDWI) to produce optimal results. OHS automatically aggregated the NDWI and EVI point data by pixel, identified an appropriate scale of analysis for Panama City and Panama City Beach, and corrected for both multiple testing and spatial dependence. When we set the scale of analysis to the pixel level (30x30m), the optimal fixed distance band is based on the average distance to 30 nearest neighbors – 114 to 148 m, depending on the indices value inside our study area boundary.

OHS results are shown in Figure 2.8 (NDWI) and Figure 2.9 (EVI) according to bin values which identify statistically significant hotspots and coldspots. Valid features and outliers of NDWI and EVI changed after the hurricane because of the indices value transformation. Before the hurricane, the total number of statistically significant NDWI hotspots ($\geq$ 95% confidence, $z \geq 1.96$) covered 61.02% of Panama City and Panama City Beach. Pixels with water bodies were observed to be stable through time since the last major weather event. Statistically significant hotspots of NDWI increased to 76.11% after the hurricane as more water inundated the study area. Statistically significant hotspots of EVI increased from 58.78% to 69.82%, which infers vegetation loss occurred in the southwestern and northeastern parts of Panama City and Panama City Beach, respectively. OOA shows hotspot areas clustered with 84.01% of the study area, which increased to 91.34% after the hurricane. It indicates more lands are inundated, and more urban vegetation is

enriched with the water content by the heavy precipitation and storm surge in the southwestern part of Panama City and Panama City Beach (Figures 2.8 and 2.9). On the other hand, OHS and OOA analysis show vegetation loss due to hurricanes, which is represented by the lower number of statistically significant (≥ 95% confidence, z ≥ 1.96) EVI clusters. About 65.46% of the area was clustered, considering the greenness of the vegetation before the hurricane, which decreased to 56.29% after the event (Figure 2.10). Figures S7 and S8 illustrate the spatial cluster and outlier of the indices NDWI and EVI before and after the hurricane event.

Our output feature class in ArcGIS Pro created Local Moran's I Index, z score, p-value, and cluster/outlier types. Using equation (3), we showed the Moran'I cluster and outlier distribution (Figures 2.11 & 2.12). OOA uses spatial lag as a variable to transform z scores which averaged the neighboring values of locations. The transformed z-score values, when using a 95% confidence level, are confined to -1.96 and +1.96 standard deviations. Accounting for 66% of the pixels values before the event, our observed p-value was smaller than 0.05, rejecting our null hypothesis because the pattern exhibited could likely be the result of random spatial processes. Our post-event NDWI scenario observed a similar distribution but with a higher number of point locations. Transformed z values (≥ 95% confidence, z ≥ 1.96) of the outliers for NDWI after the hurricane event decreased to 8.66%, which inferred more similar pixel values in the clustered pattern. Outliers of EVI show relatively static change, increasing to 8.91% from 7.56%, which suggests that more green areas (i.e., small herbs, shrubs, etc.) transformed into barren land or open space.

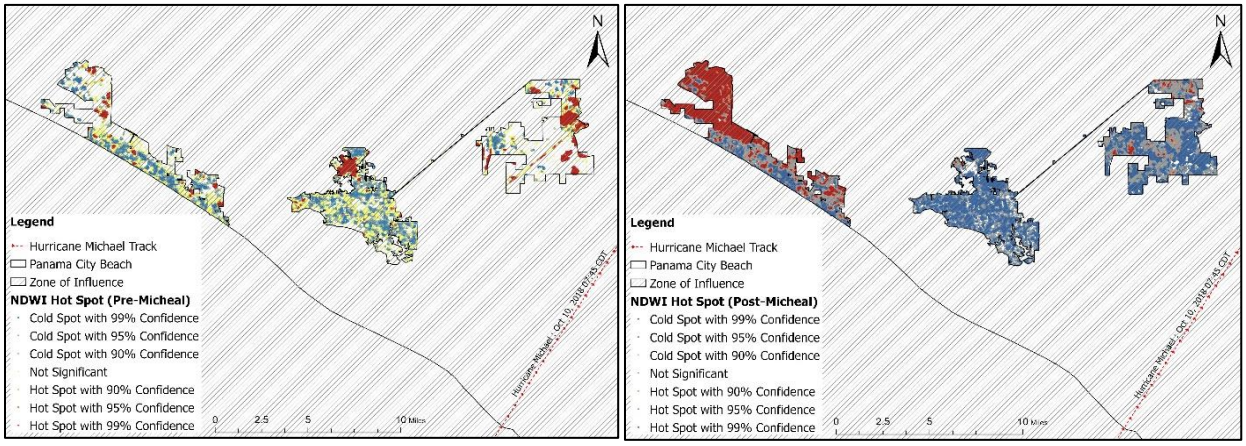

Figure 2.8: Hotspot and coldspot changes after Hurricane Michael. Red dots are illustrated as hot spots (99% confidence intervals), and blue dots are illustrated as coldspots (99% confidence intervals). Increased NDWI values after the hurricane accumulated in the southwestern part of Panama City Beach..

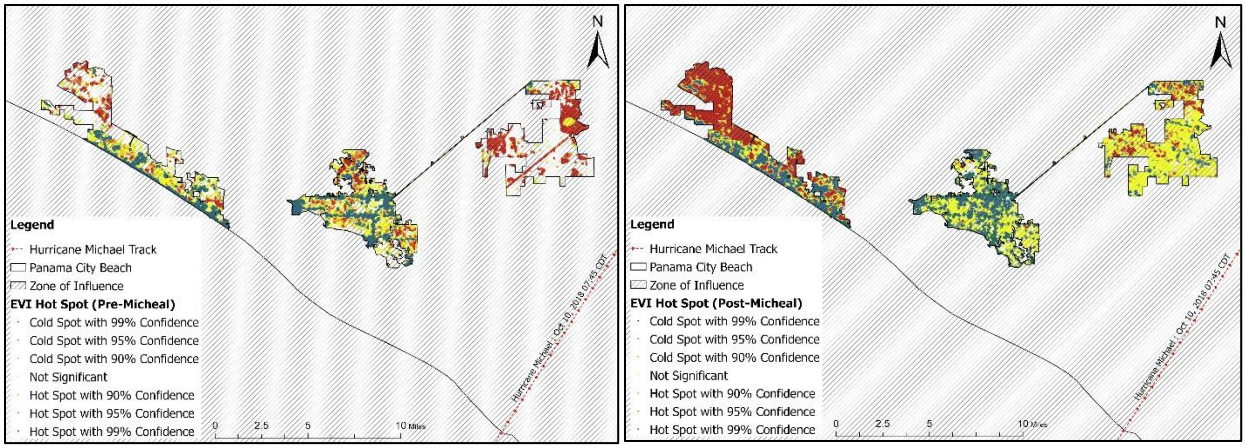

Figure 2.9: Hotspot and coldspot changes after Hurricane Michael. Red dots are illustrated as hotspots (99% confidence intervals), and yellow dots are illustrated as coldspots (99% confidence intervals). Increased EVI values after the hurricane accumulated in the southwestern part of Panama City Beach.

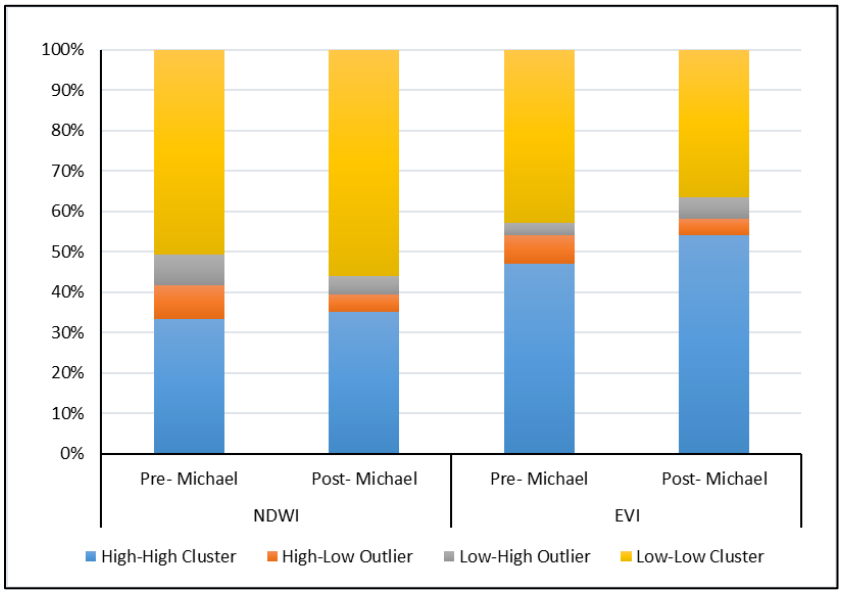

Figure 2.10: Distribution of statistically significant (≥ 95% confidence, z ≥ 1.96) pixels (cluster and outlier) from the optimized hotspot and outlier analysis based on the indices before and after Hurricane Michael.

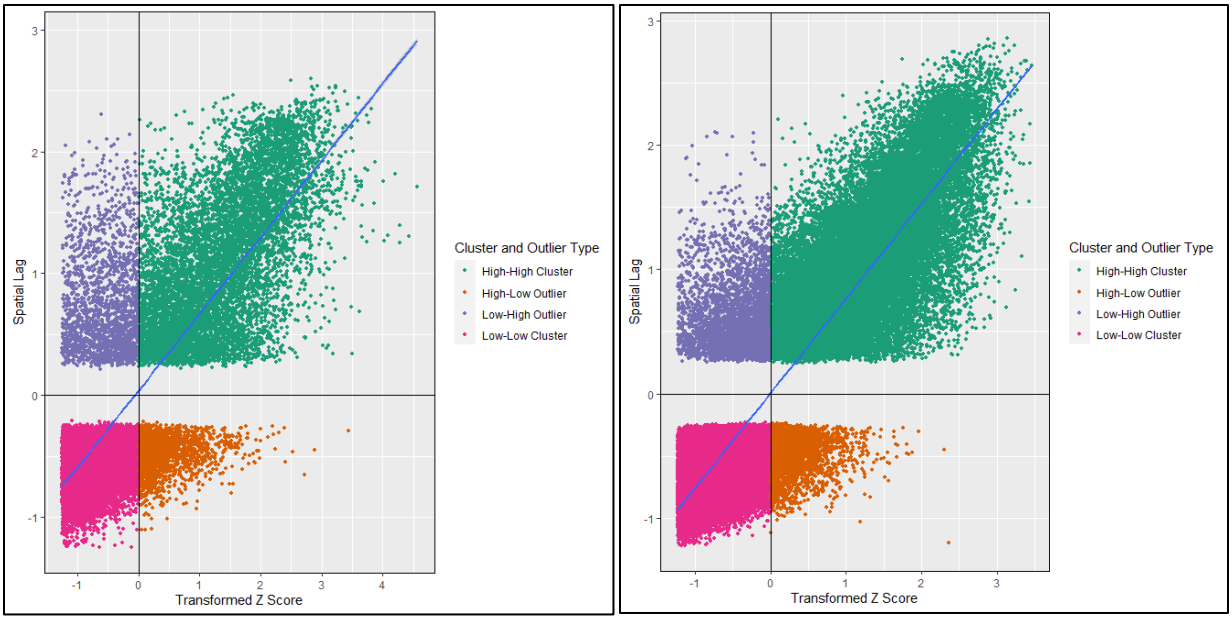

Figure 2.11: Optimal clusters and outliers based on NDWI before and after Hurricane Michael. Positive-Positive quadrants (++) NDWI values illustrate High-High cluster, and Negative-Negative quadrants (--) NDWI values illustrate Low-Low cluster. Positive-Negative (+-) quadrant NDWI values show high-low outliers, and Negative-Positive (-+) quadrant NDWI values show low-high outliers.

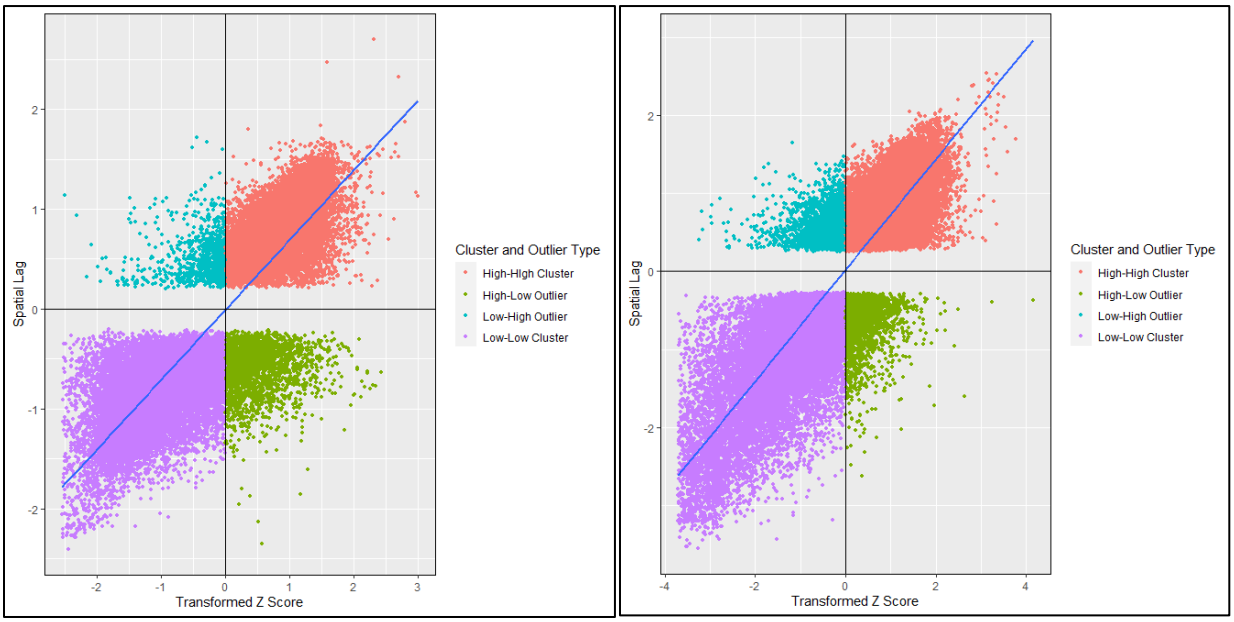

Figure 2.12: Optimal clusters and outliers based on EVI before and after Hurricane Michael. Positive-Positive quadrants (++) EVI values illustrate High-High cluster and Negative-Negative quadrants (--) EVI values illustrate Low-Low cluster. Positive-Negative (+-) quadrant EVI values show high-low outliers and Negative-Positive (-+) quadrant EVI values show low-high outliers.

Figure 2.13 shows the area of the local sum for each pixel and its neighbors in the affected CCDs (Census County Divisions). This area is then compared proportionally to the sum of all other

pixels, leading to a high-high and low-low clustering pattern when significant Z score (≥ 95% confidence, z ≥ 1.96) and vegetation indices are considered. Less water content on urban vegetation was found in Panama City than in Panama City Beach because of the proximate location near the shoreline. Vegetation cover in Southport and Youngstown was highly affected due to high wind speed (>250 km/h), as these CCD's are dominated by highly dense coastal woody wetlands. Panama City and Lynn Haven experienced less vegetation damage because of the availability of a greater impervious layer. Our analysis found Panama City Beach, Southport, and Youngstown CCD as hotspots in terms of high-water content in sustained vegetation (NDWI) and overall vegetation condition (EVI) after Hurricane Michael.

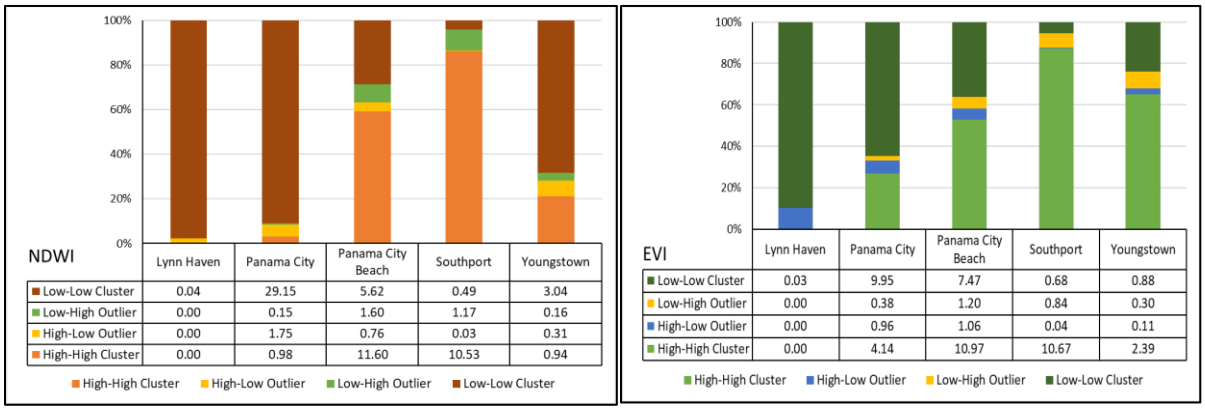

Figure 2.13: Total area (in km^2) of hotspots in CCD's after Hurricane Michael considering NDWI and EVI. Local Moran's I analysis shows High-High clustering pattern observed in Panama City Beach, Southport and Youngstown CCD

2.4 Discussion

Hurricanes impact on hotspots of urban vegetation loss

The surrounding ecosystem and populations in Panama City Beach, Florida, are facing potential risks from hurricanes. This study indicates a substantial influence of hurricanes on the alteration of urban vegetation cover, with peak gust speeds escalating from 152 km/h (Category 1 hurricane) to 225 km/h (Category 4 hurricane, and the highest gusts recorded in our data). Our investigations revealed an overall 4.91% reduction in urban vegetation after Hurricane Michael. Notably, census county divisions (CCD); Panama City Beach, Southport, and Youngstown emerge as hotspots for urban vegetation loss in the aftermath of Hurricane Michael. These regions are anticipated to remain susceptible to rapid vegetation loss due to future hurricanes.

Our study demonstrated that location, land use, and vegetation indices - NDWI and EVI, could be used to assess how a hurricane will affect built environments and human activities. The results of this study showed a considerable amount of fitness of using optimized hotspot and optimized outlier analyses to uncover clusters of changes in the urban vegetation cover associated with water content enrichment. Optimized hotspot analysis and outlier analysis could identify spatial patterns in low and high-density areas. Even though a methodology similar to this study has been used before in natural hazard assessment, our major goal was to highlight the urban vegetation damage due to high-intensity hurricanes and identify potential hotspots within a rapidly growing city on the Gulf Coast. Relevant studies; for instance, Staudhammer et al. (2011) reported a percentage of urban vegetation loss due to Hurricane Ike (2008) in Houston, Texas - similar to our study. Another study from the authors reported the clustered locations of hurricane-induced wood debris after hurricanes Ivan (2004) and Katrina (2005), which coincides to the broader goal of this study, but it did not report the potential hotspots of debris accumulation (Staudhammer et al., 2009). Similarly, Lam et al. (2011) detected and estimated changes in several land use types, including coastal forests, during hurricane Ivan and Katrina in conjunction with NDVI. Weeks Bay, Alabama, had a 6.94% increase in forest cover, according to their estimation of the relative changes in land use categories using IKONOS data taken 15 months apart. However, we used a much smaller temporal window for our change research (2 months), and we discovered a rapid decrease of urban vegetation using Landsat scenes. To further isolate the true influence of hurricanes on vegetation cover, we also incorporated the seasonality effect on EVI and NDWI for five years in our study. Wang and D'Sa, (2010) evaluated the damages from five distinct storms that struck the northern Gulf Coast between 2002 and 2008 using MODIS-based pre- and post-EVI. They concluded that the best way to identify the most likely damage area and patterns is to analyze data from two more years within a month of the hurricane overpass. However, they did not provide any statistical pattern analysis for the locations that are susceptible and frequently affected by hurricane disturbances. Potter, (2021) used USGS DOQ and NAIP (1m) imagery to analyze the changes in urban tree vegetation and the extent of shrubs or herbaceous cover on blocks located within the most flood-impacted neighborhoods of New Orleans in 2005. These images were used to track vegetation changes over a longer period. However, they did not report flood-induced water content changes. Our study added NDWI as an indicator of detecting hurricane-induced floods and water content; it scrutinizes the validity of our hotspot analysis. Hauser et al. (2015) used the hotspot

technique to assess the wetland degradation pattern after Hurricane Sandy using a stepped range of monetary ESV (economic susceptibility value) loss based on our degradation index. Van Coppenolle and Temmerman, (2020) identified global hotspots for wetland conservation with a global-scale GIS hotspot model. Shell et al. (2021) created hotspot maps to characterize the structural diversity of the US outer coastal plain mixed forest. The maps identified southern Mississippi, northern and eastern Virginia, northern North Carolina, eastern South Carolina, and the border between the states of Texas and Louisiana as the structural diversity hot spots. Harris et al. (2017) used ArcGIS hotspot analysis to identify the emerging hotspots of forest loss in Brazil, Indonesia, and the Democratic Republic of Congo (DRC) between 2000 and 2014. Their study offered that statistical data models can help isolate the most significant clusters of loss occurring over dynamic forest landscapes and provide more coherent guidance for allocating resources for forest monitoring and enforcement efforts.

Our findings from the study and the literature cited in the study showed hotspot and outlier analysis as a good starting point for those interested in understanding where future adverse climate effects, i.e., storm surge, sea level rise, drought, etc., may occur. Hurricanes often result in widespread damage to urban vegetation, leading to the disruption of existing hotspots. Areas that were once thriving with greenery may experience a sudden decline in vegetation cover due to the destructive forces of hurricanes, such as strong winds and heavy rainfall. Post-hurricane hotspot analysis becomes essential to identify new pockets of resilience or areas that require immediate attention for restoration and re-greening efforts. Hurricanes can create outliers in urban vegetation patterns by causing extreme deviations from the norm. Areas heavily impacted by hurricane-induced flooding or wind damage may exhibit vegetation conditions that deviate significantly from the surrounding urban environment. Our study executed an initial data assessment of the input features, including data outliers of NDWI and EVI for pre- and post-Micheal period. Since each input feature’s (pixel's) neighborhood is defined using pixel-based analysis to determine statistical significance, the relative increase in hotspots in our optimized hotspot analysis as time changes make apparent sense. This research did not account for any changes in the scale of analysis by comparing the pixel sizes of all data layers before and after the event. The scientific literature has emphasized the necessity for multi-scale hotspot analysis to support decision-making at multiple scales across several societal concerns. This is further evidenced by the notable changes in hotspot

placement under the diverse neighborhood distances (Guo et al., 2021; Liu et al., 2017; Lv et al., 2022).

While hurricane wind effects are probably most significant in creating tree damage, water, tree, and wind damage are all notably significant in coastal areas with relatively high concentrations of products and people (i.e., defoliation, broken stems, and branches, and uprooted or toppled trees). Following the hurricane event, changes in water bodies and coastal wetlands are visible in the study area from satellite imagery and other ground measurements. The natural resurfacing of water bodies, slow development of small plants and trees, and regeneration of coastal wetlands all assist in adjusting the shift in land use. Land cover change is a relatively static process, but the altercation of natural land use changes due to hurricanes brings about rapid changes. Although some factors typically cannot be modified by land use management (e.g., climate, topography, soil conditions), numerous tree management activities can influence factors that affect a stand's resistance to wind effects. These factors relate to tree species, stand configuration, and silvicultural treatments (Cole et al., 2021). Land use change was prompted by hurricane risk, and our findings offer important information on hazard vulnerability. Although it can be challenging to spot small-scale changes in land use brought on by hurricanes, our research looked for land use transitions and losses of vegetation cover within a short period of time. It is possible that the hotspots we identified could expand geographically and/or increase in intensity under continued climate change. Such expansion or intensification could further complicate hazard mitigation decision-making in hot spot areas, particularly for areas that are not currently considered a hotspot but may become so in the future, including areas in the southeast Atlantic coast and Gulf of Mexico. Findings from our study will assist state policymakers, and this information may also be used at the local jurisdiction level to alert communities of the risk involved in adhering to the Federal Emergency Management Agency's (FEMA) Hazard Mitigation Plan and its recommended procedures (FEMA, 2018).

Spectral homogeneity and classification-induced uncertainty

Satellite images often have spatial resolution limitations, meaning they may not capture fine-scale variations in vegetation cover. This can make it difficult to locate and define small-scale hotspots precisely, especially in places with complex vegetation patterns or heavily urbanized areas. For example, vegetation cover estimation often relies on the spectral characteristics of vegetation

captured by Landsat bands. As stated by Rapp et al. (2005) three questions should be asked when using the results of vegetation mapping from remote sensing imagery: how well the chosen classification system represents actual vegetation community composition, how effectively images from remote sensing capture the distinguishing features of each mapping unit within the classification and how well these mapping units are delineated by photo interpreters. They recommended that to improve classification accuracy, the following factors be considered when choosing a vegetation classification system: (i) enhancing class definitions to reduce ambiguity; (ii) introducing new classes to better capture the complexity of regional vegetation patterns; and (iii) employing a higher level of classification. However, when a study area is covered by vegetation of complex forms or different stages, it results in similar spectral responses among different vegetation groups or generates spectral variations for the same vegetation group (Sha et al., 2008). Difficulties or challenges are often encountered in mapping vegetation under such circumstances. Sha et al. (2008) justified to create more vegetation classes to support ecological studies of grassland change dynamics as the study area Xilin River Basin, Inner Mongolia, China, is dominated by heterogeneous plant communities. Authors believed that hard and pixel-based image classification might not be the best way to map the vegetation cover at the fine details required in their study. This led to the design and development of the Hybrid Fuzzy Classifier (HFC), a modified version of fuzzy systems. The fuzzy system acknowledges that the spectral signature of vegetation can vary, and there might be uncertainty in assigning specific pixels to vegetation cover classes (Tech, 2005). Landsat pixels can represent a mix of land cover types. Fuzzy logic allows for the characterization of pixels with a degree of membership to multiple classes (Xi et al., 2023a). This ultimately introduces spatial uncertainty into the classification of land cover because relatively homogeneous spatial extents may reflect zones of intergradation among heterogeneous map units that comprise a small fraction of an analysis area (Remmel and Perera, 2017). Therefore, transitional areas of the landscape can share properties of multiple themes in a legend, and difficult to map accurately to the most suitable themes, as in the case of mixed pixels (Li et al., 2014). In our analysis, uncertainty over barren land (23%) and impervious layer (28%) were the highest as spectral homogeneity caused less accurate land cover after the hurricane. In addition, a transition from barren land to impervious layer and vice versa before and after the hurricane did not accurately characterize the land cover due to the extent of the analysis and application of relatively coarse resolution satellite imageries.

One solution to address the classification-induced uncertainty is to adopt more advanced image classification methods, such as sub-pixel and mixed-pixel analysis, in addition to machine learning-based classifiers (Arco et al., 2022; Hung and Ridd, 2002). Choosing higher resolutions of imagery acquired by the right remote sensing sensors to increase the distinguishable possibility in image classification could be another way to deal with this uncertainty (Chen et al., 2017; Li et al., 2018). Nevertheless, higher resolutions of imagery will most likely increase the cost. Although there are some standard methods for image pre-processing, there are no super image classifiers that can be uniformly applicable to all applications (Zhou et al., 2018). Thus, it is a challenging task, as well as a hot research topic, to apply effective classifiers or to develop new powerful classifiers suitable for specific applications. Furthermore, it has been shown that auxiliary data - such as field samples, topographical features, environmental traits, and additional digital data layers - can significantly improve classification accuracy or yield a more desirable outcome. It is advisable to keep in mind that the technical improvements (designing more advanced classifiers or acquiring high-resolution imagery, etc.) cannot solve all problems that are encountered during vegetation extraction from remotely sensed data but will improve the results.

To accurately anticipate future climatic events in our study area, it is necessary to go beyond characterizing the sites of previous hurricanes and add information on the factors that influence storm activity, such as climate and human activities. On the Gulf Coast, hurricanes are a common occurrence, and they are having an increasing impact on progressively larger areas, necessitating greater research (Blake et al., 2005; NOAA, 2017c; Rappaport, 2014). Since there are so few studies that deal with the immediate assessment of hurricane damage on urban vegetation cover, our work may aid professionals and academics in their ongoing research and initiatives.

2.5 Conclusion

It is evident from our research that green cover loss and the presence of water vapor turned the land cover into a different one once a major hurricane hit. Hurricanes can cause significant damage to coastal states, and the current rise in storm frequency is concerning. The findings of our study should be used to help determine where hurricane hazard mitigation techniques should be prioritized and concentrated throughout the Gulf Coast. Although our primary focus is on the effect

of hurricanes on the cities on the Gulf Coast, it is possible to use similar methods to characterize other natural disasters in other regions. We analyzed the impact of a hurricane in a mid-size urban area on the Gulf Coast. Future research could investigate the regional scale (i.e., entire Gulf Coast urban areas) analysis using smaller pixel sizes and finer-scale aggregation patterns, such as those gained from using satellite-based land use changes.

By examining the scale of analysis setting on the ArcGIS Pro platform to characterize the unique land cover type throughout the study area, further research could enhance our techniques. This study worked only on one major hurricane event, more analysis could be done on different intensities of hurricanes and on different cities representing a variety of land use patterns. For the regions that have historically had frequent visits from large hurricanes, a comparison of various intensities is essential. Analyzing the land use change pattern is important for the Gulf Coast to oversee some land use types, especially wetlands, grasslands, and barren lands. Future research could examine additional, more in-depth land cover transitions besides vegetation in compliance with the NLCD (National Land Cover Database) land use classes.

Our statistical analysis offers a way to assess how a natural hazard altered the types of land cover over time. Given how climate change is changing the frequency, intensity, and seasonality of many natural hazards, this knowledge can be very helpful to planners and decision-makers in the field of hazard mitigation. To put it simply, the effects of climate change are diminishing the predictive power of past patterns of hazard occurrences. As a result, planners for hazard mitigation will need to employ other methods for risk mapping and estimating the likelihood of future occurrences. To effectively capture the intricacy of climate change-related naturally occurring hazards, risk mitigation planners may endeavor to integrate advanced methodologies into their risk assessments.

Supplementary Figures

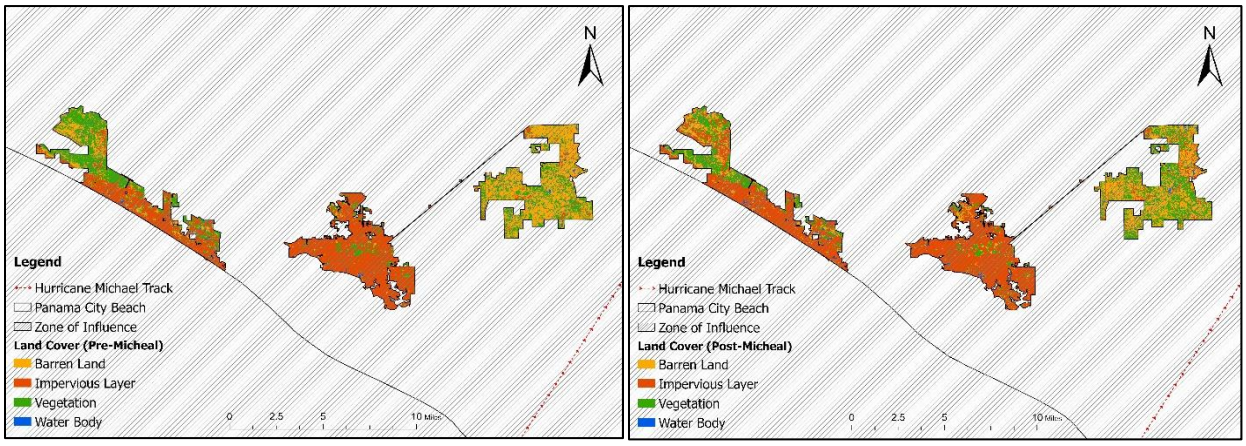

Figure S2.1: Pre-hurricane and Post-hurricane land cover in Panama City and Panama City Beach.

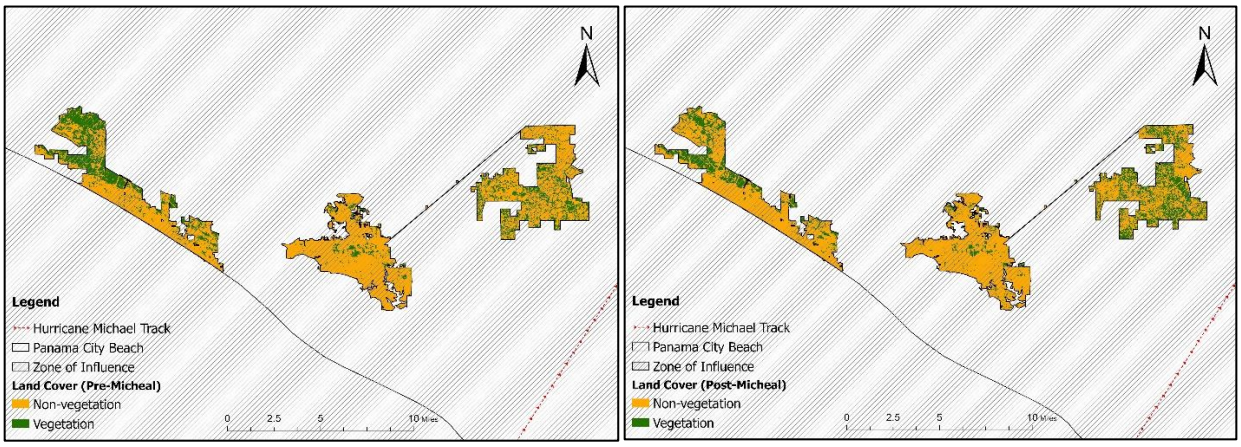

Figure S2.2: Pre-hurricane and Post-hurricane vegetation cover in Panama City and Panama City Beach.

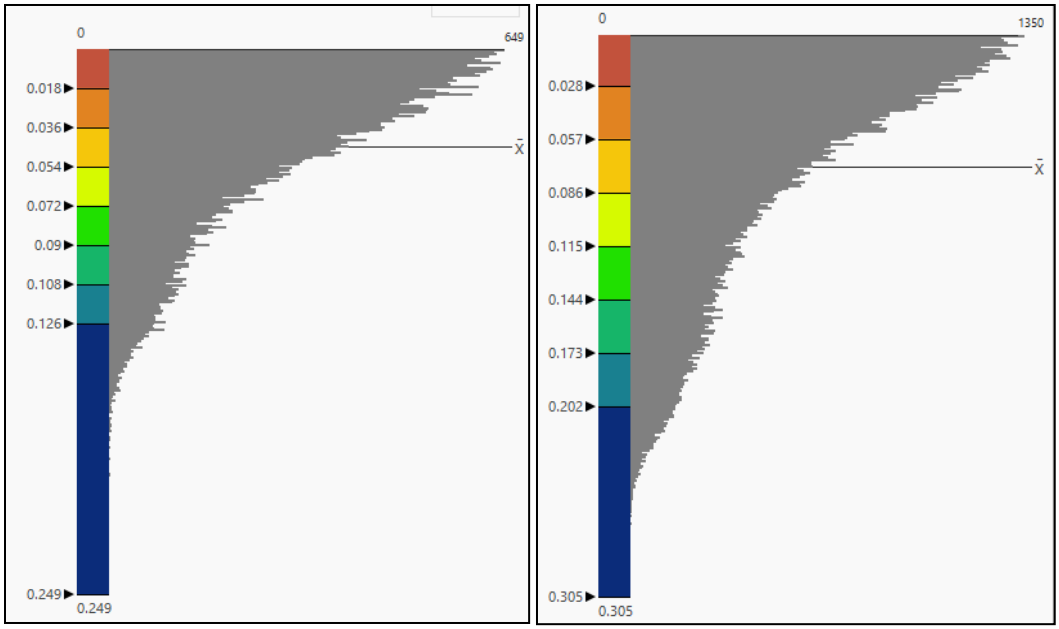

Figure S2.3: Histogram of NDWI before (May 1, 2018) and after (January 28, 2019) Hurricane Michael. NDWI: Normalized Difference Water Index,

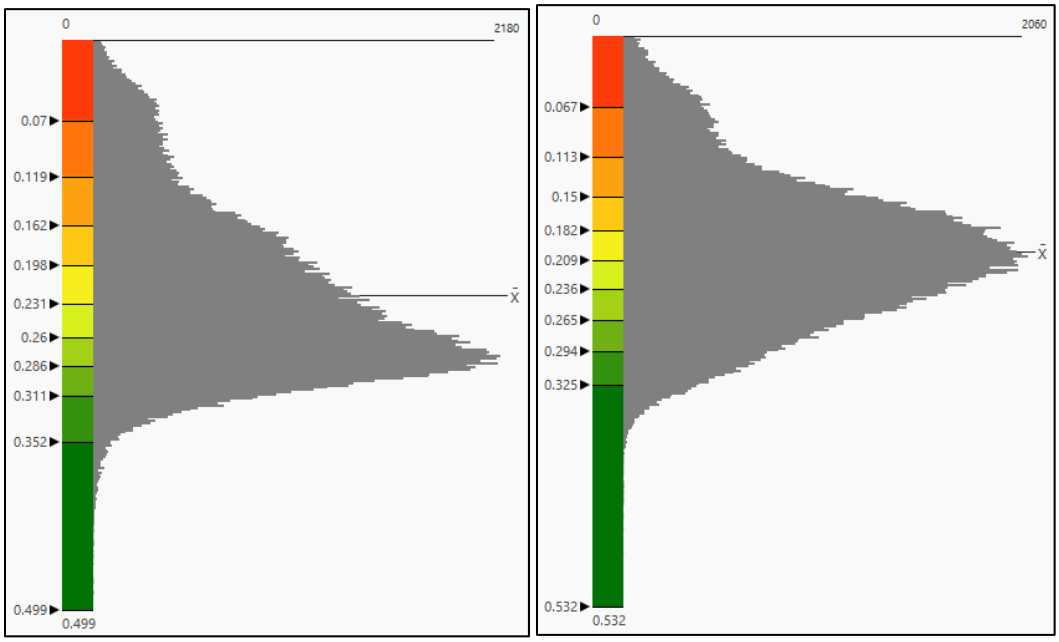

Figure S2.4: Histogram of EVI before (May 1, 2018) and after (January 28, 2019) Hurricane Michael. EVI: Enhanced Vegetation Index.

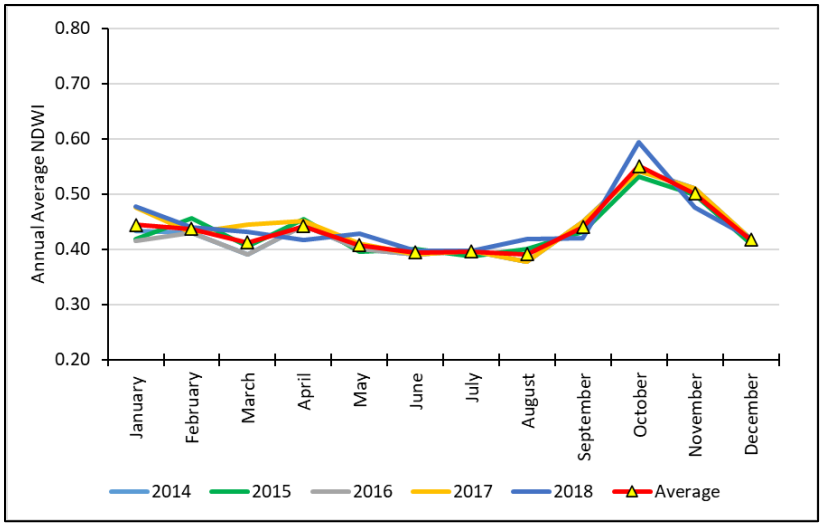

Figure S2.5: Monthly average NDWI in Panama City and Panama City Beach between 2014 and 2018.

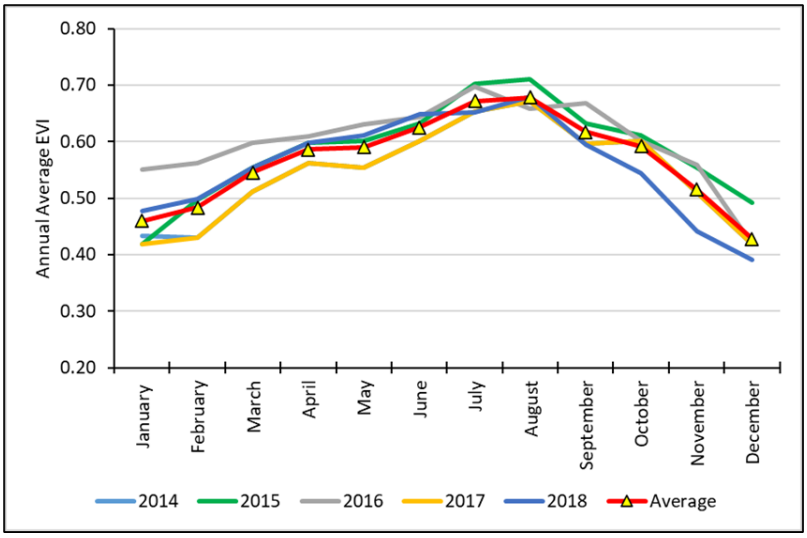

Figure S2.6: Monthly average EVI in Panama City and Panama City Beach between 2014 and 2018.

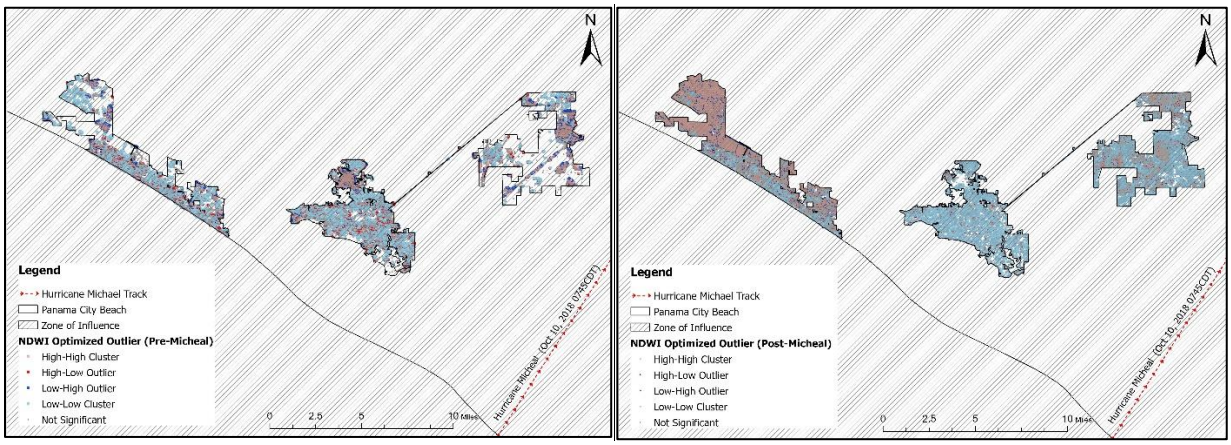

Figure S2.7: Optimal clusters and outliers based on NDWI before and after Hurricane Michael.

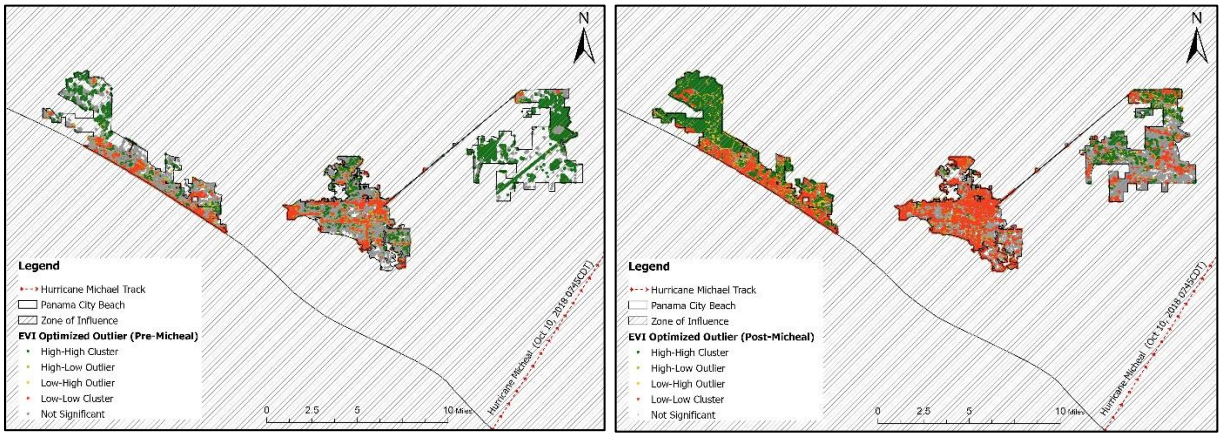

Figure S2.8: Optimal clusters and outliers based on EVI before and after Hurricane Michael.

CHAPTER 3

ASSESSING THE IMPACT OF HURRICANE IVAN ON ABOVEGROUND CARBON OF COASTAL FORESTS IN PERDIDO BAY, FLORIDA*

* Alam A., Dwivedi P. To be submitted to [Jounral of Environmental Sustainability]

Abstract

Hurricanes can physically transform forestry ecosystems, leading to immediate and potentially long-lasting impacts on carbon dynamics. We compared the average carbon in trees (saplings, bole, stump, tops) and foliage pre (2001-2003) and post (2005-2007) Hurricane Ivan for different types of tree categories in the Perdido Bay watershed, Florida. We estimated a decrease of 7,451 and 1,782 metric tons/km^2 of aboveground carbon in hardwood and mixed plots after Hurricane Ivan, respectively. Softwoods gained 1,822 metric tons/km^2 of aboveground carbon in the post-hurricane period due to post-hurricane regrowth. Aboveground carbon decreased in stands with large ($\geq$ 0.15m) and medium ($\geq$ 0.12m) diameter at breast height (d.b.h.) by 2,274 and 3,022 metric tons/km^2, respectively. Aboveground carbon in young (< 25y) taller trees (> 15m) decreased by 12,155 metric tons/km^2 of carbon immediately after the hurricane. The results of our log-linear regression model indicate that stand type (softwood/mixed/hardwood), height, physiographic class (deep sands/flatwoods/rolling uplands/small drains/swaps/bottomlands), multiplier of height and field age, along with the plot affected status were statistically significant ($p \leq 0.05$) determinants of the carbon loss from the forest stands. Over the study period, there was a decrease of approximately 38.64% of aboveground carbon in trees and 35.18% of aboveground carbon in foliage. Softwood plots had 48.31% less aboveground carbon compared to hardwood plots, while plots in flatwoods and rolling uplands had 52.73% and 63.25% less carbon than bay and wet pocosins, respectively. Post-hurricane, the carbon in the trees and foliage starts to recover gradually, taking about 15 years to come back to the original status at the landscape level. Our study provides a framework for researchers and policymakers to assess the vulnerability of coastal forests considering extreme weather events.

3.1 Introduction

The Intergovernmental Panel on Climate Change (IPCC) climate change 2023 synthesis report summarizes that human activities are the primary cause of global warming, leading to an increase in global surface temperature of 1.1°C above the pre-industrial period (1850-1900) between 2011 and 2020 (IPCC, 2023b). Human-induced climate change already impacts numerous extreme weather events and climate patterns worldwide (IPCC, 2015). As a result, there have been widespread negative consequences and associated losses and damages to the environment and human populations (Jehn et al., 2022; Kemp et al., 2022).

Due to global warming, tropical storms and hurricane activity in the Atlantic Ocean, the Caribbean, and the US Gulf of Mexico has increased since 2000 (NASA, 2022; US EPA, 2022). About 6 to 7 hurricanes have formed in the Noth Atlantic every year since 1878, and roughly 2 per year land on the coast of the US (NOAA, 2021c). According to the total annual ACE (Accumulated Cyclone Energy) Index, hurricane intensity has risen noticeably over the past 20 years, and eight of the ten most active years since 1950 have occurred since the mid-1990s (US EPA, 2022). Rising intensity (category 4 and 5) of hurricanes in recent years has meant that hurricanes travel farther inland after landfall (Figure 3.1). A more extensive landmass is impacted by these catastrophic hurricanes as they hit the US coastline and release energy inland (NOAA, 2022b). The approximate cost of damages from tropical cyclones and hurricanes on the Gulf Coast from 1980 to 2020 has been about $790 billion (NCEI, 2022; NOAA, 2021a). The US Global Change Research Program and the IPCC project that tropical cyclones and hurricanes in the Atlantic and Gulf Coast will become more intense over the 21st century, with higher wind speeds, heavier rains, and billion-dollar damages (IPCC, 2014; U.S. Global Change Research Program, 2018).

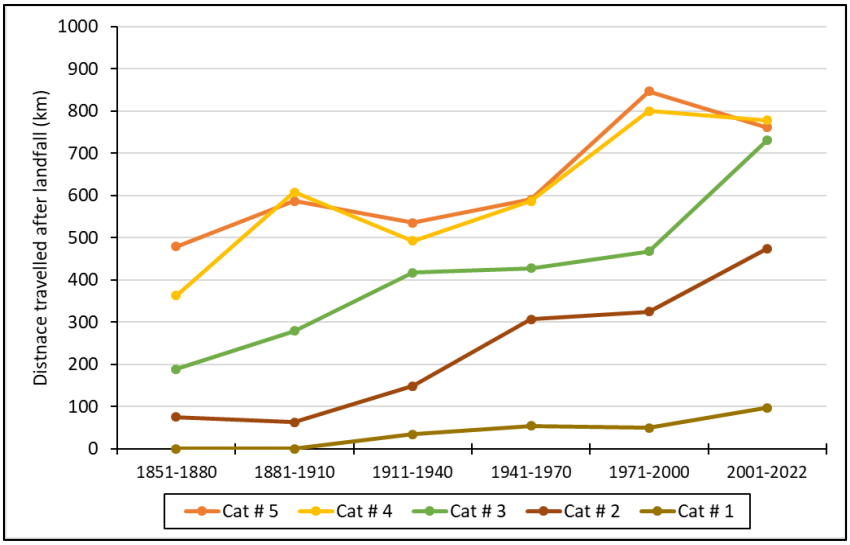

Figure 3.1: Average distance traveled by different categories of hurricanes after landfall in the US Gulf Coast, Atlantic, and Caribbean Islands since 1850 (NOAA, 2022b).

Hurricanes cause adverse impacts on forest structure and composition (Zhang et al., 2016) and have major influences on the recovery of the coastal forests (Murdiyarso et al., 2015). About 320 million large trees were severely damaged by Hurricane Katrina (Chambers et al., 2007; NASA, 2007a), and Hurricane Laura destroyed 3,642 km^2 of forested land along the US Gulf Coast (USDA, 2020). Loss of trees and forestlands compounded with carbon stock loss following a catastrophic hurricane is enormous (NASA, 2007a). Since 1851, about 97 million trees have been affected each year by tropical cyclones and hurricanes in the continental US, with an average of 26.5 million metric tons of annual carbon loss (Zeng et al., 2009). The study showed about 43.9±8.4 million metric tons and 37.9 ± 6.4 million metric tons of carbon lost due to Hurricanes Katrina and Rita in 2005, respectively (Negrón-Juárez et al., 2010). Aboveground carbon decreased by 468.9 metric tons/km^2 due to Hurricane Maria (2017) in Puerto Rico, and it is estimated that it will take 15 years for forests to recover their pre-hurricane carbon stock (Chevalier et al., 2022a). Hurricane Charley (2004) damaged 0.61 km^2 of mangrove forest land in southwest Florida, and the estimated carbon loss ranges from 427 metric tons to 3,599 metric tons of carbon (Peneva-Reed et al., 2021b).

Quantification of forest carbon is usually associated with a high degree of uncertainty due to differing methods or incomplete assessment of carbon pools after a significant hurricane (Houghton et al., 2012; Peneva-Reed et al., 2021b). Researchers are developing models to predict

the probability of hurricanes and the amount of damage inflicted by them to support overall decision-making and mitigate these catastrophic effects on forests (Blennow and Sallnäs, 2004; Peltola et al., 1999; Schmidt et al., 2010). Some models are used for quantifying damage at the single tree level (Schmidt et al., 2010), while others are used for stand-level projections (Hanewinkel et al., 2014) or regional-level assessment (Talkkari et al., 2000). There is a scarcity of studies on aboveground carbon changes at the physiological level, including sapling, bole, stump, top, and foliage. Attention is needed to monitor aboveground carbon at the overall physiological level of trees, impacting carbon sequestration, forest health, resilience, biodiversity, and ecosystem functioning.

The goal of our study is to quantify the impact of Hurricane Ivan on tree sapling, bole, stump, top, and foliage carbon in the Perdido Bay watershed. Our first objective is to compare aboveground carbon in sapling, bole, stump, top and foliage between pre (2001-2003) and post (2005-2007) Ivan period. Secondly, we assess the changes of aboveground carbon in different physiological levels of trees after Hurricane Ivan and the relevance of different tree characteristics using log-linear modeling. Our study on aboveground carbon across different physiological levels will provide valuable insights into forest health and resilience, especially after catastrophic hurricanes. This assessment will also enhance our understanding of biodiversity patterns in forests. In addition to biodiversity, our study will pave the way to comprehensively explore the relationships between carbon dynamics and ecosystem biodiversity.

3.2 Methods and Methodology

Perdido Bay and Hurricane Ivan

Perdido Bay covers approximately 1.3 km^2. Its watershed encompasses over 32.3 km^2 of land, tributaries, lagoons, and bayous in Florida and Alabama. Perdido Bay is oriented almost perpendicular to the Gulf of Mexico, with a length of 53 km and an average width of 4 km (Taylor et al., 2002). Perdido Bay is connected to the Gulf of Mexico through Perdido, and the Gulf Intracoastal Waterway (GIWW) passes through the southern portion of the bay, including areas along the coastal and inland sections of Escambia County in Florida and Baldwin and Escambia Counties in Alabama. Hurricane Ivan, a Cape Verde-type hurricane, hit Perdido Bay on the morning of 16 September in 2004 as a category 3 hurricane with sustained winds of 193 km/h and

a 4.3m storm surge, causing tremendous wind and water damage (National Weather Service, 2005). Hurricane Ivan ravaged the coastlines of Mississippi, Alabama, and Florida, producing waves over 15 m high offshore. By the time it completely dissipated nearly a week later, Ivan had claimed the lives of 57 people and caused more than $27 billion of damage (in 2017 dollars) (National Weather Service, 2005; Stewart, 2011).

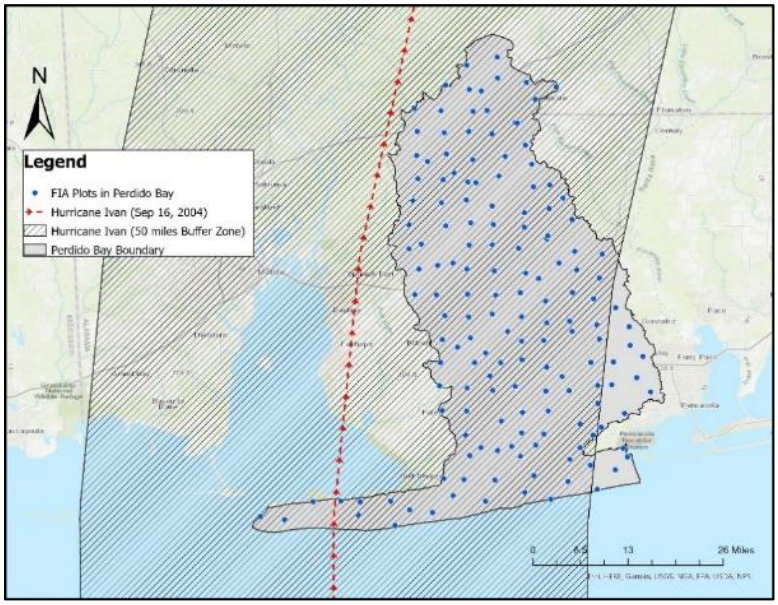

Figure 3.2: Blue dots represent FIA plots in the Perdido Bay watershed. The survey cycle of our research is 2001-2007.

Data Collection and Data Processing

We obtained the Forest Inventory Analysis (FIA) database for Florida and Alabama from the FIA DataMart website (https://apps.fs.usda.gov/fia/datamart/datamart.html), then selected plot data within our study area and processed these data following the steps outlined in Figure 3.3. To ensure accurate data integration into an SQL database, we referred to the user's guides for database description and population estimation. We utilized the "RSQLite" and "sqldf" packages in R programming software v3.0.1 to connect and manage the database (Appendix 2). We extracted data from three database tables, namely PLOT, COND, and TREE, for 2001 to 2020, as FIA started annualizing data from 1997 in the Gulf Coast states. We focused only on accessible forestland for our study, and the filtered data for these 20 years were exported to .csv files for further processing in ArcGIS Pro and geolocation cross-validation with our study area. Due to data integrity and landowner privacy concerns, FIA does not offer the exact geolocation in their database system,

but rather an approximate location. We shared our FIA plot locations with the USDA Southern Research Station scientists to validate the geolocation for our area of interest. Blue dots in Figure 3.2 show the FIA plots inside the Perdido Bay boundary, and Table 3.1 shows the 'county' and 'stand type' wise plot affected status before and after hurricane Ivan. Forest inventory plans are designed to meet sampling error standards for area, volume, growth, and removals provided in the Forest Service directive (FSH 4809.11) known as the Forest Survey Handbook. These standards, along with other guidelines, are aimed at obtaining comprehensive and comparable information on timber resources for all parts of the country. FIA inventories are commonly designed to meet the specified sampling errors at the State level at the 67% confidence limit (one standard error). We followed the FIA sampling errors for the southern region to estimate aboveground carbon across the Perdido Bay watershed.

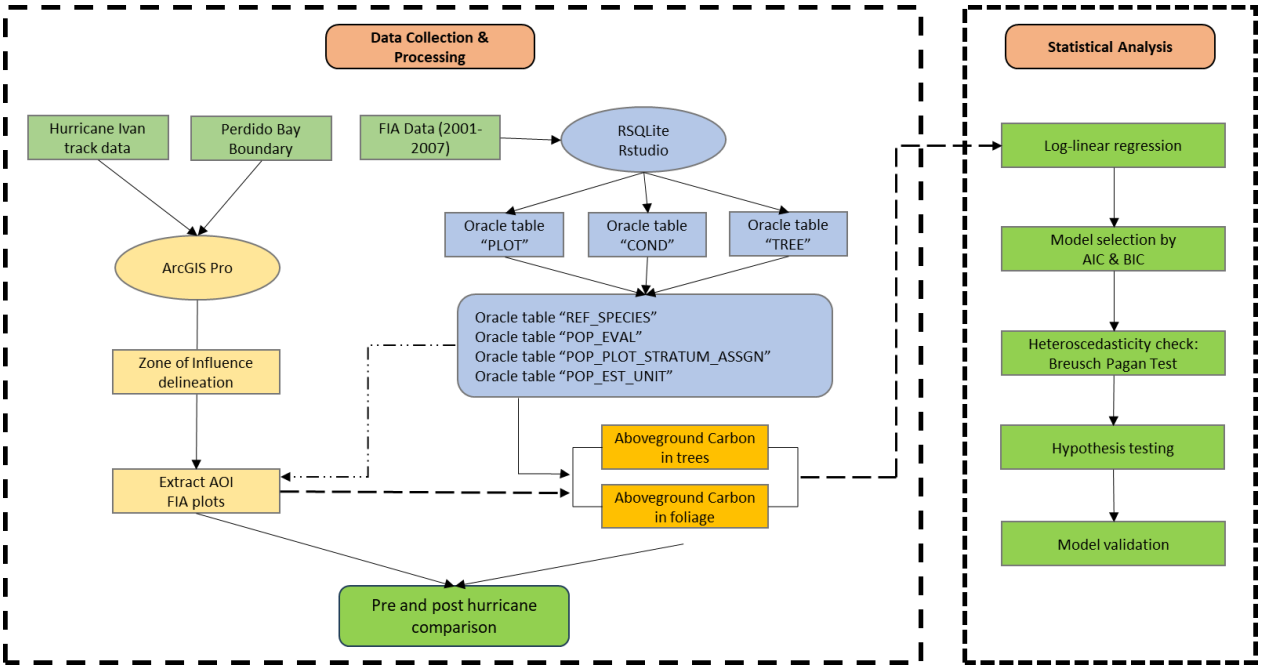

Figure 3.3: Process flow diagram of processing FIA data from SQL database to regression-friendly data format .csv files. The dotted line with the arrow shows the intermediate process in the flow diagram.

Table 3.1: Affected and non-affected plots with stand type in three different counties in the Perdido Bay watershed. Affected plots are marked with bold fonts in the table.

Year vs Stand Type	Plot Affected Status	Baldwin	Colbert	Escambia	Total
Hardwood		10	0	0	10
2001	No	2	0	0	2
2002	No	2	0	0	2
2003	No	3	0	0	3
2004	***Yes***	***1***	***0***	***0***	***1***
2007	No	2	0	0	2
Mixed		46	3	19	68
2001	No	5	1	0	6
2002	No	9	0	4	13
2003	No	5	0	4	9
2004	No	1	0	0	1
2004	***Yes***	***8***	***0***	***4***	***12***
2005	No	8	1	0	9
2006	No	6	1	5	12
2007	No	4	0	2	6
Softwood		18	1	2	21
2001	No	5	0	0	5
2002	No	3	0	0	3
2003	No	2	0	0	2
2004	***Yes***	***3***	***0***	***1***	***4***
2005	No	2	0	0	2
2006	No	0	1	0	1
2007	No	3	0	1	4

Aboveground carbon calculation for trees and foliage

To calculate carbon in foliage, we used the Jenkins equation Eq. (4) mentioned in (USFS, 2015) to estimate total aboveground carbon (metric tons/km^2) (includes stem wood (bole), stump, bark, top, limbs, and foliage). The diameter of each sampled plot was used to estimate the carbon. In FIA data processing, individual tree values are expanded to per acre values using the TPA_UNADJ variable, the value of which is a constant equal to 6.01 for trees with a diameter at breast height (d.b.h.) $\geq$ 12.7 cm (5 inches) or a constant equal to 74.96 for trees with d.b.h. $\leq$ 12.6 cm (4.9 inches) for plots that are not subdivided into differing conditions. In the case of subdivided plots, the TPA_UNADJ variable can vary according to the size of the condition in which the tree falls (USFS, 2018). Then, a population expansion factor is applied, which represents a stratum divided by the number of sampled plots in that stratum.

Aboveground Carbon in Trees = 0.5(exp(Jenkins_Total_B1 + Jenkins_Total_B2 * ln(Diameter*2.54)) * 2.2046)* (4)

In addition to PLOT, COND, and TREE table database, we extracted three more database tables; Reference Species ('REF_SPECIES'), Population Evaluation ('POP_EVAL') and Population Plot Stratum Assignment ('POP_PLOT_STRATUM_ASSGN') to calculate aboveground carbon using Eq. (5) mentioned in the FIA data user's guide (USFS, 2018, 2015). This formula excludes foliage of live trees with a diameter at breast height (d.b.h.) ≥1.0 inch, and dead trees with a d.b.h. ≥5.0 inches (USFS, 2015). Finally, we calculated the aboveground carbon (metric tons/km^2) by multiplying with the population expansion factor (USFS, 2018).

Aboveground Carbon in Trees without Foliage = 0.5(Drybio_Bole+Drybio_Stump + Drybio_Top + Drybio_Sapling + Drybio_Wdld_Spp)* (5)

Log-linear Regression

Log-linear regression model uses a logarithmic transformation of the input data before fitting it to a linear equation. This transformation helps to account for non-linear relationships in the data and results in a more accurate prediction of those relationships (Benedetti and Brown, 1978). In log-linear regression, the model is specified as:

$$Ln\ (Y) = \beta_0 + \beta_1 X_1 + \beta_2 X_2 + \ldots + \beta_p X_p + \varepsilon \quad (6)$$

where Y is the dependent variable, X_1, X_2, …, X_p are the independent variables, β_0 is the intercept, β_1, β_2, …, β_p are the coefficients or parameters that describe the relationship between the independent and dependent variables, and ε is the error term. We decomposed Eq. 6 to derivate our log-linear equation for aboveground carbon in Eq. 7.

$$Log\ (Aboveground\ Carbon\ in\ Trees/in\ Foliage) = \beta_0 + \beta_1 * Inventory\ Year + \beta_2 * County + \beta_3 * Height + \beta_4 * Diameter + \beta_5 * Stand\ Age + \beta_6 * Elevation + \beta_7 * Plot\ Affected\ Status + \beta_8 * Soil\ Physiographic\ Zone + \beta_9 * Stand\ Type + \varepsilon \quad (7)$$

Since the presence of heteroskedasticity makes the least-squares standard errors incorrect, we used "sandwich" package in Rstudio to adjust heteroskedasticity errors in our model (Zeileis, 2006, 2004; Zeileis et al., 2020). We used the most common robust type standard errors *vcovHC(type =*

"HC1") in our analysis. HC1 applies a degrees of freedom-based correction, (n−1)/(n− k), where n is the number of observations and k is the number of explanatory or predictor variables in the model (Rstudio, 2022). We used the *coeftest()* function to estimate heteroskedasticity-adjusted standard errors in our models.

Model Selection through ICs (Information Criterion) and Heteroscedasticity test

The information criterion, or ICs, are model selection routines that seek to balance the reduction in the sum of squared errors with the cost of adding additional parameters (Burnham and Anderson, 2004). We used AIC, the most common information criterion, to compare and select the best regression model (Fabozzi et al., 2014a; Rouder et al., 2016). Our model selection approach also considered BIC, a selection criterion based on information theory but set within a Bayesian context other than AIC (Benedetti and Brown, 1978; Claeskens and Jansen, 2015; Kingdom and Prins, 2016; Fabozzi et al., 2014b; Hurvich and Tsai, 1989; Yang, 2005). For our model selection, we devised four different models (Table 3.2). For model 1, we used year and county as fixed effects and the rest of the variables as variable effects. In model 2, we multiplied the average tree height and stand age to observe the effects of interaction between these two variables in the model. We considered the 'basal area' as a block variable in model 3 to oversee the character of multicollinearity with tree 'height' and 'diameter.' For model 4, we removed the variable 'height' from the model to see the effect of tree 'height' in our regression model comparison. We used the Breusch Pagan Test (BP Test) for the heteroscedasticity check in the selected model. BP test is used for heteroscedasticity in a linear regression model and assumes that the error terms are normally distributed. It tests whether the variance of the errors from regression is dependent on the values of the independent variables (Claeskens and Jansen, 2015; Halunga et al., 2017).

Table 3.2: Models used to identify the "best" in model selection step fitting best regression model for aboveground carbon.

Log-linear regression for AG Carbon in Trees	Model
log (Aboveground Carbon in Trees) ~ Year + Height + Diameter+ Plot Affected Status + Stand Age +Elevation + Soil Physiographic Zone + Stand Type	1
log (Aboveground Carbon in Trees) ~ Year + Diameter+ Plot Affected Status + Height * Stand Age +Elevation + Soil Physiographic Zone + Stand Type	2
log (Aboveground Carbon in Trees) ~ Year + Diameter+ Plot Affected Status + Height + Stand Age +Elevation + Soil Physiographic Zone + Stand Type + Basal Area	3
log (Aboveground Carbon in Trees) ~ Year + Diameter+ Plot Affected Status + Stand Age +Elevation + Soil Physiographic Zone + Stand Type	4
Log-linear regression for AG Carbon in Foliage	**Model**
log (Aboveground Carbon in Foliage) ~ Year + Height + Diameter+ Plot Affected Status + Stand Age +Elevation + Soil Physiographic Zone + Stand Type	1
log (Aboveground Carbon in Foliage) ~ Year + Diameter+ Plot Affected Status + Height + Stand Age +Elevation + Soil Physiographic Zone + Stand Type + Basal Area	2
log (Aboveground Carbon in Foliage) ~ Year + Diameter+ Plot Affected Status + Height * Stand Age +Elevation + Soil Physiographic Zone + Stand Type	3
log (Aboveground Carbon in Foliage) ~ Year + + Diameter+ Plot Affected Status + Stand Age +Elevation + Soil Physiographic Zone + Stand Type	4

3.3 Results

Aboveground carbon scenarios before and after Hurricane Ivan

We compared the average aboveground carbon in pre- and post-hurricane periods with different FIA data variables (stand type, stand size, physiographic class, height and stand age). About 94% of FIA plots were affected due to Hurricane Ivan in 2004. FIA plots in Baldwin and Escambia County were affected most, 70% and 29% plots, respectively. Escambia County in Alabama, located outside the hurricane influence zone (80 km), survived with most of the plots. Supplementary Figure S3.1 shows county-wise aboveground carbon distribution in trees (top, bole, stump, sapling) and in foliage before and after the hurricane. Our study found that the average aboveground carbon in trees in Baldwin County was about 8,794 metric tons/km^2 before the hurricane and decreased to 7,006 metric tons/km^2 after Hurricane Ivan. Aboveground carbon in foliage was observed with a decrease from 719 metric tons/km^2 to 565 metric tons/km^2 after the hurricane. Due to the unavailability of FIA data in Escambia (AL) County in 2002-2004 and 2007, it was difficult to estimate aboveground carbon change after the hurricane there. However, a sharp decrease was observed in our analysis, which inferred the possible impact of the hurricane on aboveground carbon. In Escambia (FL) county, aboveground carbon in trees decreased from 13,078 metric tons/km^2 to 6,564 metric tons/km^2 in the post-hurricane period. Correspondingly, aboveground carbon in foliage decreased from 475 metric tons/km^2 to 294 metric tons/km^2 in the

post-hurricane period. Overall, aboveground carbon decreased from 10,151 metric tons/km^2 to 8,145 metric tons/km^2 (Figure 3.4). Carbon in bole decreased markedly from 6,206 to 4,789 metric tons/km^2 in the post-hurricane period. Carbon decreased by about 116 metric tons/km^2 and 252 metric tons/km^2, respectively, in stump and foliage in the post-hurricane period.

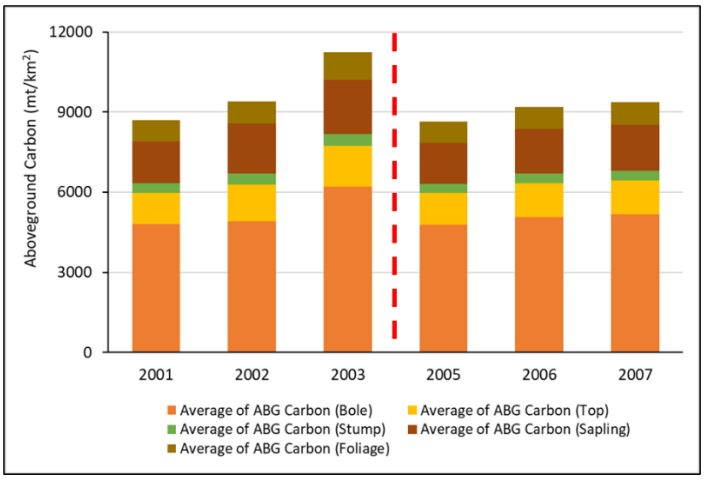

Figure 3.4: Change of aboveground carbon in bole, stump, top, sapling, and foliage (metric tons/km^2) before and after Hurricane Ivan. Red dotted line shows the intervention by Hurricane Ivan in 2004. ABG stands for aboveground carbon in the graph.

Figure 3.5 shows the aboveground carbon changes before and after Hurricane Ivan as per 'stand type' (hardwood, mixed, and softwood) and 'stand size' (large, medium, and small diameter). Plots with hardwoods were affected the most, as the carbon decreased from 13,796 to 4,051 metric tons/km^2. The carbon on mixed plots decreased from 10,141 to 8,358 metric tons/km^2. Plots with hardwood (Sweetgum, Nuttall oak, Willow oak) and mixed (hardwoods + softwoods) observed a carbon decrease (11.45% and 3.66%, respectively) after the hurricane. However, more carbon (8.34% increase) was observed in softwoods (loblolly pine, slash pine, sand pine, and longleaf pine) after the hurricane inventory in 2005. The carbon decrease rate in large and medium diameter trees was respectively 6.67% and 5.43% higher than small diameter trees due to the greater number of dead trees in the inventory year 2006. Foliage decreased in all stand size classes, however, as small-diameter trees increased from 545 to 1,242 metric tons/km^2 in the post-hurricane period.

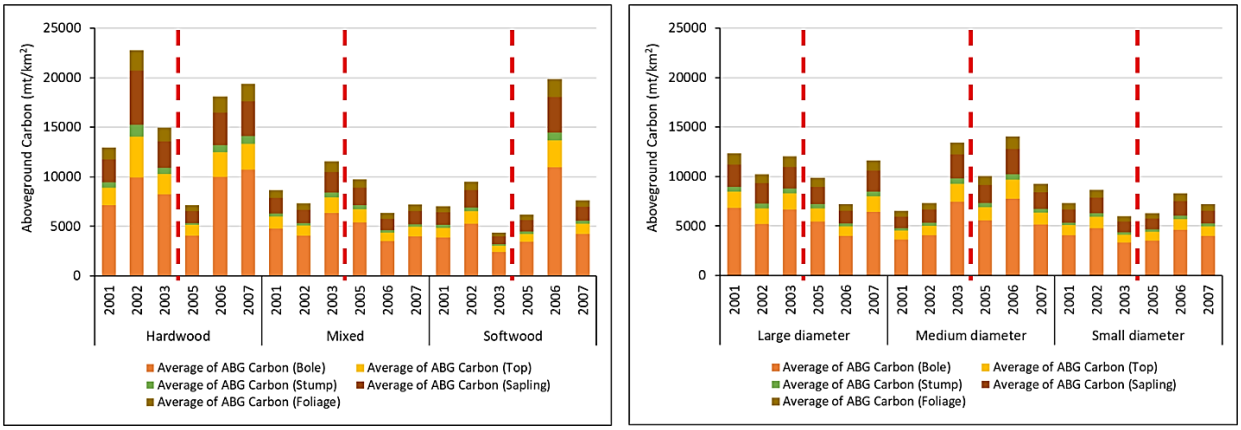

Figure 3.5: Change of aboveground carbon in bole, stump, top, sapling, and foliage (metric tons/km^2) before and after hurricane Ivan as per stand type and stand size. Red dotted line shows the intervention by Hurricane Ivan in 2004. ABG stands for aboveground carbon in the graph.

Figure 3.6 provides an illustration of how trees with different heights and stand ages were impacted by the hurricane. Plots containing relatively taller trees experienced significant carbon loss from the hurricane, primarily due to the higher carbon content in the 'bole', 'stump', 'top', and 'sapling', resulting in more carbon being stored in the 'foliage.' Among the relatively taller trees, those with heights ranging from 15 meters to 20 meters exhibited a sharp decrease in aboveground carbon from 16,665 metric tons/km^2 to 7,273 metric tons/km^2 after the hurricane. Specifically, the carbon in 'saplings' and 'bole' of taller and larger trees decreased by 73.34% (from 3,416 metric tons/km^2 to 960 metric tons/km^2) and 64.44% (from 10,320 metric tons/km^2 to 3,807 metric tons/km^2), respectively, compared to the pre-hurricane period. However, the carbon in 'foliage' increased from 1,269 metric tons/km^2 to 2,202 metric tons/km^2, indicating the regeneration of tree leaves and branches. Regarding stand age, plots with a stand age of less than 25 years were the most affected, experiencing a decrease in carbon from 12,691 metric tons/km^2 to 5,008 metric tons/km^2 after the hurricane. Similarly, plots with trees of middle age (26 years to 50 years) showed a similar trend, while relatively older trees (51 years to 75 years) gained more than 50% carbon after the hurricane. Our analysis found that carbon in the top of the trees increased from 2,518 metric tons/km^2 to 3,732 metric tons/km^2, and foliage carbon increased from 1,269 metric tons/km^2 to 2,094 metric tons/km^2 after the hurricane.

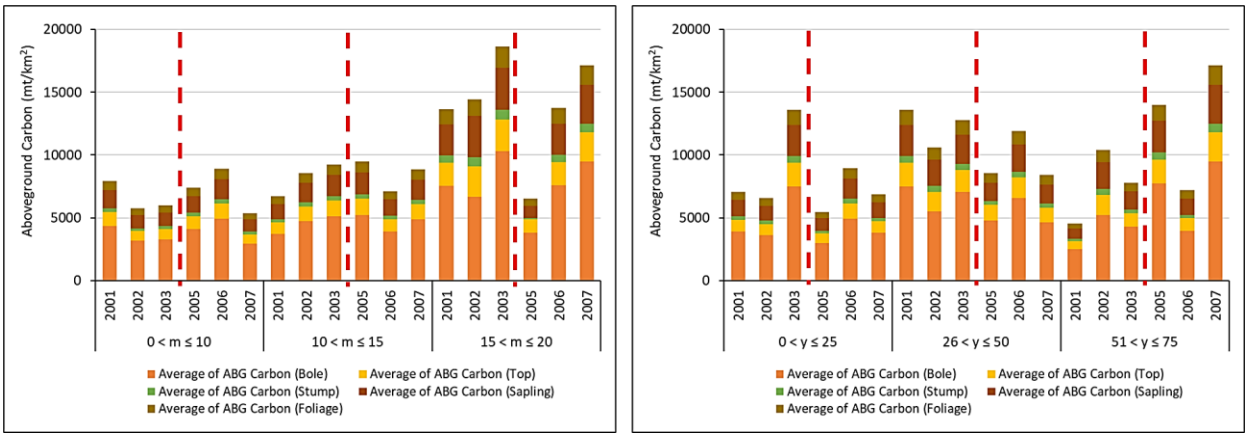

Figure 3.6: Change of aboveground carbon (metric tons/km^2) in trees and foliage related to height (in meters) and stand age (in years) of the sampled plots before and after Hurricane Ivan. Red dotted line shows the intervention by Hurricane Ivan in 2004

Figure 3.7 illustrates that carbon decreased after the hurricane regardless of the physiographic zone. Plots located in bays and wet pocosins, which are low, wet, and boggy sites characterized by peaty or organic soils, were the most affected. The carbon in the tree 'bole' and 'sapling' decreased by 46.42% and 46.17%, respectively, compared to the pre-hurricane period. Additionally, plots in deep sands, flatwoods, and bottomlands also experienced decreases in carbon, including carbon in 'foliage,' which decreased from 8,21 metric tons/km^2 to 5.72 metric tons/km^2, 6.46 metric tons/km^2 to 4.80 metric tons/km^2, and 9.69 metric tons/km^2 to 8.42 metric tons/km^2, respectively. On the other hand, plots in rolling uplands and small drains were less affected, as their carbon profiles remained relatively stable. However, there was a decrease of 2.96 metric tons/km^2 in 'sapling' carbon in small drains after the hurricane.

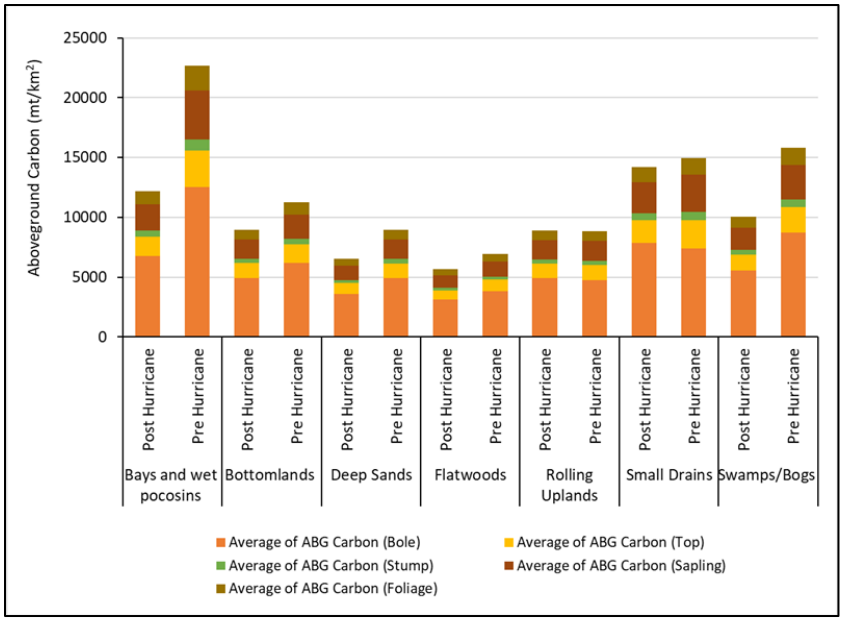

Figure 3.7: Distribution of aboveground carbon changes before (2001-2003) and after (2005-2007) Hurricane Ivan period considering physiographic classes available in the Gulf Coast

Regression diagnostics from model selection

Figure 3.8 presents log-linear regression models for estimating aboveground carbon in trees (bole, stump, top, and sapling) and foliage. The results indicate that, 'height', 'physiographic class', 'field age' and 'stand type' variables are statistically significant ($p \leq 0.05$) for estimating carbon in trees, while 'height', 'field age', 'stand size', and 'stand type' are statistically significant for estimating carbon in foliage. Our residual sum of squares (RSS) estimation identifies "Model 2" as the best for estimating carbon in trees in trees (Model 2_{RSS} = 25.45), and "Model 3" as the best for estimating carbon in foliage (Model 3_{RSS} = 18.547). Supplementary Table S3.1 illustrates the result of model selection. Our model selection criteria AIC and BIC, and the weight of the AIC and BIC show "Model 3" works better for estimating carbon in trees in trees and foliage only. We used biophysical variables (Height and Stand Age) to interact in the model (Model 3), and later dropped them from the model (Model 4) to see how our parameter estimate differentiated the model variability. As per the conditions of AIC and BIC; lower the better – AIC_t for model 3 is 5312.93 (AIC_{wt} = 66%) and BIC_t for model 3 is 5453.32 (BIC_{wt} = 71%), and AIC_f for model 3 is 9556.44 (AIC_{wf} = 58%) and BIC_f for model 3 is 9696.83 (BIC_{wt} = 66%).

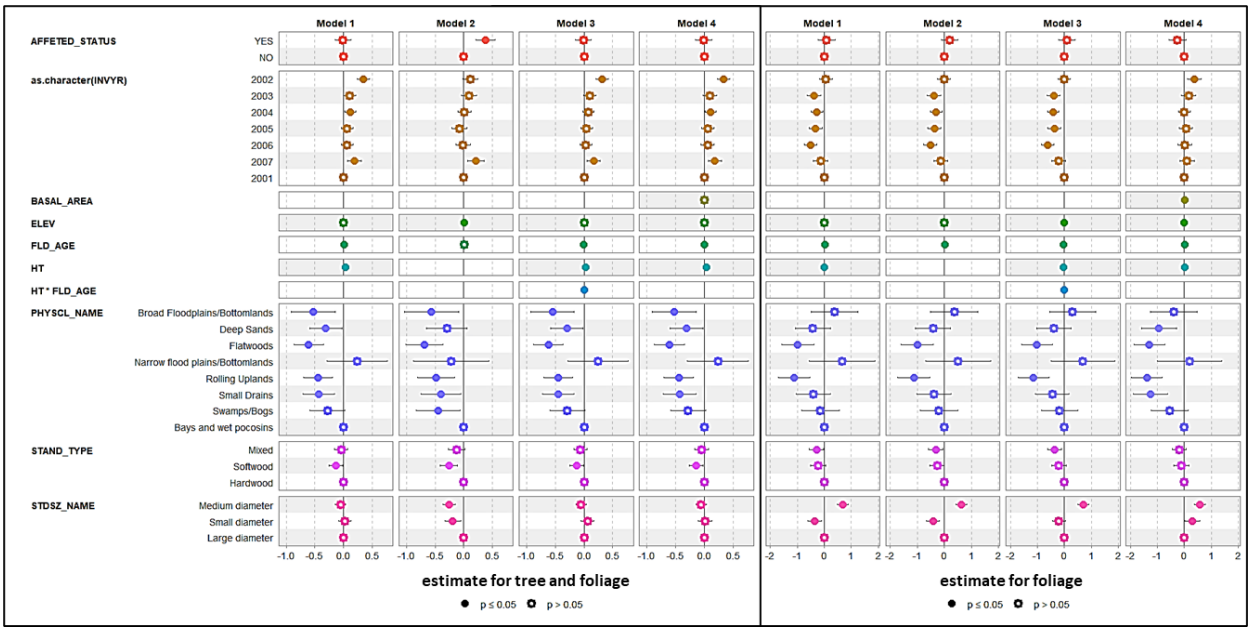

Figure 3.8: Log-linear model using different biophysical parameters and two fixed effects (inventory year "INVYR" and COUNTY); All models were performed with 95% CIs. The coefficient estimate on the left of "0" shows the negative change of the biophysical parameters and fixed effects in the model.

Table 3.3 shows the Breusch-Pagan (BP) heteroscedasticity test for model 3- aboveground carbon in trees and foliage only. Since both the p-values in the models are not less than $\alpha = .05$, we fail to reject the null hypothesis (H_0). Thus, we assume that homoscedasticity is present in our selected model. Regression diagnostics show no pattern in the residual plot of the model (Supplementary Figures S3.2 & S3.3). This suggests we can assume a linear relationship between the predictors and the outcome variables.

Table 3.3: Breusch-Pagan (BP) heteroscedasticity test for selected model

Selected Model	**BP test statistic**	**df**	**p-value**	**Status**
Model 3 – log (Aboveground Carbon with Foliage) ~ Year + Diameter+ Plot Affected Status + Height + Stand Age +Elevation + Soil Physiographic Zone + Tree Class + Basal Area	401.93	22	0.05 < 0.47	Homoscedastic
*Model 3 – log (Foliage) ~ Year + Diameter+ Plot Affected Status + Height * Stand Age +Elevation + Soil Physiographic Zone + Tree Class+ Affected Status + Stand Age +Elevation + Soil Physiographic Zone + Stand Type*	402.88	22	0.05 < 0.51	Homoscedastic

Figure 3.9 displays parameter estimates ($p \leq 0.05$) from our best model for quantifying aboveground carbon in trees and foliage. Our findings reveal a negative trend in aboveground carbon productivity following the 2005 hurricane event. Both fixed effects, 'inventory year' and 'affected status' of FIA plot showed variable impacts after the hurricane (Figure 3.8). Aboveground carbon in trees and foliage started decreasing after Hurricane Ivan, with a higher rate of decrease observed in 'foliage' compared to trees (Figure 3.9). More dead trees were reported in the 2005 annualized data, resulting in a 19% increase in the rate of carbon decrease compared to 2001. Plots dominated with 'Softwood' stand type exhibited 48.30% higher aboveground carbon compared to 'hardwood' stand type and 24.25% higher than 'mixed' stand type. Carbon in 'medium diameter' stands (≥ 5.0 inches d.b.h.) and 'small diameter' stands (< 5.0 inches d.b.h.) changed by 15.40% and 9.25 %, respectively, compared to trees with 'large diameter' (≥ 11.0 inches d.b.h. for 'hardwoods' and ≥ 9.0 inches d.b.h. for 'softwoods'). Aboveground carbon in 'foliage' was higher in plots with 'medium diameter' stands compared to 'large diameter' stands (Figure 3.10). Remarkably, aboveground carbon was higher in 'rolling uplands' (58.78%) and 'flatwoods' (63.25%) compared to 'bays and wet pocosins'. Interaction variable 'height * field age' shows a significant change in the foliage loss; about 65.06% increase of foliage loss was reported in the study period. The 'elevation' of plots, 'field age', and 'height' of trees in the affected plots showed small impacts (~0.01% - 2.20%) on the overall carbon profile in the model during the study period (2001-2007).

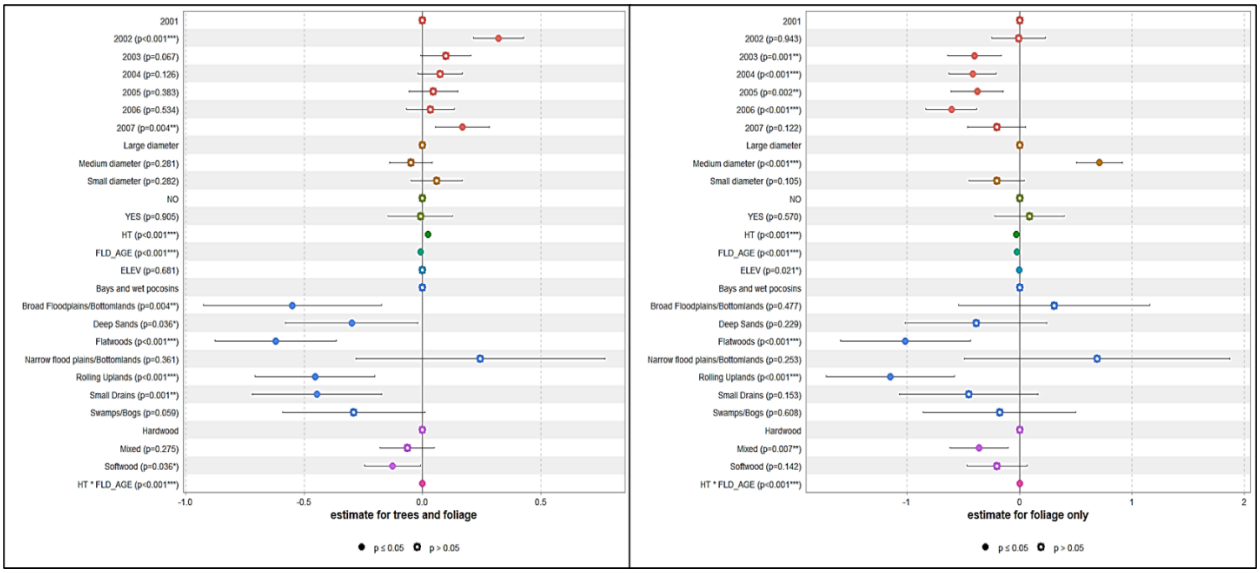

Figure 3.9: Coefficients of the log-linear regression model for aboveground carbon (metric tons/km^2) with and foliage. Error bars show the significant difference between plot samples and the variability of standard deviation around the mean value.

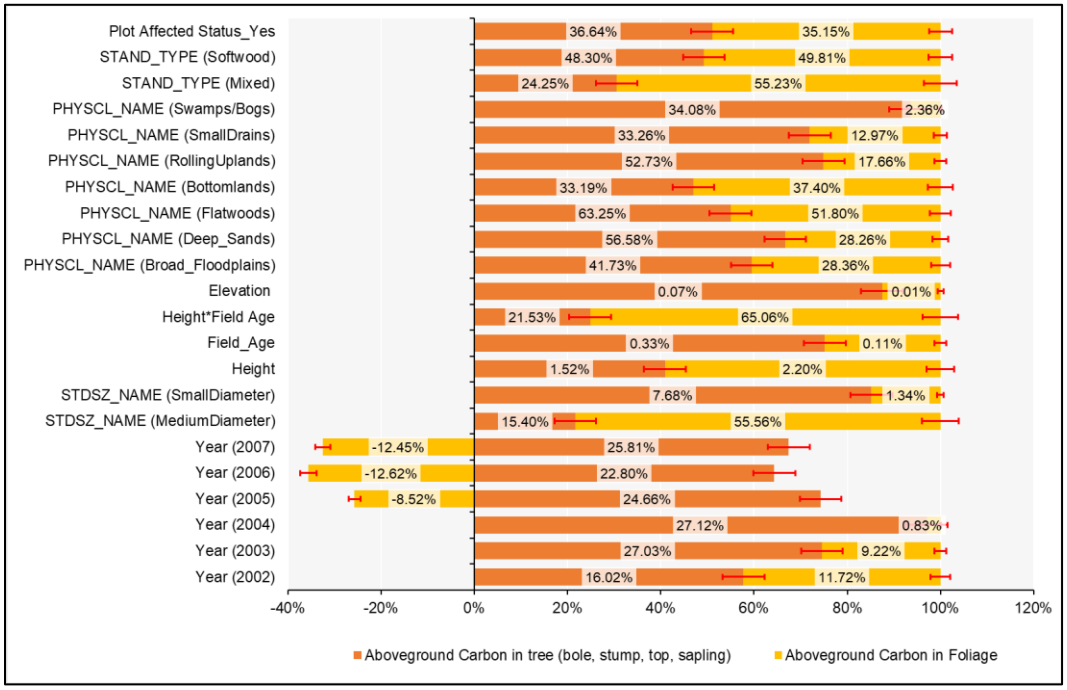

Figure 3.10: Estimates of relative changes in aboveground carbon (metric tons/km^2) in trees and foliage (metric tons/km^2) only compared to the year 2001. Error bars show the significant difference between plot samples and the variability of standard deviation around the mean value.

3.4 Discussion

Forest structure and hurricane effects on aboveground carbon

Pre-hurricane stand characteristics were important factors that determined the vulnerability of the trees to hurricane damage. Hurricane Ivan showed a disproportionate impact on large and small-diameter trees, as well as softwood-dominated stands. In the affected plots, the average aboveground carbon loss was estimated to be about 2,600 metric tons/km^2. Our results were consistent with previous research that found hurricanes caused the most damage to large-diameter stands in major forest types in the southeastern US (Ojha et al., 2020; Platt et al., 2000; Sharma et al., 2021; Zampieri et al., 2020). Chevalier et al. (2022a, 2022b) applied experimental forest management techniques by trimming the canopy to regenerate aboveground carbon but reported continued carbon loss in larger trees after severe Hurricane Maria. This suggests that even though management practices may aid in recovery, large trees still face challenges in retaining aboveground carbon after severe hurricane events.

Correspondingly, younger and smaller trees have a higher ratio of living sapwood to heartwood than older trees, which makes them elastic and flexible (USDA, 2021). Our results coincided with the findings (USDA, 2021), and the elasticity of the smaller softwoods stand out as potentially resistant to aboveground carbon loss in small-diameter trees. This resulted in about 1.24% more aboveground carbon decrease in large-diameter trees than the smaller trees. Stand age is an important factor that influences the amount of aboveground carbon in trees and foliage. As stands age, trees tend to grow taller and increase in diameter, leading to greater overall biomass and carbon storage. When large trees have attained their near maximum tree height, further growth is allocated to diameter increase, thus decreasing height-to-diameter ratios in very mature trees, and potentially making them relatively more windfirm (Sharma et al., 2021). Our findings aligned with the results from Valinger and Fridman (2011) and Xi et al. (2008), which show that taller, older trees lower the stability of stands due to a lower ratio of living sapwood and their increased vulnerability to windthrow.

Studies estimating aboveground carbon by physical characteristics of stands and a physiographic class of landform are very limited. Our study quantified the aboveground carbon in all physiographic classes available in Perdido Bay. Melson et al. (2011) estimated live tree carbon

stored in the Pacific Northwest region using the height and DBH of the trees, but they did not report the tree carbon distribution across different physiographic soil types. Castañeda-Moya et al. (2020) and Rivera-Monroy et al. (2019) quantified how Hurricane Irma influenced soil nutrient pools, vertical accretion, and plant phosphorus uptake after its passage across the Florida Coastal Everglades in September 2017. However, they focused more on soil nutrients than aboveground carbon in trees and foliage. Our study attempted to describe the distribution of aboveground carbon in rolling uplands, deep sands, swamps, bay and wet pocosins. Kuhn et al. (2021) estimated the volumetric change of biochemical properties (carbon, nitrogen, phosphorus, and sulfur) of soil in coastal wetlands after Hurricane Harvey in August 2017. They also reported the root biomass change both in marsh and mangrove stands, but their experimental plot was smaller compared to our study area. Their study did not quantify the aboveground carbon in marshlands. Our study created a scope of using physiographic classes to estimate aboveground carbon not only for overseeing a regional variance of carbon distribution across the stands but also for maintaining healthy vegetation after a major hurricane.

The carbon stored in the plant foliage is a crucial component of the carbon cycle and essential to ecosystem functioning. Foliage carbon is instrumental in photosynthesis, in which plants use sunlight and carbon dioxide from the atmosphere to produce sugars, cellulose, and other organic compounds. However, while several studies (Coulston et al., 2015; Hoover and Smith, 2023; Lu et al., 2015; Ryan et al., 1997) focus on changes in aboveground carbon in trees, including the bole, top, stump, and sapling, the carbon stored in foliage is often overlooked.

Log-linear regression on estimating aboveground carbon

Log-linear regression is commonly used for estimating aboveground carbon in forests, as biomass and carbon are closely related. Log-linear regression models have the capability of capturing the non-linear relationship between carbon and predictor variables (Auret and Aldrich, 2012), such as tree diameter and height. In particular, the log transformation of the response variable (aboveground carbon) and/or the predictor variables can help to stabilize the variance and make the relationship between the variables more linear (Ma et al., 2018). Using a log-linear regression model for estimating aboveground carbon also has several advantages. First, the log-linear regression model can account for the fact that the relationship between carbon and predictor

variables is often non-linear, with diminishing returns as trees get larger (Clerici et al., 2016; Trautenmüller et al., 2021). Second, the log transformation can help to reduce the impact of outliers and make the model more robust to deviations from normality in the data (von Eye and Mun, 2013). Third, the log-linear regression model can facilitate the estimation of confidence intervals (Heinze et al., 2018) and prediction intervals for carbon estimates, which can be useful for assessing the uncertainty associated with the estimates. In addition, log-linear regression models are often preferred over linear models because they can handle a wider range of carbon values, including very large values that can occur in forests with large trees or high biomass. Using a linear model for estimating carbon can result in biased estimates or poor prediction performance when there are large differences in carbon values across the data set (Ploton et al., 2020). Moreover, log-linear models are also preferred because they are often more parsimonious and have better statistical properties than non-linear models. This means that log-linear regression models can provide accurate estimates of aboveground carbon while using fewer parameters, which can improve model precision and reduce overfitting (Wang et al., 2023).

The general approach for modeling hurricane effects on aboveground carbon using log-linear regression is similar to that for estimating aboveground carbon but with the addition of hurricane-related predictor variables. In this case, the categorical predictor variables might represent forest types, physiographic classes, stand size, or other qualitative factors that may affect aboveground carbon stocks. Abdul-Hamid et al. (2022), Pati et al. (2022), and Peneva-Reed et al. (2021b) used allometric equations to estimate aboveground carbon for different tree species after natural intervention. However, allometric equations have some limitations, with limited geographic and size applicability, limited accuracy, and limited consideration of site-specific factors (Vorster et al., 2020). Allometric equations assume a linear relationship between tree size and carbon stocks, which may not hold true for all tree species or all stages of tree growth. This can result in underestimation or overestimation of biomass or carbon stocks (Köhl et al., 2017). Log-linear regression models can be more flexible than allometric equations because they can incorporate multiple predictor variables. This can help to account for the effects of these variables on aboveground carbon stocks, which may not be captured by simple allometric equations.

3.5 Conclusion

Forests are crucial for mitigating climate change by absorbing carbon from the atmosphere and storing it in biomass and soils. However, climate change can increase the frequency and intensity of extreme weather events such as hurricanes, which can have significant impacts on forest structure and aboveground carbon stocks. Hurricanes can cause defoliation, damage or loss of trees, and soil erosion, which can alter ecosystem structure and function, reduce carbon sequestration, and contribute to climate change. Moreover, changes in forest structure and function due to hurricanes can affect the water balance of forests, affecting the evapotranspiration rates and leading to changes in regional climate patterns. It is therefore important to understand the interaction between forest structure, hurricanes, and climate change to predict the impacts of these disturbances on carbon stocks and climate and to develop effective management strategies to reduce the vulnerability of forests to hurricanes and maximize their capacity to sequester carbon and mitigate climate change.

To assess the impact of natural disasters such as Hurricane Ivan on aboveground carbon in coastal forests, a log-linear regression modeling approach with categorical variables was adopted. This approach can estimate aboveground carbon in forests and identify the factors that influence carbon sequestration. Our study found that ‘stand type’, ‘height’, ‘physiographic class’, and hurricane ‘affected status’ of the FIA plots are statistically significant factors. The rate of aboveground carbon change in foliage is observed to be higher than that of trees, and foliage carbon is a major source of energy and nutrients for many organisms in ecosystems. Therefore, adding foliage carbon in the log-linear regression model provides another dimension to see the carbon dynamics after a major hurricane. We also found that the aboveground carbon decrease in ‘hardwood’ stand type is more significant than in ‘softwood’ stand type, varying by the predominant tree diameter of the stands.

Our study provides several conclusions that can be used as a basis for resistance, resilience, and adaptation of southern US coastal forests and of forests in other locations to the increased incidents of hurricanes and climate change. Forest management will benefit from an improved understanding of the mechanisms behind the resistance and resilience of forest stands and species to catastrophic wind. Our study also provides a framework for researchers and policymakers to

assess the vulnerability of coastal forests and facilitate strategic planning to protect forests as carbon sinks. Future studies should include water level and storm surge information in the affected areas to examine how flooding and salinity affect coastal forests and marsh migration into inland areas. Modeling studies should evaluate the impacts of future storm surges, salinity, and land use changes on coastal forests to inform forest management. Since our current study did not explore the accounting of carbon growth due to replantation of softwood species, this could bring new avenues in sustainable forest management practices.

Supplementary Tables

Table S3.1: Log-linear model selection considering Akaike Information Criterion (AIC) and Bayesian Information Criterion (BIC).

Log-linear regression for AG Carbon with Foliage	**AICc**	**AICw**	**BIC**	**BICw**
M1 – log (Aboveground Carbon with Foliage) ~ Year + Height + Diameter+ Plot Affected Status + Stand Age +Elevation + Soil Physiographic Zone + Tree Class	5360.24	0.15	5494.79	0.11
*M2 – log (Aboveground Carbon with Foliage) ~ Year + Diameter+ Plot Affected Status + Height * Stand Age +Elevation + Soil Physiographic Zone + Tree Class*	6497.54	0.16	6626.26	0.12
M3 – log (Aboveground Carbon with Foliage) ~ Year + Diameter+ Plot Affected Status + Height + Stand Age +Elevation + Soil Physiographic Zone + Tree Class + Basal Area	**5312.93**	**0.66**	**5453.32**	**0.71**
M4 – log (Aboveground Carbon with Foliage) ~ Year + Diameter+ Plot Affected Status + Stand Age +Elevation + Soil Physiographic Zone + Tree Class	5362.26	0.01	5502.64	0.02
Log-linear regression for AG Carbon in Foliage Only	**AICc**	**AICw**	**BIC**	**BICw**
M1 – log (Foliage) ~ Year + Height + Diameter+ Plot Affected Status + Stand Age +Elevation + Soil Physiographic Zone + Tree Class	9680.34	0.17	9814.89	0.12
M2 – log (Foliage) ~ Year + Diameter+ Plot Affected Status + Height + Stand Age +Elevation + Soil Physiographic Zone + Tree Class + Basal Area	9704.40	0.22	9833.12	0.16
M3 – log (Foliage) ~ Year + Diameter+ Plot Affected Status + Height * Stand Age +Elevation + Soil Physiographic Zone + Tree Class	**9556.44**	**0.58**	**9696.83**	**0.66**
M4 – log (Foliage) ~ Year + Diameter+ Plot Affected Status + Stand Age +Elevation + Soil Physiographic Zone + Tree Class	9583.19	0.03	9723.58	0.05

*** t stands model for carbon in trees with foliage and f stands model for carbon in foliage only. wt and wf stands for weightage of the model for trees and foliage in the selection*

Supplementary Figures

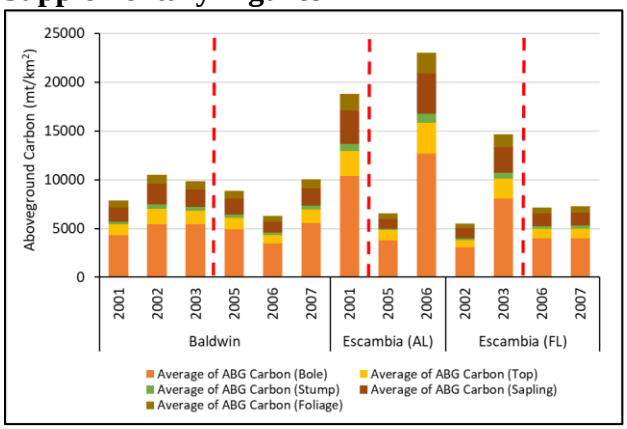

Figure S3.1: Distribution of aboveground carbon changes before (2001-2003) and after (2005-2007) hurricane Ivan period in Baldwin and Escambia (AL, FL) counties. Due to geographic location of the watershed boundary and county area size, some inventory years plot data were not available.

Regression Diagnostics for predicting aboveground carbon in trees

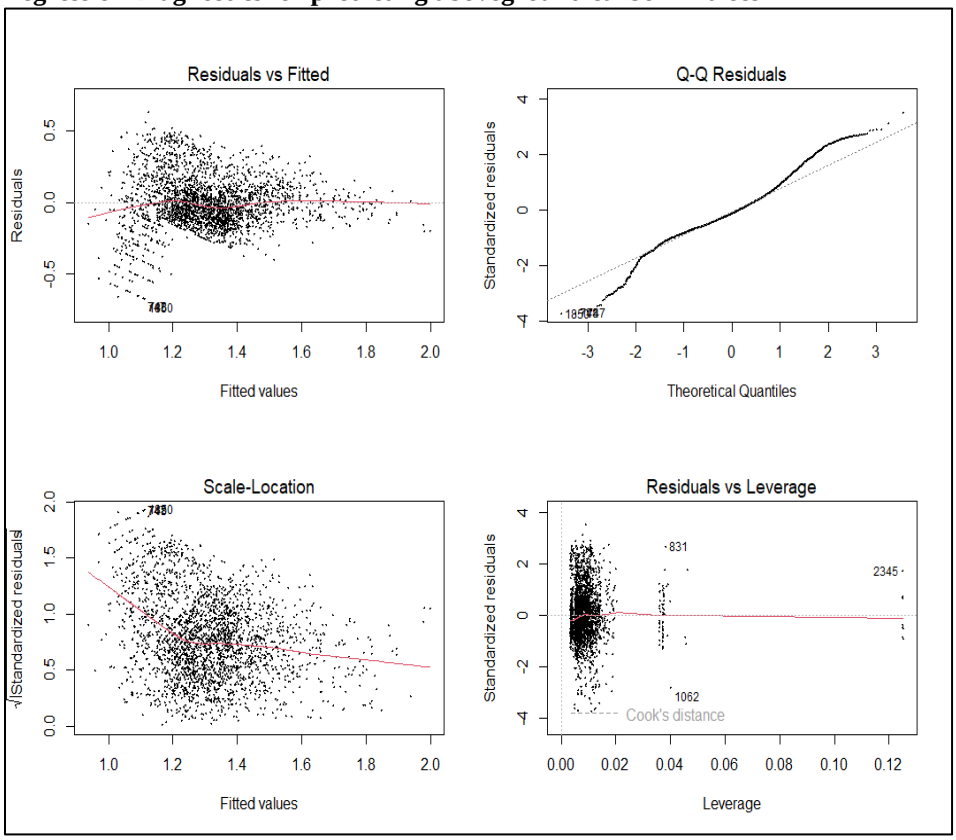

Figure S3.2: 1) Residuals vs Fitted - Used to check the linear relationship assumptions. A horizontal line, without distinct patterns is an indication for a linear relationship, what is good, 2) Normal Q-Q. Used to examine whether the residuals are normally distributed. It's good if residuals points follow the straight dashed line, 3) Scale-Location (or Spread-Location). Used to check the homogeneity of variance of the residuals (homoscedasticity). Horizontal line with equally spread points is a good indication of

homoscedasticity. 4) Residuals vs Leverage. Used to identify influential cases, that is extreme values that might influence the regression results when included or excluded from the analysis.

Regression diagnostics for predicting aboveground carbon in foliage

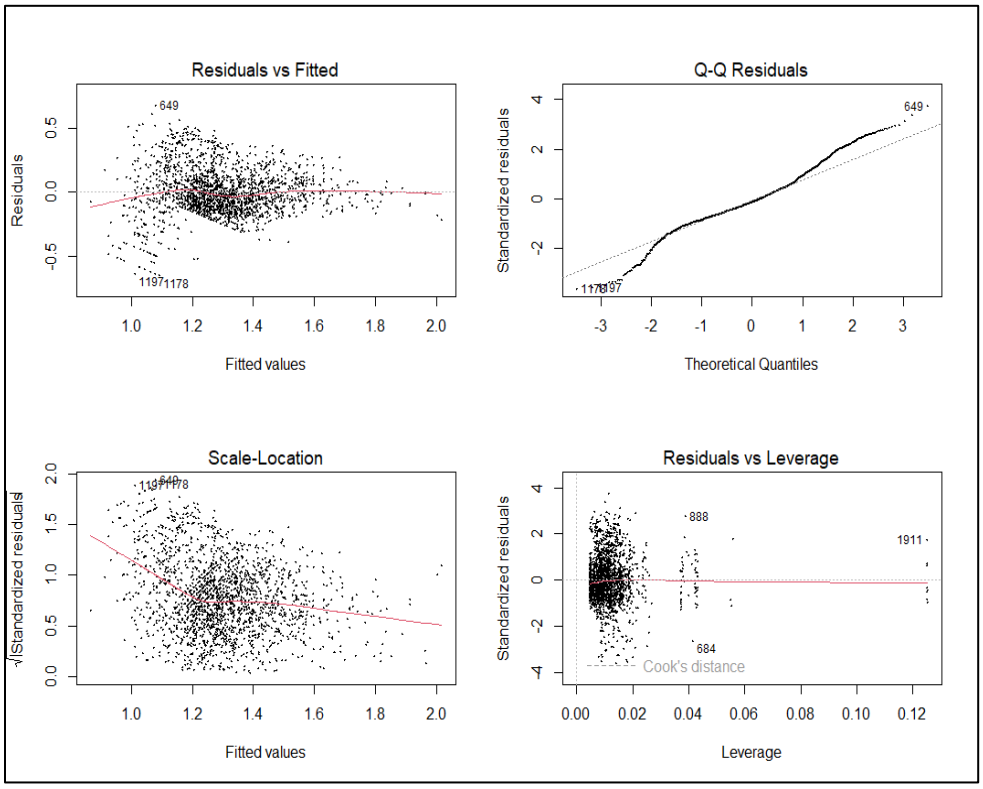

Figure S3.3: 1) Residuals vs Fitted - Used to check the linear relationship assumptions. A horizontal line, without distinct patterns is an indication for a linear relationship, what is good, 2) Normal Q-Q. Used to examine whether the residuals are normally distributed. It's good if residuals points follow the straight dashed line, 3) Scale-Location (or Spread-Location). Used to check the homogeneity of variance of the residuals (homoscedasticity). Horizontal line with equally spread points is a good indication of homoscedasticity. 4) Residuals vs Leverage. Used to identify influential cases, that is extreme values that might influence the regression results when included or excluded from the analysis.

CHAPTER 4

IS HURRICANE-INDUCED URBAN AND FOREST LAND CHANGE DRIVING CARBON DYNAMICS IN THE GULF OF MEXICO? A COMPREHENSIVE LAND USE SCENARIO ANALYSIS ON THE PERDIDO WATERSHED*

*Alam A., Dwivedi P. To be submitted to [Jounral of Land Use Policy]

Abstract

The urbanization rate in the Gulf of Mexico region has been steadily rising by 2.55% since 2001, even as the frequency of hurricane landfalls has increased. The combined impact of this growing urbanization and the more frequent hurricanes affects land use and associated carbon dynamics. No prior research has examined this combined impact of urbanization growth and increasing hurricane occurrences on land use and carbon dynamics at the watershed level. Our research objectives are to predict anticipated changes in land use resulting from urbanization growth and the expected responses of landowners to more frequent hurricanes. We also aim to assess how these projected land use changes impact carbon dynamics at the watershed level. We utilized a Multi-Layer Perceptron-Cellular Automata (MLP-CA) model for land use forecasting and the Integrated Valuation of Ecosystem Services and Tradeoffs (InVEST) model to quantify carbon storage in the Perdido watershed, situated in the Panhandle of Florida. We ran the MLP-CA model with six land use scenarios: LUR+CFR, LUR+FR25%, LUR+FR50%, HUR+CFR, HUR+FR25%, and HUR+FR50%. LUR and HUR indicate low and high urbanization rates. CFR indicates current forestlands at the present rate of hurricane risks. FR25% and FR50% indicate changes in forestlands relative to increased tropical storm and hurricane rates (25% and 50%) from 2000-2020 levels. In comparison to 2021, the urban land area within these scenarios ranged from 5.28% to 6.12%, while the forestland area spanned from 40.30% to 48.71%. Nevertheless, forestland conservation in the LUR+FR50% and HUR+FR50% scenarios displayed only minor disparities compared to LUR+FR25% and HUR+FR25%, respectively. Cropland and Pasture are set to diminish by 1.87% to 0.85% in FR25% and FR50% scenarios. Our InVEST model discerns an increase in carbon storage within forestland, shrubs, cropland, and pasture. As hurricane frequencies increase from 25% to 50%, overall carbon storage in forestlands ranges from 447.52 thousand metric tons to 604.95 thousand metric tons under a low urbanization rate and from 442.43 thousand metric tons to 591.49 thousand metric tons under the high urbanization rate. Carbon loss in Shrub ranges from 3.88 thousand metric tons to 6.89 thousand metric tons. Cropland and pasture will lose about 3.61 thousand metric tons to 7.35 thousand metric tons of carbon with a 50% increase in hurricanes. Our research insights equip relevant stakeholder groups with valuable

information on decision-making processes and facilitate sustainable land use and conservation efforts.

4.1 Introduction

The Intergovernmental Panel on Climate Change (IPCC) climate change 2023 synthesis report states that human activities are the primary cause of global warming, leading to an increase in global surface temperature of 1.1°C above the pre-industrial period (1850-1900) between 2011 and 2020 (IPCC, 2023b). Human-induced climate change already affects numerous extreme weather events and climate patterns worldwide (IPCC, 2015). As a result, there have been widespread negative consequences and associated losses and damages to the environment and human populations (Jehn et al., 2022; Kemp et al., 2022).

Due to global warming, tropical storms and hurricane activity in the Atlantic Ocean, the Caribbean, and the US Gulf of Mexico has increased since 2000 (NASA, 2022; US EPA, 2022). About 6 to 7 hurricanes have formed in the North Atlantic every year since 1878, and roughly 2 per year land on the US coast (NOAA, 2021). According to the total annual ACE (Accumulated Cyclone Energy) Index, hurricane intensity has risen noticeably over the past 20 years (Figure 1a), and eight of the ten most active years since 1950 have occurred since the mid-1990s (US EPA, 2022). The approximate cost of damages from tropical cyclones and hurricanes on the Gulf Coast from 1980 to 2020 has been about $790 billion (NCEI, 2022; NOAA, 2021). Since 2001, this cumulative damage has cost more than $550 billion than in previous decades. The US Global Change Research Program and the IPCC project that tropical cyclones and hurricanes in the Atlantic and Gulf Coast will become more intense over the 21st century, with higher wind speeds, heavier rains, and billion-dollar damages (IPCC, 2014; U.S. Global Change Research Program, 2018). In addition to the economic loss, hurricanes take several lives every year. Hurricanes have claimed about 2,907 lives since 2001, and the devastating Hurricane Katrina alone in 2005 left more than 2,000 people dead along the Gulf Coast (Figure 4.1).

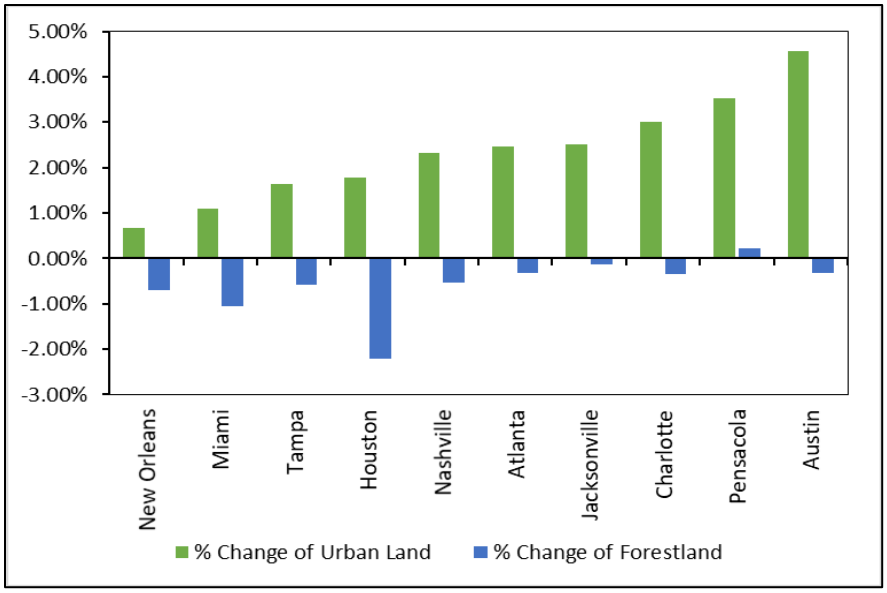

Figure 4.1: Yearly percentage change of urban land and forestland from 2001 to 2021 in the major cities of Gulf Coast and southern states. This percentage change calculated from NLCD 2001 to NLCD 2021 (MRLC, 2023, 2017).

Urban land cover represents a relatively small amount of the total land cover at approximately 5% coverage of the Gulf of Mexico region (NOAA, 2022c). Despite experiencing catastrophic hurricanes every year, urban land in the Gulf Coast and southern states is increasing. From New Orleans to Austin, urban expansion ranges from 0.66% to 4.57% every year since 2001 (MRLC, 2023). While this urban expansion is significant across the region, this increase in development occurred at a much higher pace in some geographic regions. Areas of change were most common between Houston, Texas, and Orlando, Florida, and were somewhat more prevalent in the counties not immediately along the coast. According to the 2017 Ecosystem Status Report update for the Gulf of Mexico, the Gulf Coast experienced a more than 15% urban land use increase, including open space in the urban areas (Karnauskas et al., 2017; NOAA, 2017a). From 1996 to 2010, the amount of developed area increased in the Gulf of Mexico by 3,979 km^2, which represents a 17% rate of growth. New development across the Gulf of Mexico during the 14-year time came from lands previously categorized as agriculture (31%), upland forest (25%), wetlands (17%), shrub (14%), and grass (9%). An additional 3% came from barren land and water features (NOAA, 2017a). Development intensity increased on 455 km^2 of already developed land; this type of change is commonly associated with increasing density of housing or infill development within city limits (NOAA, 2017b).

Concurrently, forestland decreased in cities and surrounding watersheds by 0.23% to 2.21% every year since 2001. The Gulf of Mexico Regional Land Cover Change Report (1996-2010) estimated about 34,252 km^2 of forestland changed to other land cover types. About 22,548 km^2 of forestland were lost from 1996 to 2010 (Homer et al., 2020; Mendoza-González et al., 2012; NOAA, 2017a). Most of the forestland losses in the land cover consisted of changes from forest to grassland and shrub. Approximately 1,512 km^2 of forest were lost to development/urban land during the study period, accounting for 4% of the net losses. Of these losses, 1,028 km^2 were upland forests, and 484 km^2 were wetland forests (NOAA, 2017a, 2017b). In addition, about 2,580 km^2 of wetlands decreased from 1996 to 2010, and were primarily lost to water (48%) (NOAA, 2010).

Hurricanes, coupled with induced land use change, may impact total atmospheric and terrestrial carbon storage capabilities (Jones et al., 2017; McNulty, 2002). By using the Dynamic Land Ecosystem Model (DLEM) in combination with spatially explicit, long-term historical data series on multiple environmental factors, Tian et al. (2012) examined the century-scale responses of ecosystem carbon storage and flux to multiple environmental changes (i.e., land use, climate, nitrogen disposition, atmospheric CO_2, etc.) in the Gulf Coast. During the study period 1895-2007, the Gulf Coast ecosystem experienced a net carbon sink of 0.80 ± 0.38 Pg through an increase in vegetation carbon pool (Tian et al., 2012). Piao et al. (2018) estimated net land carbon sink and its driving factors using atmospheric inversions and terrestrial carbon models across seven continents. The linear trend of net land carbon sink was about 0.13 ± 0.05 Pg C yr^{-1} during 1998–2012, which was three times larger than during 1980–1998 (0.04 ± 0.05 Pg C yr^{-1}). This included the land use emissions during the slow warming process in the atmosphere. Delphin et al. (2013) used land cover maps, FIA (Forest Inventory and Analysis) data, and the InVEST (Integrated Valuation of Ecosystem Services and Tradeoffs) model to determine potential damage to subtropical forests from hurricanes in the Lower Suwannee River (LS) and Pensacola Bay (PB) watersheds in Florida, US. They divided the study area into two risk zones: high and low. Results showed that 31% and 0.5% of the total aboveground carbon storage in the LS and PB, respectively, was in high forest damage risk (HR) zones.

Land use change is the most dynamic driving factor of terrestrial carbon stock change, yet this dynamic is not well understood associated with hurricane impact (Arneth et al., 2017; Fahey et al.,

2010; Philpott et al., 2008; Schulp et al., 2008; Zaehle et al., 2007). In this context, the objectives of this study are twofold: (1) to predict land use changes in 2050, taking into account hurricane frequency, and (2) to monitor carbon dynamics in conservation easements. To achieve these objectives, we have developed a land use projection model for the year 2050, which we have integrated with the InVEST (Integrated Valuation of Ecosystem Services and Tradeoffs) Carbon Storage and Sequestration model. This combined approach allows us not only to forecast future land use changes but also to evaluate the corresponding shifts in carbon storage expected by 2050. The outcomes of this research hold significant relevance for various stakeholder groups, including policymakers, urban planners, conservationists, and landowners. By providing insights into the anticipated evolution of ecosystem services in the Gulf Coast region, our study furnishes these stakeholders with valuable information that can inform decision-making processes. Moreover, it facilitates the implementation of sustainable land use and conservation strategies, thereby contributing to the responsible management of the area's natural resources and environmental assets.

4.2 Methods

Study Area

Perdido Bay watershed is located on the Alabama-Florida border (Figure 4.2), a small estuarine system fed by freshwater from the Perdido River, which is designated an Outstanding Florida Water. Besides Perdido Bay, the system includes Tarkiln Bay, Arnica Bay, Bay La Launch and Bayou St. John. The bays are separated from the Gulf of Mexico by Perdido Key, and water exchange takes place through Perdido Pass. The system is bounded by two barrier islands, Perdido Key and Santa Rosa Island. The bay system is characterized by saltwater sounds and marshes. Species dominant in the region include fishes and birds, several of which are rare and/or endangered. As of NLCD 2021, forestland (39.46%) and wetland (22.46%) are the dominant land use in the Perdido watershed, total encompassing about 2570 km^2. About 10% of the total land area is developed and Cropland and pasture account for 16.72% of the entire watershed area.

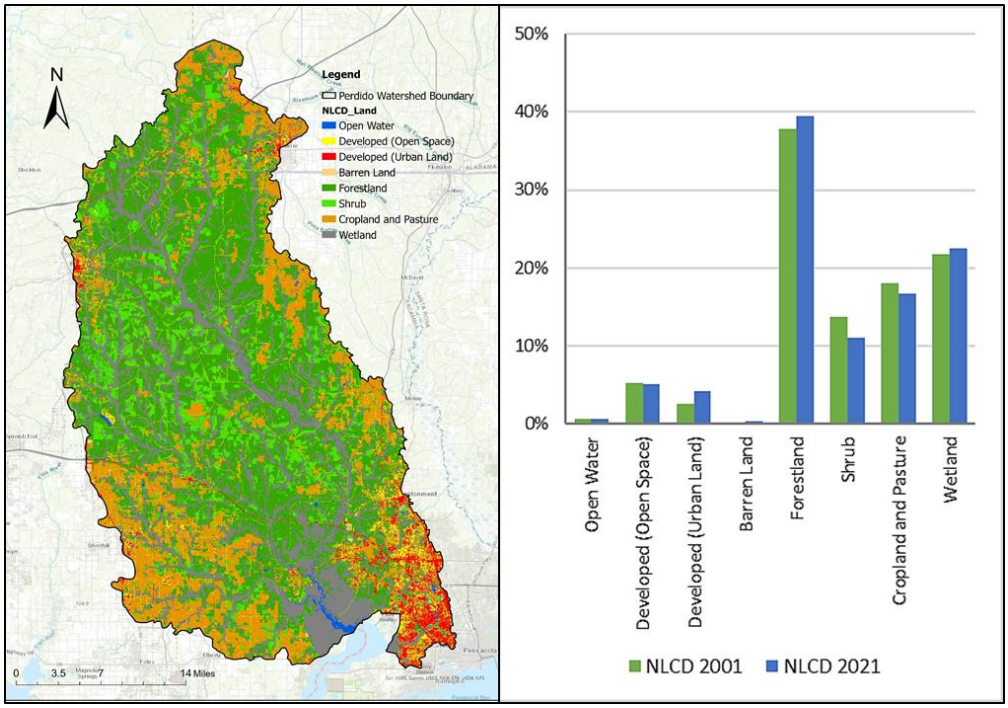

Figure 4.2: Location of Perdido watershed (Alabama and Florida)

National Land Cover Database (NLCD)

We used the National Land Cover Database (NLCD) for the Perdido watershed. Table 4.1 shows the relevant dataset used in our analysis, and Figure 4.3 shows the methodological flowchart of our analysis. The National Land Cover Database (NLCD) provides nationwide data on land cover and land cover change at a 30m resolution with a 16-class legend based on a modified Anderson Level II classification system (MRLC, 2017). In our analysis, we used NLCD 2001 and newly released NLCD 2021 data, which represents the latest evolution of NLCD land cover products focused on providing innovative land cover and land cover change data for the United States. We reclassified 16 land use classes into eight major land use classes – developed (low intensity), developed (medium intensity), and developed (high intensity) to developed (urban land); deciduous forest, evergreen forest, and mixed forest to forestland; shrub, grassland and herbaceous to shrub; hay, pasture and cultivated crops to cropland and pasture; woody wetlands and emergent herbaceous wetlands to wetland.

Table 4.1: Spatial and Survey data sources used for land use and carbon storage estimation

Data Layer Name	Format	Unit	Source
National Land Cover Dataset (NLCD)	.tif	Meter	U.S. Geological Survey
Perdido Watershed	.shp	km^2	Natural Resources Conservation Service
Roads and Rails	.shp	Meter	Department of Transport
Digital Elevation Model (DEM)	.tif	Meter	U.S. Geological Survey
US Protected Areas Database	.shp	km^2	U.S. Geological Survey
Forest Landowners Survey	.xlsx	km^2	Personal Communication
Aboveground Carbon	.tif	metric tons/km^2	Oak Ridge National Laboratory
Belowground Carbon	.tif	metric tons/km^2	Oak Ridge National Laboratory
Soil organic Carbon	.tif	metric tons/km^2	Natural Resources Conservation Service
Dead organic Carbon	.tif	metric tons/km^2	Natural Resources Conservation Service

Multi-layer Perceptron (MLP) and Markov Model

We used the Artificial Neural Network (ANN) based Multi-layer Perceptron (MLP) technique to identify the land use transitions from one class to another in NLCD 2001 and NLCD 2021. Artificial Neural Network (ANN) is a technique or approach to information processing inspired by the workings of the biological nervous system, especially on human brain cells, in processing information (Lee et al., 1990; Tian et al., 2021). Multilayer Neural Network, better known as Multilayer Perceptron (MLP), is a neural network consisting of the input layer, hidden layer, and output layer network (Joshi, 2023; Taud and Mas, 2018a). In this analysis ANN based MLP works in four different stages - (1) determining input and network architecture, (2) creating a network using a portion of pixels from the input, (3) testing the network using all pixels from inputs, and (4) uses information that has been generated by the network to predict future land use changes (Geidarov, 2017; Subiyanto et al., 2021; Taud and Mas, 2018b). At first, we defined the original transition probability matrices of land use classes using Equation 1. A transition probability matrix is a square matrix that shows the probability of transitioning between states in a Markov chain. Each entry in the matrix is a non-negative real number representing a probability.

The matrix is non-negative and has unit row sums.

$$P = \begin{bmatrix} p_{11} & p_{12} & \cdots & p_{1n} \\ p_{21} & p_{22} & \cdots & p_{2n} \\ & \cdots & \cdots & \\ p_{n1} & p_{n2} & \cdots & p_{nn} \end{bmatrix} \quad (1)$$

In the above matrix, P_{ij} is the transformation probability of the *i*th type land into the *j*th type land from prophase (2001) to telophase (2021); *n* is the land use type of studied area Perdido. P_{ij} should meet the following conditions, i.e., $0 \leq P_{ij} \leq 1(i, j = 1, 2, 3, ..., n)$ and $\sum_{i=1}^{n} Pij = 1(i, j = 1, 2, 3, ..., n)$.

For training and validation, MLP requires examples of pixels that went through each of the transitions being modeled between the two dates of land cover information – NLCD 2001 and NLCD 2021 in our case. It also needs examples of all persistence classes – pixels eligible to go through one of the transitions being modeled but did not. In this analysis, we used seven transition sub-models, developed (Open Space) to developed (Urban Land), barren land to forestland, forestland to shrub, forestland to cropland and pasture, shrub to forestland, cropland and pasture to forestland and wetland to open water. These sub-models were subjected to our historical land use change analysis. MLP indicated the number of pixels that went through the smallest transition being modeled as well as the minimum number that persisted in these 7 sub-models. MLP used half of the specified sample for training and half for testing.

From the outputs of the MLP, we used the transition maps in our Markov model to predict the future land use in the Perdido Bay watershed. The Markov process is a special random movement from one state to another state at each time step. A first-order Markov model is the model of a system in which probability distribution over the next state is assumed to depend only on the current state but not on previous ones (non-aftereffect) (Guan et al., 2011; Rai et al., 2017; Rimal et al., 2018). According to non-after effect of the Markov process and probability formulae of the Bayes condition, the forecast model of Markov is obtained using Equation 2.

$$P_{(n)} = P_{(n-1)}P_{ij} \quad (2)$$

where $P_{(n)}$ is the state probability of any time and $P_{(n-1)}$ is the preliminary state probability.

Land Use Scenario Projection for 2050

We ran our Markov model for six different scenarios: LUR+CFR, LUR+FR25%, LUR+FR50%, HUR+CFR, HUR+FR25%, and HUR+FR50%. For our analysis, we compared the NLCD 2001 and NLCD 2021 developed (urban land) area to estimate the per-year growth up to 2050. To comply with the current and future trends of the urban growth, we observed ten fast-growing urban areas in the Gulf Coast and Southeast – New Orleans, LA (0.66%), Miami, FL (1.10%), Tampa, FL (1.63%), Houston, TX (1.79%), Nashville, TN (2.33%), Atlanta, GA (2.45%), Jacksonville, FL (2.50%), Charlotte, NC (3.01%), Pensacola, FL (3.53%) and Austin, TX (4.50%) (MRLC, 2023). In this research, we used Jacksonville, FL (2.5%) for the LUR and Austin, TX (4.5%) for the HUR compared to the current growth rate in Perdido (2.67%). All the growth rates are accounted for with historical land use change and catastrophic hurricane effects from 2001 to 2021.

We conducted a forest landowners survey (Auburn University) in the 12 different countries in the Gulf Coast to see how they use their forestland in different purposes and how they want to use their forestland in the future (Supplementary Table S4.1) if the owned forestlands hit by a catastrophic hurricane. Depending upon the responses, we used three different scenarios for future forestland change - (1) Current Forestland Ratio (CFR), (2) Forestland Ratio with tropical storm and hurricane rates increase 25% from 2000-2020 levels (FR25%) and (3) Forestland Ratio with tropical storm and hurricane rates increase 50% from 2000-2020 levels (FR50%). Finally, we ran six different scenarios (Table 4.2) in our analysis. These scenarios estimate how urban land growth interacts with forestland conservation if the current hurricane landfall increases from 25% to 50% at the end of 2050 in the Perdido watershed.

Table 4.2: Future land use and forestland conservation scenarios for MLP-CA model

Scenario name	Description
LUR+CFR	Low Urbanization rate + Current Forestland Ratio
LUR+FR25%	Low Urbanization rate + Forestland Ratio with tropical storm and hurricane rates increase 25% from 2000-2020 levels
LUR+FR50%	Low Urbanization rate + Forestland Ratio with tropical storm and hurricane rates increase 50% from 2000-2020 levels
HUR+CFR	High Urbanization rate + Current Forestland Ratio
HUR+FR25%	High Urbanization rate + Forestland Ratio with tropical storm and hurricane rates increase 25% from 2000-2020 levels
HUR+FR50%	High Urbanization rate + Forestland Ratio with tropical storm and hurricane rates increase 50% from 2000-2020 levels

Estimation of Conservation Easements

We used the Protected Areas Database of the United States (PAD-US) v2.0 with our land use scenario analysis to estimate the changes in conservation easements in the Perdido Bay watershed. We intended to align the USGS Gap Analysis Project (GAP) to provide landscape (e.g., state, watershed, regional, and national) assessments of the conservation status of native vertebrate species and natural land cover types and to facilitate the application of this information to land management activities (NCED, 2022; USGS, 2022). In consequence, we considered the dominant land use – forestland, cropland and pasture and wetland inside each easement for future prediction. Finally, we estimated the land use difference from the baseline year 2021 to the prediction year 2050 for forestland, cropland, pasture, and wetland.

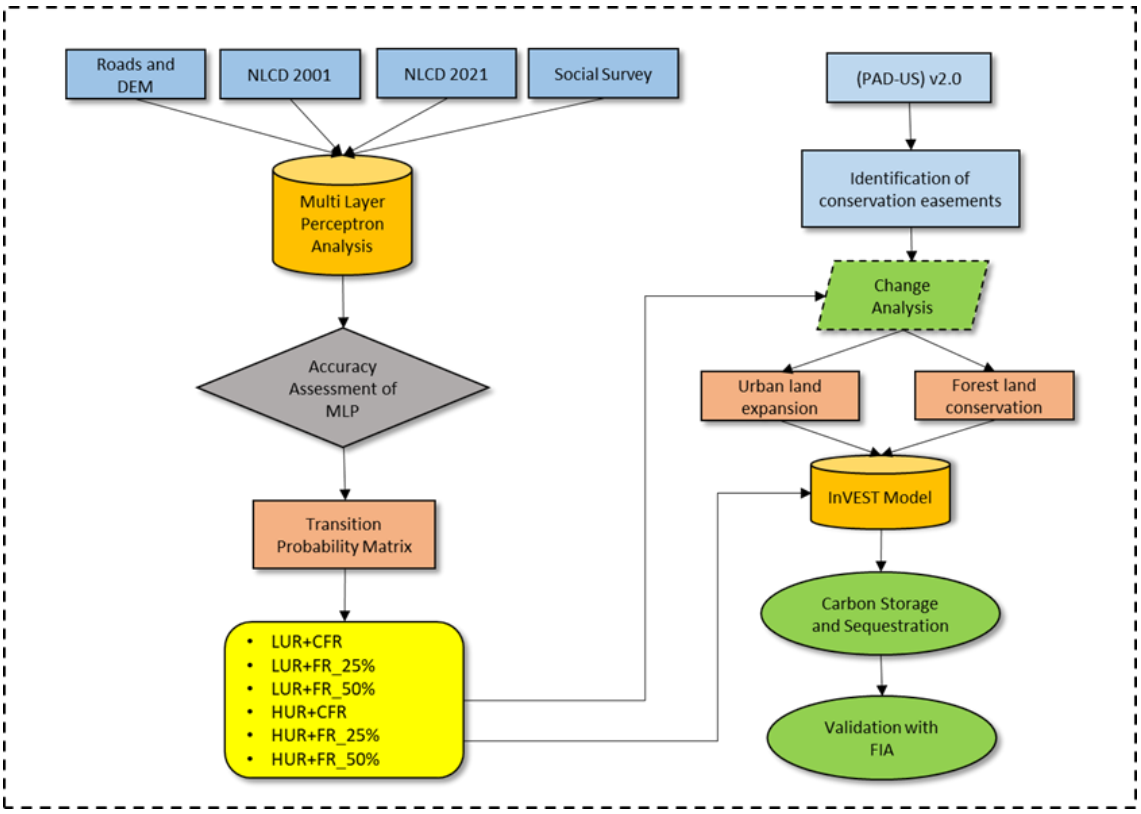

Figure 4.3: Methodological flowchart for estimating future land use and carbon storage in different urbanization rates and forestland change scenarios.

Estimation of Carbon Storage

We used the InVEST Carbon Storage and Sequestration model, developed by the Natural Capital Project of Stanford University, along with land use scenarios in three carbon pools (aboveground carbon, belowground carbon and soil organic carbon, dead organic carbon) to estimate the amount of carbon stored or the amount of carbon stored by the end of 2050 in the Perdido Bay watershed. Aboveground and belowground dataset provide temporally consistent and harmonized global maps of aboveground and belowground biomass carbon density for the year 2010 at a 300-m spatial resolution. The aboveground biomass map integrates land-cover specific, remotely sensed maps of woody, grassland, cropland, and tundra biomass. The belowground biomass map similarly combines matching maps derived from each aboveground biomass map and land-cover specific empirical models (ORNL, 2020; Spawn et al., 2020). Aboveground and belowground maps were then integrated separately using ancillary maps of percent tree cover and land cover and a rule-based decision tree. We converted the resolution into 30m to parameterize the InVEST model with soil organic carbon data from Gridded SSURGO (gSSURGO) (NRCS, 2020). Before feeding into

the InVEST model, we added the value look-up table with SSURGO in the ArcGIS platform to generate soil organic carbon maps. Because the death organic carbon data are difficult to obtain, and the impact on the overall carbon storage is very small (Lai et al., 2016; Zhu et al., 2021), therefore, this study does not consider the impact of this part on carbon storage. Finally, we used land use scenario maps, and the amount of carbon stored in carbon pools in the InVEST Carbon Storage and Sequestration model. We followed the data preparation and model parametrization process using the documentation from (Nelson et al., 2010; Standford University, 2018).

$$C_i = C_{i\text{-}aboveground} + C_{i\text{-}belowground} + C_{i\text{-}soil} + C_{i\text{-}dead} \quad (3)$$

$$C_{total} = \sum_{i=1}^{n} x\ C_i\ x\ S_i \quad (4)$$

In Equations 3 and 4, *i* represents the *i*th land-use type; C_i represents the total carbon density of soil and organisms of land type *I*, $C_{i\text{-}aboveground}$ refers to the carbon density of aboveground organisms of land type *i*, $C_{i\text{-}belowground}$ refers to the carbon density of ground type *i* underground organisms, $C_{i\text{-}soil}$ refers to the soil organic matter carbon density in the soil layer of land category *i* at a certain depth (0–100 cm in this study). $C_{i\text{-}dead}$ refers to the dead organic matter carbon density of land category *i*. All carbon densities are measured in metric tons/pixel. C_{total} represents total Carbon storage in metric tons; S_i represents the total area of land-use type *i*; *n* represents the total number of land use types.

InVEST model simplifies the carbon cycle, assuming that none of the land use types in the landscape are gaining or losing carbon over time. Instead, it is assumed that all land use types are at some fixed storage level equal to the average of measured storage levels within that land use type. The InVEST model also does not capture carbon that moves from one pool to another. For example, if trees in a forest die due to disease, much of the carbon stored in aboveground biomass becomes carbon stored in other (dead) organic material. To overcome this issue, we utilized FIA (Forest Inventory Analysis, US Forest Service) 2021 inventory year data for comparing InVEST model results to FIA carbon estimation. We followed the steps mentioned in the FIA User Guide for Phase 2 v 6.1 to calculate carbon storage in the Perdido watershed.

4.3 Results

Land use projection for 2050

Figure 4.4(a) depicts the land use change from 2001 to 2050 using the MLP-CA model. Considering the current urban land growth in the Gulf Coast, open space is experiencing a sharp decline from the baseline period of 2021. Cropland and pasture, shrub, and barren land are decreasing than the state of 2001 and 2021. Historical land use (2001-2021) shows about 26.70% more open space was available than that of the projection period (2021-2050). Our MLP-CA model iterates these changes transformed mostly into urban land (23.11%) for the next 30 years from the historical level. Figure 4.4(b) illustrates historic land use change and projected land use change for different land use classes. Urban land, barren land, and forestland increased every year at a rate of 1.46%, 0.34%, and 0.07%, respectively, from the historical level. From 2001-2021, the increased rate was 3.35%, 0.76%, and 0.22%, respectively in these three land use classes. Shrub, developed (open space) and cropland and pasture are also decreasing from the historical level - 0.11%, 0.95%, and 0.18% per year, respectively. Open water will increase 0.13% per year and wetland will decrease by 0.12% per year at the end of the prediction period.

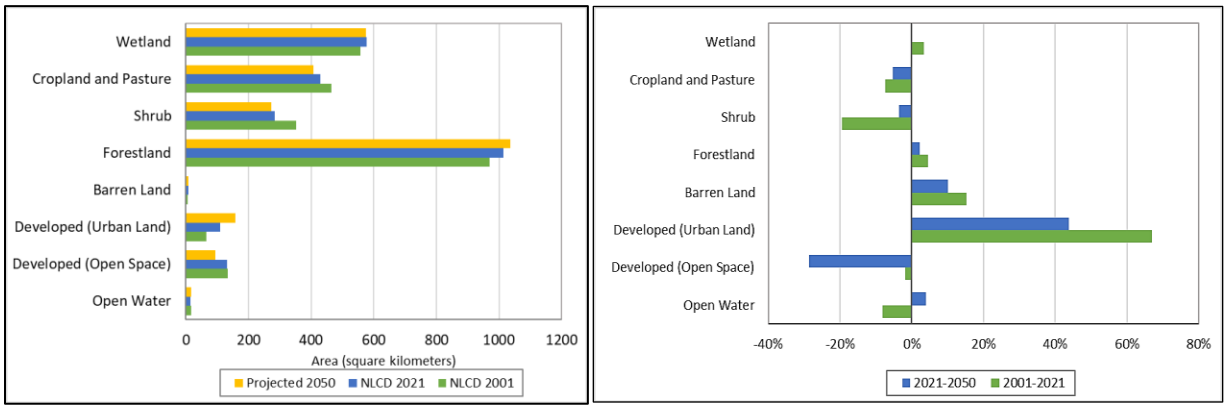

Figure 4.4: (a) Land use (km^2) in NLCD 2001, 2021 and MLP CA based on projected year 2050, (b) relative change of land use classes from NLCD 2001 to NLCD 2021 and NLCD 2021 to Projected 2050.

Figure 4.5 shows the land use transition for baseline 2021 to 2050. Our model predicts that 41% of the total developed open space land will change into urban land at the end of 2050. About 10.37% of Cropland and Pasture, 25.43% of Shrub and 1% of barren land are predicted to change into Forestland. Correspondingly, 18% of the forestland and 1% of cropland and pasture will change into Shrub. About 1% of wetlands will be lost to water at the end of 2050.

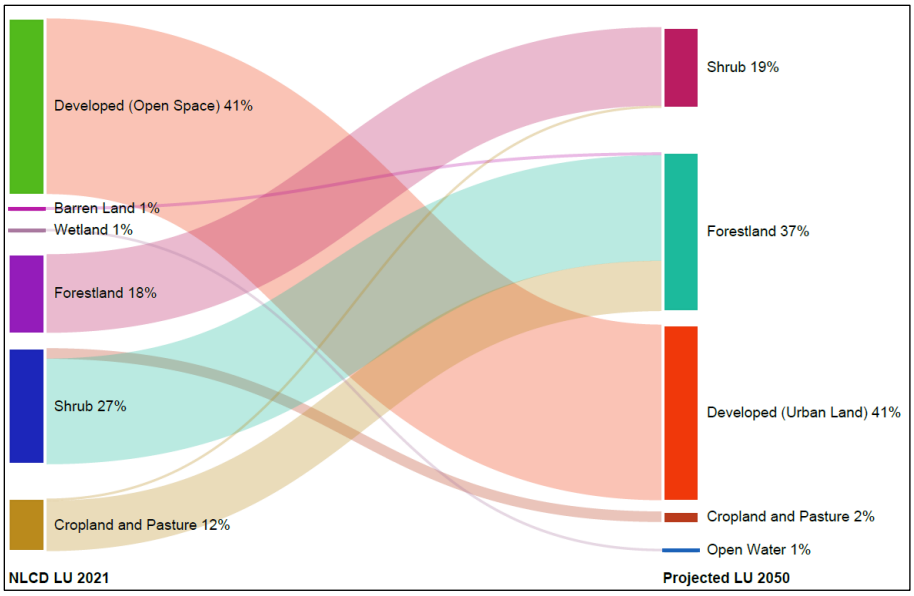

Figure 4.5: Sankey diagram shows land use transitions from 2021 to 2050. This diagram consists of MLP transition sub models: developed (open space) to developed (urban land), barren land to forestland, forestland to shrub, forestland to cropland and pasture, shrub to forestland, cropland and pasture to forestland and wetland to open water.

Transition Probability Matrix

Our scenario analysis on urban land and forestland shows indifferent results in land use change due to projected hurricanes in the next 30 years. Our analysis considered three different rates for future urban growth: low (2.5%), current (2.67%), and high (4.5%). MLP-CA model accounts for a two-forestland ratio level compared to 2021; forestland Ratio with tropical storm and hurricane rates increased 25% from 2000-2020 levels and 50% from 2000-2020 levels. Our social survey in the Perdido Bay watershed revealed that landowners opt to sell 8.95% to 29.12% of their total forestland if the tropical storm and hurricane rates increase from 25% to 50% at the end of 2050. Furthermore, a significant portion of landowners between 15.69% and 25.26% - want to conserve their forestland under the increased hurricane scenarios.. We feed the forestland ratio and urban land growth rate in the MLP model to create the transition probability matrix (Figure 4.6) from the baseline 2021 to projection 2050. Red cells in the matrix show a higher transition probability (conversion), and blue cells stand for a lower transition probability (persistence). MLP model predicts the probability of converting open space to urban land increasing by time, ranging from 19.62% to 35.86% - approximately 0.65% to 1.19% per year considering the forestland ratio changes due to increased tropical storm and hurricane from 25% to 50%. Increased tropical storm and hurricane intensities in the future will drive more landowners to conserve their forestlands; the

probability of the current forestlands will rise to 92% from 75% by the end of the projection period, coupled with future urban growth. Correspondingly, the probability of croplands and pasture will decrease by 16.72% and 18.94%, respectively, under the same land use scenarios.

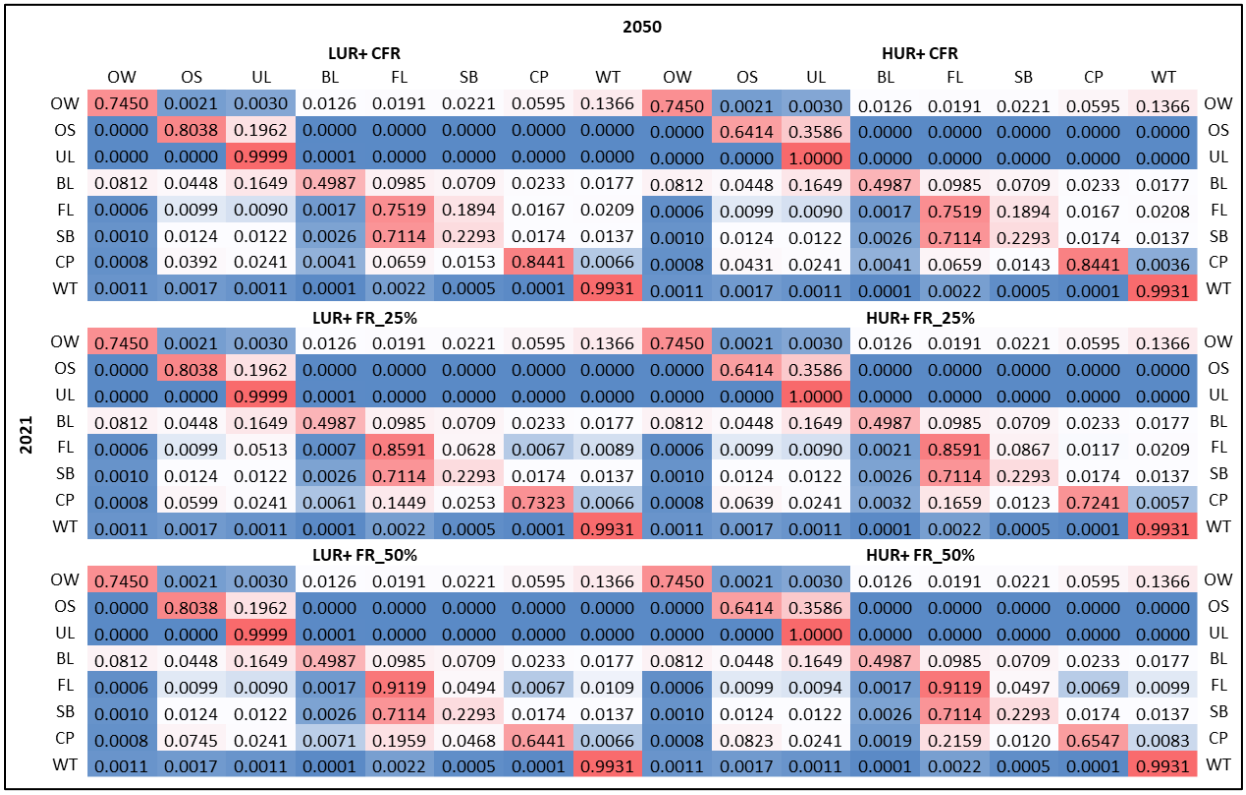

2050

2021	LUR+ CFR								HUR+ CFR								
	OW	OS	UL	BL	FL	SB	CP	WT	OW	OS	UL	BL	FL	SB	CP	WT	
OW	0.7450	0.0021	0.0030	0.0126	0.0191	0.0221	0.0595	0.1366	0.7450	0.0021	0.0030	0.0126	0.0191	0.0221	0.0595	0.1366	OW
OS	0.0000	0.8038	0.1962	0.0000	0.0000	0.0000	0.0000	0.0000	0.0000	0.6414	0.3586	0.0000	0.0000	0.0000	0.0000	0.0000	OS
UL	0.0000	0.0000	0.9999	0.0001	0.0000	0.0000	0.0000	0.0000	0.0000	0.0000	1.0000	0.0000	0.0000	0.0000	0.0000	0.0000	UL
BL	0.0812	0.0448	0.1649	0.4987	0.0985	0.0709	0.0233	0.0177	0.0812	0.0448	0.1649	0.4987	0.0985	0.0709	0.0233	0.0177	BL
FL	0.0006	0.0099	0.0090	0.0017	0.7519	0.1894	0.0167	0.0209	0.0006	0.0099	0.0090	0.0017	0.7519	0.1894	0.0167	0.0208	FL
SB	0.0010	0.0124	0.0122	0.0026	0.7114	0.2293	0.0174	0.0137	0.0010	0.0124	0.0122	0.0026	0.7114	0.2293	0.0174	0.0137	SB
CP	0.0008	0.0392	0.0241	0.0041	0.0659	0.0153	0.8441	0.0066	0.0008	0.0431	0.0241	0.0041	0.0659	0.0143	0.8441	0.0036	CP
WT	0.0011	0.0017	0.0011	0.0001	0.0022	0.0005	0.0001	0.9931	0.0011	0.0017	0.0011	0.0001	0.0022	0.0005	0.0001	0.9931	WT
	LUR+ FR_25%								HUR+ FR_25%								
OW	0.7450	0.0021	0.0030	0.0126	0.0191	0.0221	0.0595	0.1366	0.7450	0.0021	0.0030	0.0126	0.0191	0.0221	0.0595	0.1366	OW
OS	0.0000	0.8038	0.1962	0.0000	0.0000	0.0000	0.0000	0.0000	0.0000	0.6414	0.3586	0.0000	0.0000	0.0000	0.0000	0.0000	OS
UL	0.0000	0.0000	0.9999	0.0001	0.0000	0.0000	0.0000	0.0000	0.0000	0.0000	1.0000	0.0000	0.0000	0.0000	0.0000	0.0000	UL
BL	0.0812	0.0448	0.1649	0.4987	0.0985	0.0709	0.0233	0.0177	0.0812	0.0448	0.1649	0.4987	0.0985	0.0709	0.0233	0.0177	BL
FL	0.0006	0.0099	0.0513	0.0007	0.8591	0.0628	0.0067	0.0089	0.0006	0.0099	0.0090	0.0021	0.8591	0.0867	0.0117	0.0209	FL
SB	0.0010	0.0124	0.0122	0.0026	0.7114	0.2293	0.0174	0.0137	0.0010	0.0124	0.0122	0.0026	0.7114	0.2293	0.0174	0.0137	SB
CP	0.0008	0.0599	0.0241	0.0061	0.1449	0.0253	0.7323	0.0066	0.0008	0.0639	0.0241	0.0032	0.1659	0.0123	0.7241	0.0057	CP
WT	0.0011	0.0017	0.0011	0.0001	0.0022	0.0005	0.0001	0.9931	0.0011	0.0017	0.0011	0.0001	0.0022	0.0005	0.0001	0.9931	WT
	LUR+ FR_50%								HUR+ FR_50%								
OW	0.7450	0.0021	0.0030	0.0126	0.0191	0.0221	0.0595	0.1366	0.7450	0.0021	0.0030	0.0126	0.0191	0.0221	0.0595	0.1366	OW
OS	0.0000	0.8038	0.1962	0.0000	0.0000	0.0000	0.0000	0.0000	0.0000	0.6414	0.3586	0.0000	0.0000	0.0000	0.0000	0.0000	OS
UL	0.0000	0.0000	0.9999	0.0001	0.0000	0.0000	0.0000	0.0000	0.0000	0.0000	1.0000	0.0000	0.0000	0.0000	0.0000	0.0000	UL
BL	0.0812	0.0448	0.1649	0.4987	0.0985	0.0709	0.0233	0.0177	0.0812	0.0448	0.1649	0.4987	0.0985	0.0709	0.0233	0.0177	BL
FL	0.0006	0.0099	0.0090	0.0017	0.9119	0.0494	0.0067	0.0109	0.0006	0.0099	0.0094	0.0017	0.9119	0.0497	0.0069	0.0099	FL
SB	0.0010	0.0124	0.0122	0.0026	0.7114	0.2293	0.0174	0.0137	0.0010	0.0124	0.0122	0.0026	0.7114	0.2293	0.0174	0.0137	SB
CP	0.0008	0.0745	0.0241	0.0071	0.1959	0.0468	0.6441	0.0066	0.0008	0.0823	0.0241	0.0019	0.2159	0.0120	0.6547	0.0083	CP
WT	0.0011	0.0017	0.0011	0.0001	0.0022	0.0005	0.0001	0.9931	0.0011	0.0017	0.0011	0.0001	0.0022	0.0005	0.0001	0.9931	WT

Figure 4.6: Transition probability matrix of sub-models for six land use scenarios in MLP model from the baseline year 2021 to the projected year 2050.

Future Land Use Scenario Analysis

Figure 4.7 represents the maps of six different land use scenarios. From the baseline level 2021, urban land area in six different scenarios ranges from 5.28% to 6.12%, and forestland area ranges from 40.30% to 48.71%. Historic urban land growth counted the hurricane's impact on the existing land use. With an increasing growth rate of urban land and tropical storm and hurricane rates increasing 25%-50% from 2000-2020 levels, more landowners opt to conserve their existing forestlands to combat the extreme weather events. However, forestland conservation in LUR+FR50% and HUR+FR50% scenarios show a marginal difference compared to LUR+FR25% and HUR+FR25%: 0.31% and 0.79%, respectively (Figure 4.7). The imperviousness character of developed open space and developed urban land and interchanged in the MLP model considering

the trend of 2001-2021 land use change. This implies that the future development of urban growth will comprise the land parcel that comes from developed open space. Conversely, shrubs will decrease from the current level to FR25% and FR50% scenarios by 4.05% and 1.46%, respectively, in the high urbanization rate and 5.05% and 0.53%, respectively, in the low urbanization rate. Cropland and pasture will decrease at a rate of 1.87% to 0.85% in both FR25% and FR50% scenarios. Wetlands and open water will not experience a considerable amount of change from the historical level.

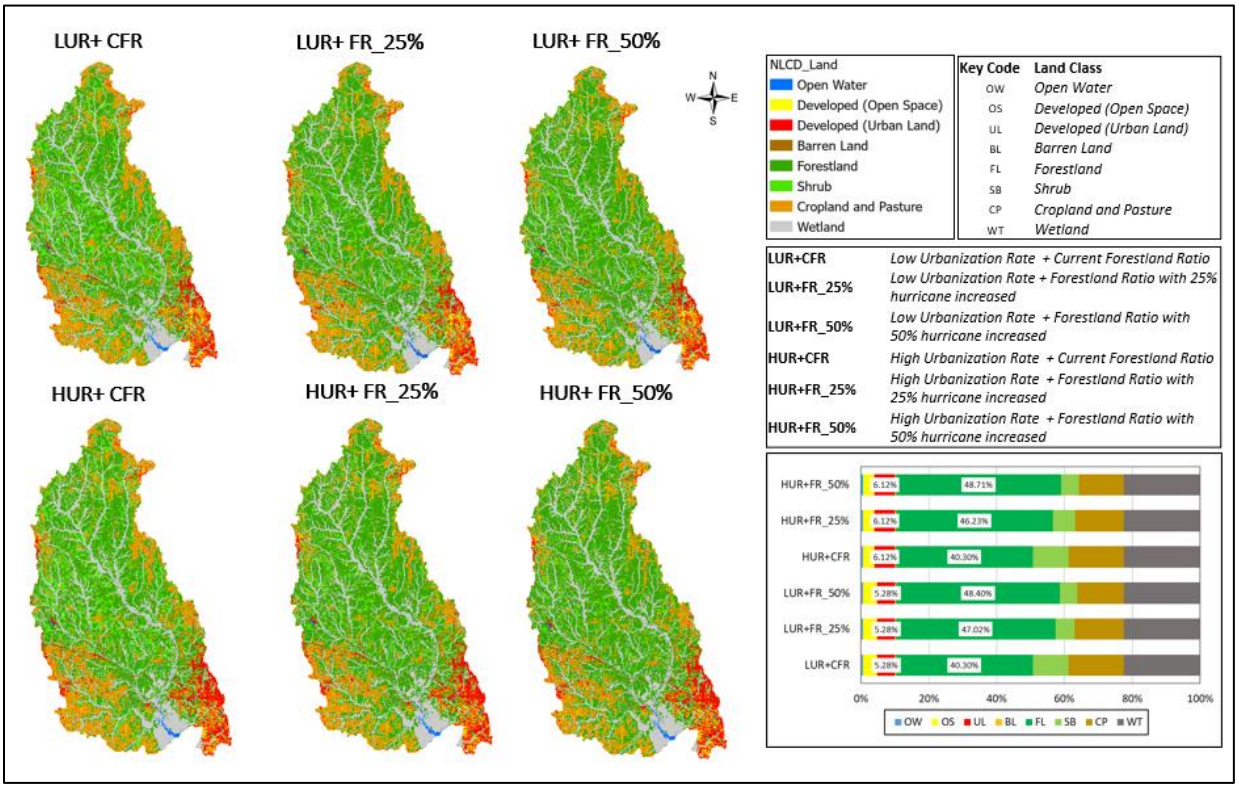

Figure 4.7: Maps of projected land use in 2050 in different land use scenarios. Graph in the bottom right corner shows the distribution of land use changes in different land use scenarios. Table in the middle describes different land use scenarios. Key code used in the analysis for space utilization in graphical representation.

From baseline 2021 to different land use scenarios in 2050, we found land area increase in urban land, forestland, and open water (Figure 4.8). The expansion of urban land is anticipated to vary between 23.67% and 43.26%, corresponding to low and high urbanization rates. These projections take into account an increase in tropical storms and hurricanes by 25% to 50% over the next three decades. In conjunction with urban land, forestland will also experience a sharp increase (2.14%

to 23.45%) due to the conservation of forestlands by the landowners. As more intense hurricanes are predicted in the next 30 years than in the 2001-2021 period, our model showed more forestlands would be conserved in the low urbanization rate (17.01%) scenario compared to the high urbanization rate (14.91%) scenario. Open water will experience an increase of 0.98%. In contrast, open space, barren land, shrub, cropland and pasture, and wetland are predicted to decrease in all the scenarios. The reduction in open spaces is particularly pronounced due to rapid urban expansion in the Gulf Coast, with a 19.62% decrease in the low urbanization scenario and a 35.86% decrease in the high urbanization scenario. This illustrates how increased urbanization will force more open spaces to grow as urban land and reveal greater imperviousness further. Crop and pasture lands will decrease alarmingly in all scenarios, 12.91% in FR25% and 19.96% in FR50% scenarios, respectively. Shrub will experience the highest decrease in the next 30 years, ranging from 3.37% to 53.36% loss in all scenarios. Barren land will decrease by 9.8%, and wetlands will remain similar compared to the baseline.

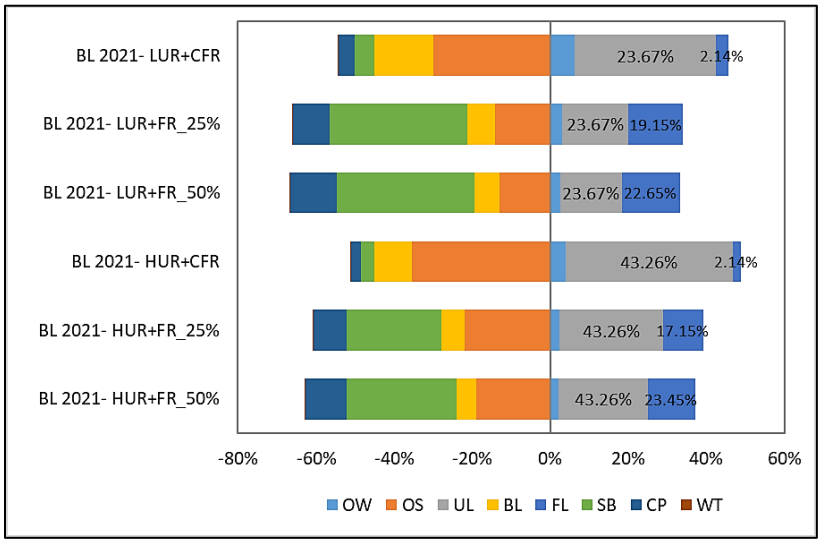

Figure 4.8: Changes in land uses from baseline year 2021 to 2050 in different land use scenarios. Data labels marked only for the scenario parameters; urban land and forestland.

Forestland conservation in conservation easements

Figure 4.9 shows changes in dominant land use categories across all conservation easements: forestland, wetland, and Cropland and Pasture from baseline 2021 to projected land use scenarios. Cropland and pasture will decrease significantly in all the scenarios, i.e., 31.25% to 66.91% from LUR+CFR to HUR+FR50%. With the current forestland growth trend in the Perdido Bay

watershed, the loss of cropland and pasture is relatively lower than FR25% and FR50%. Conserving more forestland in the future will offset 13.79% to 34.65% of cropland and pasture in LUR+FR25% and LUR+FR50%, respectively, and 14.39% to 22.01% in HUR+FR25% and HUR+FR50% within the easements. Forestland in the easements will see growth from baseline to all land use scenarios. If tropical storms and hurricanes increase by 25% to 50% from 2000-2020 levels, landowners will conserve about 5.63% to 6.82% more forestlands in lower urbanization rate and 5.24% to 6.99% more forestland in higher urbanization rate scenarios. Wetlands within the easements are anticipated to remain relatively stable compared to the baseline – about 0.08% to 0.12% decrease across all land use scenarios.

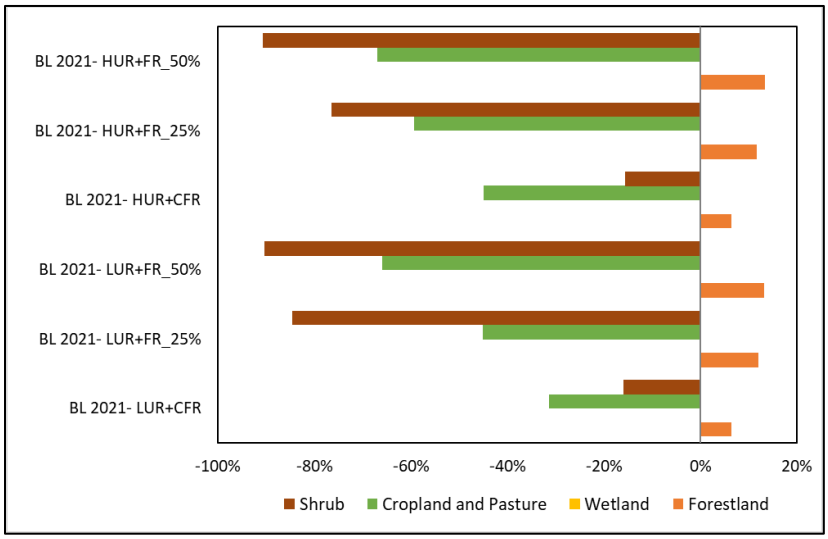

Figure 4.9: Changes of forestland, wetland, and Cropland and Pasture in different Land use scenarios in all conservation easements in Perdido.

Table 4.3 shows the land use transition in the conservation easements in future land use scenarios. As more hurricanes hit the Perdido Bay watershed, more conservation easement owners opt to conserve their lands into forestlands mainly emphasized on converting cropland and pasture. Our model predicts lands from cropland and pasture and shrubs will convert into forestland in current land use scenarios, approximately 0.28 km^2 of land. If hurricane increases by 25% by 2050, forestland will increase from 0.59 km^2 to 0.61 km^2, considering high and low urbanization rate, respectively. Correspondingly, hurricane increases by 50% will conserve 0.67 km^2 to 0.68 km^2 of forestland in low and high urbanization rate scenarios. About 0.03 to 0.04 km^2 of wetlands will convert into water across all land use scenarios.

Table 4.3: Land use transition from baseline 2021 to projected scenarios in conservation easements. Land classes in the rows are stand for 2021 NLCD and columns are in MLP-CA projected 2050. Transition areas are represented in km^2.

Land use Scenarios		Forestland	Open Water	Shrub
LURCFR	Cropland and Pasture	**0.28**	0.00	0.00
	Forestland	0.00	0.00	**0.01**
	Shrub	**0.06**	0.00	0.00
	Wetland	0.00	**0.04**	0.00
LUR+FR25%	Cropland and Pasture	**0.37**	0.00	0.00
	Shrub	**0.24**	0.00	0.00
	Wetland	0.00	**0.04**	0.00
LUR+FR50%	Cropland and Pasture	**0.41**	0.00	0.00
	Shrub	**0.26**	0.00	0.00
	Wetland	0.00	**0.04**	0.00
HURCFR	Cropland and Pasture	**0.28**	0.00	0.00
	Forestland	0.00	0.00	**0.01**
	Shrub	**0.06**	0.00	0.00
	Wetland	0.00	**0.03**	0.00
HUR+FR25%	Cropland and Pasture	**0.37**	0.00	0.00
	Shrub	**0.22**	0.00	0.00
	Wetland	0.00	**0.03**	0.00
HUR+FR50%	Cropland and Pasture	**0.42**	0.00	0.00
	Shrub	**0.26**	0.00	0.00
	Wetland	0.00	**0.03**	0.00

Carbon storage and sequestration

Figure 4.10 shows the spatial distribution of overall carbon storage (aboveground, belowground, soil organic carbon, and dead organic carbon) in each pixel in different land use scenarios using the InVEST model. Supplementary Table S4.2 illustrates the model output for aboveground, belowground, and soil organic carbon in six different scenarios across all land use classes. Considering the future hurricane's impact on forestland conservation, our model predicts more carbon will store in forestland, shrub and cropland and pasture. Figure 4.11 shows the spatial distribution of total carbon loss and sequestration across all future land use scenarios. With the increasing hurricane rate from 25% to 50%, about 447.52 thousand metric tons to 604.95 thousand

metric tons of carbon store in forestlands, considering the low urbanization rate. In high urbanization rate, forestland stores 442.43 thousand metric tons to 591.49 thousand metric tons in the terrestrial ecosystem. Figure 4.12 reflects the relative change of carbon across different land use classes from the baseline to the projection period 2050. Cropland and pasture show a similar trend, from current scenarios to future scenarios of hurricane carbon storage will see a decreasing trend. About 3.61 thousand metric tons to 7.35 thousand metric tons will be lost if the tropical storm and hurricane rates increase 50% from 2000-2020 levels. . However, the current scenario and 25% increase in tropical storms and hurricanes will store about 435.20 and 143.36 thousand metric tons of carbon at a low urbanization rate and 435.22 and 126.74 thousand metric tons of carbon in a high urbanization rate, respectively. Urban land, open space, wetlands, and open water all exhibit carbon loss during the projection period. In low and high urban growth rate scenarios, wetland will lose roughly 1.95 thousand to 2.85 thousand metric tons of carbon, open space will lose roughly 12.31 thousand to 16.95 thousand metric tons, and urban land will lose 6.19 thousand to 18.35 thousand metric tons.

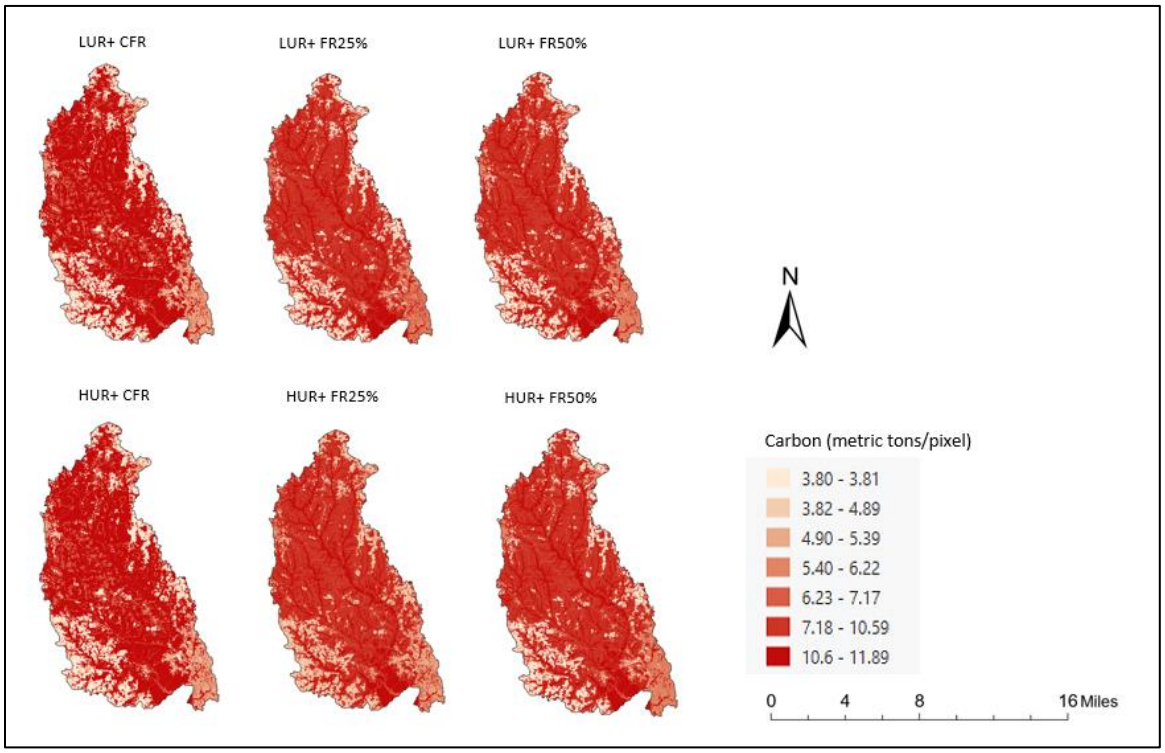

Figure 4.10: Spatial distribution of future (2050) carbon storage (metric tons/pixel) in different land use scenarios. Storage Carbon includes aboveground carbon, belowground carbon, soil organic carbon and dead organic carbon.

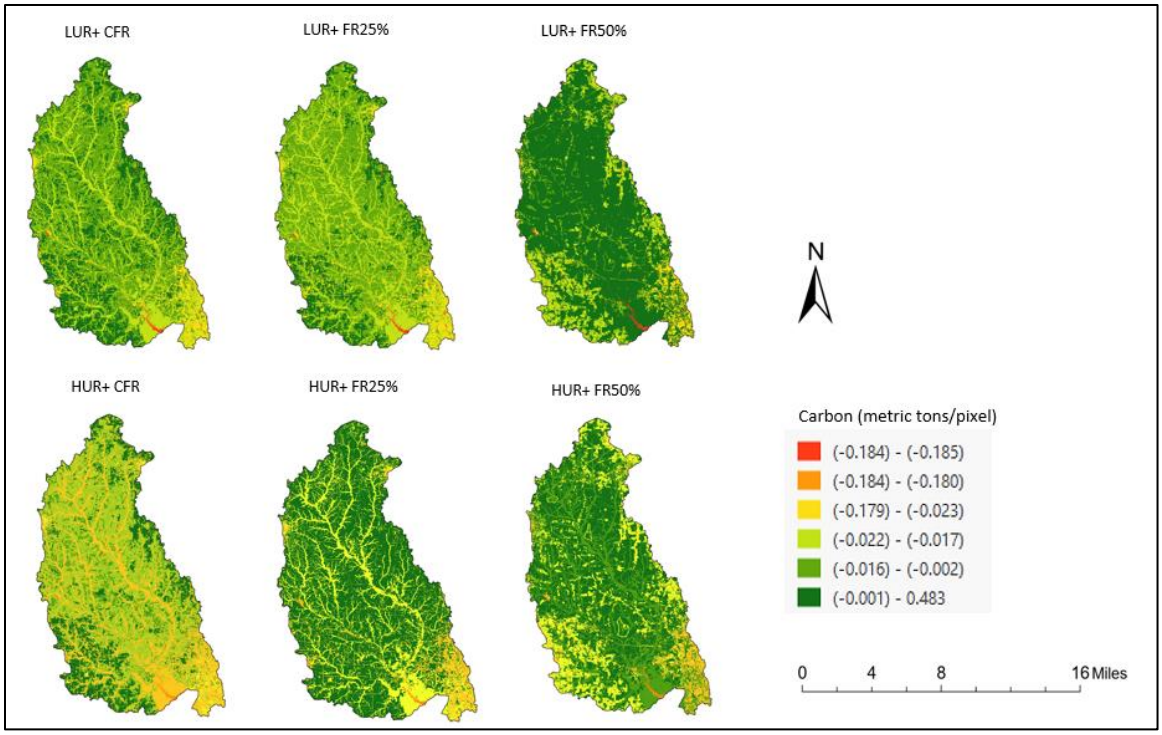

Figure 4.11: Spatial distribution of overall carbon (metric tons/pixel) change in different land use scenarios relative to the baseline (2021). Storage Carbon includes aboveground carbon, belowground carbon, soil organic carbon and dead organic carbon. Negative values stand for carbon lost in the projection period and positive values stand for carbon sequestration in the projection period.

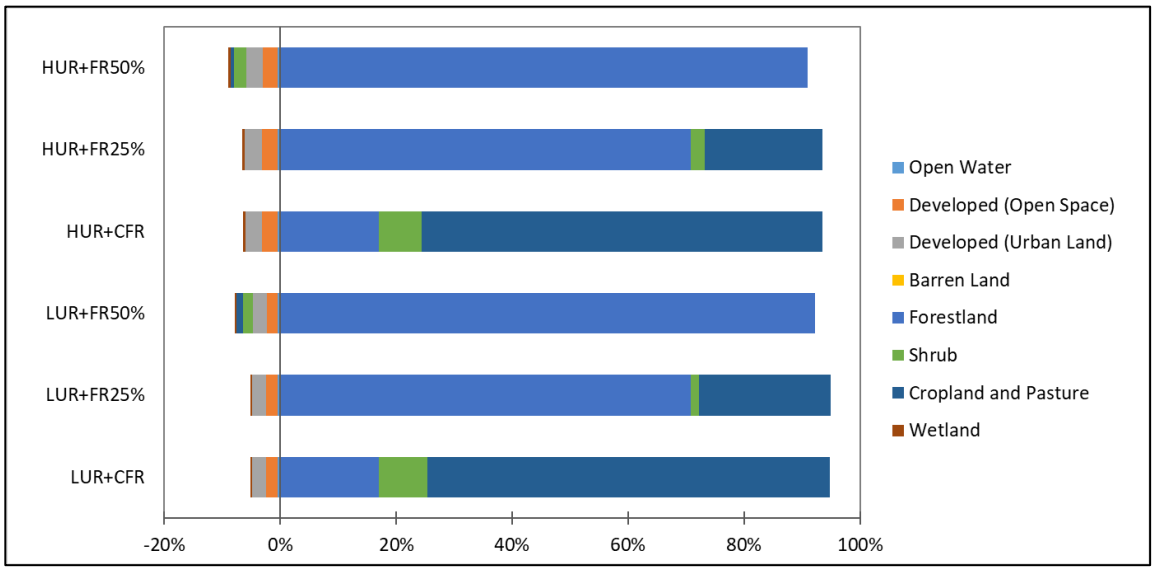

Figure 4.12: Relative change of carbon across all land classes in different scenarios relative to baseline (2021). Negative values stand for the carbon lost in the projection period, and positive values stand for carbon sequestration in the projection period.

Table 4.4 shows the estimated carbon across all land use scenarios in all nine conservation easements in the Perdido Bay watershed. Overall carbon loss in open water ranges from 0.17

thousand metric tons to 0.19 metric tons in LUR+CFR to HUR+FR50% scenarios. Carbon loss in wetland is estimated at about 0.01 thousand metric tons to 0.02 thousand metric tons; 8.55% and 23.23% less carbon estimated in LUR+CFR to HUR+FR50% scenarios, respectively, compared to baseline 2021. Correspondingly, forestland, shrubs, cropland and pasture store carbon across all scenarios. Landowners will conserve more of their forestlands as tropical storms and hurricanes are predicted to increase by 20% to 50% of 2000-2020 levels, reflects InVEST model output coincidence with our land use MLP-CA model. About 1.95 thousand metric tons to 2.93 thousand metric tons of carbon will be stored in all land use scenarios from LUR+CFR to HUR+FR50%. Shrub and cropland and pasture show a similar trend. Shrub predicts s a small contribution to carbon storage in the conservation easements comprising up to 0.08 thousand metric tons of carbon across all land use scenarios. Cropland and pasture will store about 0.09 to 0.81 thousand metric tons of carbon in LUR+FR50% and LUR+CFR, and 0.02 to 0.78 thousand metric tons of carbon in HUR+FR25% and HUR+CFR.

Table 4.4: Estimated carbon storage (thousand metric tons) across all conservation easements in different land use scenarios in Perdido Watershed. Negative values stand for carbon lost in the projection period and positive values stand for carbon sequestration in the projection period.

Land Class	LUR+CFR	LUR+FR25%	LUR+FR50%	HUR+CFR	HUR+FR25%	HUR+FR50%
Open Water	-0.18	-0.18	-0.18	-0.16	-0.16	-0.16
	(0.00%)	(0.00%)	(0.00%)	(-11.90%)	(-11.90%)	(-11.90%)
Forestland	1.96	2.64	2.94	1.96	2.64	2.93
	(16.58%)	(56.58%)	(74.65%)	(16.21%)	(56.78%)	(73.91%)
Shrub	0.08	0.01	0.00	0.08	0.02	0.00
	(-22.34%)	(-93.47%)	(-100.00%)	(-22.64%)	(-84.54%)	(-100.00%)
Cropland and Pasture	0.81	0.30	0.19	0.78	0.27	0.09
	(-28.68%)	(-73.74%)	(-91.87%)	(-31.57%)	(-75.88%)	(-91.95%)
Wetland	-0.01	-0.01	-0.01	-0.02	-0.03	-0.04
	(-93.92%)	(-95.31%)	(95.71%)	(-88.10%)	(-83.11%)	(-79.19%)
Total Carbon	**2.66**	**2.75**	**2.85**	**2.63**	**2.74**	**2.82**
(thousand metric tons)	**(3.98%)**	**(7.62%)**	**(11.26%)**	**(2.88%)**	**(7.14%)**	**(10.41%)**

4.4 Discussion

Hurricane Impact on land use scenarios

We observed the land use change due to the increased frequency and intensity of catastrophic hurricanes in the Gulf of Mexico, focusing on urban expansion and forestland conservation in 2050. Our results suggested urban land would be increased irrespective of hurricane and land use

scenarios with the current growth rate pattern. For analytical comparability, we fed the growth rate pattern of urban expansion and forestland ratio in our MLP-CA model. Our model considers the historical pattern of hurricane intensities (Chan et al., 2021; Emanuel, 2021) and its impact on land use (NOAA, 2015); parallelly, we used the NOAA predicted hurricane scenario to estimate the land use changes with a better understanding (NOAA, 2023). In terms of estimated urban land use change in the Perdido watershed, our study coincided with (Li et al., 2016). They monitored urban dynamics using nighttime light imagery to characterize the extent of urban development in the Southeast US. By using the NLCD data, we identified the historical (2001-2021) annual growth rate for the ten fastest growing urban centers in the Southeast and Gulf Coast. We utilized this information to estimate different urban growth rate scenarios in the Perdido watershed. Our result has found similarity with Wang et al. (2014), who used a spatially downscaled Global Circulation Model to predict environmental partakers that affect urban growth substantially in the Gulf Coast.

The impact of catastrophic hurricanes on forestlands in the Gulf Coast is profound, as hurricanes can result in severe tree damage, changes in forest structure, and long-term ecological consequences (Lugo, 2008; Sharma et al., 2021). Understanding how hurricanes affect Gulf Coast forestlands is crucial for forest management, conservation efforts, and adaptation strategies (Needham et al., 2012). For example, high winds and storm surges can cause tree damage, uprooting, and defoliation. These disturbances often lead to changes in forest structure and composition, affecting species diversity and abundance (Castañeda-Moya et al., 2020b; Sharma et al., 2021). The response of forestlands to hurricanes depends on factors such as forest type, age, and prior management practices (Henderson et al., 2022; Polinko et al., 2022). While older, mixed-species forests may be more resilient to hurricanes, younger, monoculture plantations are often more susceptible to damage. Silvicultural practices that encourage structural diversity and selective harvesting can enhance the resilience of forestlands on the Gulf Coast (Polinko et al., 2022; Xi et al., 2008b). In addition to their ecological impact, hurricane-induced land use change has significant economic consequences for forestland owners and timber industries (Beach et al., 2010; Prestemon and Holmes, 2010). High winds can uproot trees, break branches, or damage the trunk, rendering the timber unsuitable for commercial use (Alabama Forestry Commission, 2022; Kinnucan, 2016). In our landowner's survey, we found these uncertainties in processing commercial timbers after intense hurricanes, and the landowners are more interested in converting

or selling the existing forestland if the future hurricane scenarios prevail by 25% to 50%. Consequently, more forestlands will be converted into other land uses, especially pasture and open space. Forestlands are often managed for both conservation and commercial purposes, and hurricanes can have a direct impact on the economic viability of these lands. The economic implication of hurricane impacts on forestlands necessitates robust risk management and insurance strategies for landowners (Kinnucan, 2016; Stanturf et al., 2007). In addition to the immediate loss of standing timber, reforestation efforts following a hurricane can be costly. Forestland owners must invest in replanting new trees and managing the land to ensure a healthy, productive forest in the future. This incurs expenses related to seedlings, site preparation, and ongoing maintenance. Future research could be implemented to explore the avenue of commercial forestland risk management and how the economic value triggers land use conversion amid uncertainties.

Importance of carbon sequestration by land use change

Terrestrial ecosystems, which store more carbon than the atmosphere, are vital to influencing carbon dioxide-driven climate change (Ades et al., 2022; NOAA, 2019). Studies are not accounting for carbon storage and sequestration occurred by climate change actions, especially hurricanes (McNulty, 2002) We employed the InVEST Carbon Storage and Sequestration model to estimate the amount of carbon (aboveground carbon, belowground carbon, soil organic carbon and dead organic carbon) currently stored in a landscape and the amount of carbon sequestered over time. The forestland area accounts for about 40% to 48% of the total area across all land use scenarios. The main reason for the increase in carbon storage is the conservation of forestland due to the increased possibility of hurricanes. Carbon storage increased by forestland accounts for 79% to 91% of the total carbon storage across land use scenarios. This ratio also supports the carbon uptake in the conservation easements located in Perdido. However, due to land conversion from cropland to forestland, carbon loss increases by 22% to 26%. Belowground carbon and soil organic carbon generally remain in the soil for years (USDA, 2016). Since cropland and pasture loss is a complex process, climate factors are accountable for shifting the land parcel to forest conservation, especially on the Gulf Coast, where a hurricane is a common phenomenon (EPA, 2019). About 376 thousand metric tons to 549 thousand metric tons of carbon will be sequestered due to increased forestland conservation, as per our model output. This correspondingly accumulates

about 0.67 thousand metric tons to 1.29 thousand metric tons of sequestered carbon across all conservation easements.

Carbon sequestration is important for several critical reasons, and it involves capturing and storing carbon dioxide (CO_2) from the atmosphere (McNulty, 2002). Given that CO_2 is a major greenhouse gas responsible for global warming, sequestering carbon helps reduce the concentration of CO_2 in the atmosphere. This, in turn, mitigates the effects of climate change, such as rising temperatures, extreme weather events, and sea-level rise. It also helps stabilize the climate by offsetting the emissions of CO_2, allowing us to work towards achieving the goals of the Paris Agreement to limit global temperature increase (UNFCCC, 2015). Ecosystems with high carbon sequestration potential, such as forests and wetlands, tend to be rich in biodiversity. Conserving these ecosystems by proper land use management not only stores carbon but also supports a wide range of plant and animal species crucial for ecological balance (Buotte et al., 2020; Weiskopf et al., 2020). Protecting and enhancing carbon sequestration also helps maintain valuable ecosystem services, clean water, air purification, and habitat for wildlife. Some agricultural practices, such as agroforestry and soil carbon sequestration, can enhance carbon storage while promoting more sustainable and resilient agricultural systems. This can benefit food security and the livelihoods of farmers (Kay et al., 2019). Carbon markets and carbon offset programs offer economic incentives for sequestering carbon. These mechanisms can provide revenue for landowners and communities engaged in responsible land use and carbon capture activities (Barbato and Strong, 2017; Pape et al., 2016). Coastal ecosystems like mangroves and seagrasses sequester carbon while also acting as natural buffers against storm surges, protecting communities from the impacts of sea-level rise and extreme weather events (Castañeda-Moya et al., 2020c; Osland et al., 2017). As we transition to a low-carbon and sustainable future, carbon sequestration becomes essential. It helps build resilience in ecosystems and societies, ensuring a more sustainable and stable world for future generations.

Limitations of InVEST Carbon and Sequestration Model

InVEST Carbon and Sequestration Model simplifies the carbon cycle, which allows it to run with relatively little information but also leads to important limitations. For example, the model assumes that none of the LULC types in the landscape are gaining or losing carbon over time. Instead, it is

assumed that all LULC types are at some fixed storage level equal to the average of measured storage levels within that LULC type (Abd El-Hamid and Hafiz, 2022; Thamo and Pannell, 2016). Under this assumption, the only changes in carbon storage over time are due to changes from one LULC type to another. Therefore, any pixel that does not change its LULC type will have a sequestration value of 0 over time. As a matter of fact, many regions are going through natural succession or are recuperating from previous land use (Stanford University, 2016). One possible solution to the issue is to create more LULC kinds by classifying LULC types into age groups, like three different ages of forests. Subsequently, in certain conditions, packages may transition between age classes, which could alter their carbon storage values.

A second limitation is that because the model relies on carbon storage estimates for each LULC type, the results are only as detailed and reliable as the LULC classification used and the carbon pool values supplied (Grafius et al., 2016). There are LULC categories that clearly differ in terms of carbon storage (i.e., open woodland vs. tropical forest), but there can also be substantial variance within a single LULC type. For instance, the amount of rainfall, temperature, elevation, and time elapsed since a significant disturbance all influence the amount of carbon stored in a "tropical moist forest" (e.g., clear-cut or forest fire or hurricane). The variety of carbon storage values within coarsely defined LULC types can be partly recovered by using a LULC classification system and related carbon pool table, which stratifies coarsely defined LULC types with relevant environmental and management variables (He et al., 2016; Toru and Kibret, 2019). For example, forest LULC types can be stratified by elevation, climate bands, or time intervals since a major disturbance. Of course, this more detailed approach requires data describing the amount of carbon stored in each of the carbon pools for each of the finer LULC classes.

An additional constraint of the model is its inability to account for carbon that is transferred between different pools. A large portion of the carbon stored in aboveground biomass, for instance, is converted into carbon stored in other (dead) organic material when disease kills trees in a forest (USFS, 2016). Furthermore, after a forest's trees are harvested, the branches, stems, bark, etc., are left as slashes on the ground. The model assumes that wood-slash carbon "instantaneously" reaches the atmosphere (Stanford University, 2016; Xi et al., 2023b). However, FIA (Forest Inventory Analysis, US Forest Service) data considers the atmospheric and ecological process of overall

carbon though their sub-cycle period data inventory (Schimel and Chadwick, 2013; USFS, 2016). FIA counts all the sampled trees inside the plot and subplot during the survey cycle. Hence, little uncertainty and minimal error of carbon estimation is ensured considering geographical and soil physiographic variance (USFS, 2018). To ascertain the accuracy of our carbon results, we used InVEST vs. FIA differences to oversee the estimated carbon in both the InVEST model and FIA using NLCD 2021 data. Our InVEST model result of carbon estimation has a closer match with FIA; average carbon storage resulted in InVEST ~ 328.79 metric tons/ha, and average carbon storage reported in FIA 2021 ~ 348.91 metric tons/ha. Figure 4.13 shows the relative estimated difference of overall carbon (metric tons) between InVEST Carbon Storage and Sequestration Model and FIA. Our estimation shows that about 2%-15% of carbon was underestimated in the InVEST model compared to the FIA estimated carbon for 2021. Carbon in barren land and wetlands was overestimated by 3% and 15%, respectively. Open space (10.71%) and forestland (15.25%) show higher variability in estimation using baseline NLCD 2001 for the InVEST model. These confer complex carbon cycle, and its associated dynamics bring uncertainty in estimating carbon for future land use.

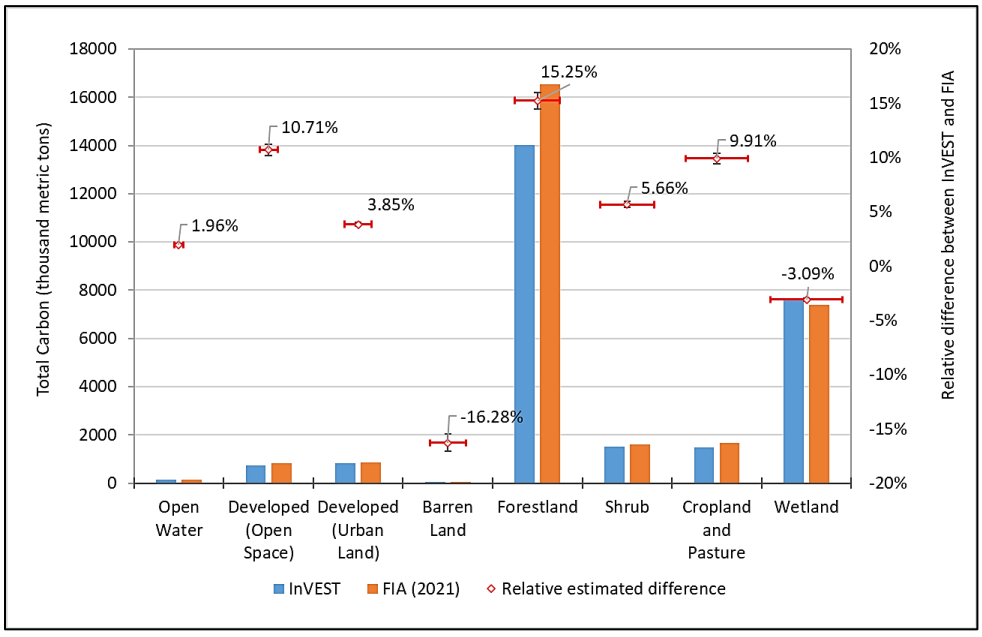

Figure 4.13: Relative estimated difference of overall carbon (metric tons) between InVEST Carbon Storage and Sequestration Model and FIA (2021). Error bars show the variability of InVEST model output and reported carbon value as per FIA 2021.

Finally, while most sequestration follows a nonlinear path such that carbon is sequestered at a higher rate in the first few years and a lower rate in subsequent years, the model's valuation of carbon sequestration assumes a linear change in carbon storage over time. Due to discounting, the assumption of a constant rate of change will tend to undervalue sequestered carbon, as a nonlinear path of sequestration is more socially acceptable than a linear path.

4.5 Conclusion

Hurricanes have the capacity to reshape the urban landscape, alter the way we conserve forests, and influence the long-term carbon balance. In our investigation of these effects, we utilized the Multi-Layer Perceptron-Cellular Automata (MLP-CA) model to predict future land use in 2050 and the InVEST model to quantify carbon storage in the Perdido Bay watershed. The MLP-CA model was employed to simulate six distinct land use scenarios. When compared to the conditions in 2021, the urban land area in these scenarios ranged from 5.28% to 6.12%, while the forested area spanned from 40.30% to 48.71%. Notably, scenarios LUR+FR50% and HUR+FR50% showed little difference in forest conservation compared to LUR+FR25% and HUR+FR25%. Shrubland is also expected to decrease from current levels to FR25% and FR50% scenarios, declining by 4.05% and 1.46% in high urban growth scenarios and by 5.05% and 0.53% in low urban growth scenarios. Cropland and pasture are projected to decrease by 1.87% to 0.85% in FR25% and FR50% scenarios. Our InVEST model reveals increased carbon storage within forested areas, shrubland, cropland, and pasture. As hurricane scenarios progress from 25% to 50%, overall carbon storage in forested areas ranges from 493.31 thousand metric tons to 666.85 thousand metric tons under low urban growth and from 487.70 thousand metric tons to 652.01 thousand metric tons under high urban growth. Carbon loss in shrubland ranges from 4.28 thousand metric tons to 7.59 thousand metric tons. Cropland and pasture are expected to lose approximately 3.98 thousand metric tons to 8.11 thousand metric tons of carbon with a 50% increase in hurricane intensity.

Although future urban land and forestland are growing as per our MLP-CA model, a satellite-based (i.e., Landsat, Sentinel, etc.) image analysis could be a great tip for this kind of research. NLCD data has been serving enormously over the years to scientists, policymakers, and

landowners. Satellite-based analysis and projection with recent time data could provide a more precise estimation on land use change. In addition, future research could emphasize the inclusion of climate factors, i.e., hurricane intensity, wind speed, storm surge, etc. in the MLP-CA model. This will allow us to trigger the uncertainties in the prediction model. Correspondingly, more research needs to be done to eliminate the limitations of the InVEST model, particularly on non-linear carbon cycles with actual sequestration paths.

Supplementary Tables

Table S4.1: Future forestland scenarios in Perdido due to 25% and 50% increase of hurricanes from 2021 level. Unit are in km^2.

	Current Level			25% Increase			50% Increase		
County	**Sell**	**Convert**	**Conserve**	**Sell**	**Convert**	**Conserve**	**Sell**	**Convert**	**Conserve**
Escambia	29.67	15.29	12.54	20.69	17.50	12.00	36.18	23.12	11.66
Bay	103.86	609.25	244.69	444.25	606.74	429.60	461.68	616.35	433.65
Baldwin	37.84	91.94	42.81	46.48	98.80	34.89	59.12	119.72	37.65
Total (km^2)	69.34	289.89	121.40	206.92	292.54	192.79	225.35	307.16	195.40

Table S4.2: InVEST model output for aboveground, belowground, soil organic and dead organic carbon in six different scenarios across all land use classes. Units in this table are in metric tons/km^2. LUR and HUR indicate low and high urbanization rates. CFR indicates current forestlands at the present rate of hurricane risks. FR25% and FR50% indicate changes in forestlands relative to increased (25% and 50%) hurricane risks.

	LUR+FR50%			
Land Class	**Aboveground Carbon**	**Belowground Carbon**	**Soil Organic Carbon**	**Dead Organic Carbon**
Open Water	19.96	8.56	48.61	2.15
Developed (Open Space)	23.71	9.42	34.25	1.60
Developed (Urban Land)	18.28	8.51	30.49	1.34
Barren Land	13.00	6.39	33.60	1.33
Forestland	45.05	14.68	56.11	2.32
Shrub	43.29	14.13	54.13	2.32
Cropland and Pasture	10.68	4.00	26.27	1.22
Wetland	56.09	16.72	56.92	2.43
	LUR+FR25%			
Land Class	**Aboveground Carbon**	**Belowground Carbon**	**Soil Organic Carbon**	**Dead Organic Carbon**
Open Water	19.96	8.56	48.61	2.15
Developed (Open Space)	23.71	9.42	34.25	1.60
Developed (Urban Land)	18.28	8.51	30.49	1.34
Barren Land	13.00	6.39	33.60	1.33
Forestland	45.59	14.85	56.57	2.33
Shrub	43.96	14.30	54.54	2.33
Cropland and Pasture	10.75	4.01	26.40	1.23
Wetland	56.09	16.72	56.92	2.43
	LUR+CFR			
Land Class	**Aboveground Carbon**	**Belowground Carbon**	**Soil Organic Carbon**	**Dead Organic Carbon**
Open Water	19.96	8.56	48.61	2.15
Developed (Open Space)	23.71	9.42	34.25	1.60
Developed (Urban Land)	18.28	8.51	30.49	1.34

Barren Land	13.00	6.39	33.60	1.33
Forestland	45.84	15.09	57.10	2.38
Shrub	48.63	15.20	56.92	2.29
Cropland and Pasture	11.20	4.14	27.29	1.26
Wetland	56.09	16.72	56.92	2.43

HUR+FR50%

Land Class	Aboveground Carbon	Belowground Carbon	Soil Organic Carbon	Dead Organic Carbon
Open Water	20.00	8.56	48.60	2.16
Developed (Open Space)	24.31	9.48	34.82	1.67
Developed (Urban Land)	18.71	8.61	30.70	1.34
Barren Land	13.02	6.40	33.64	1.33
Forestland	44.83	14.60	55.91	2.31
Shrub	43.34	14.15	54.17	2.32
Cropland and Pasture	10.66	4.01	26.26	1.22
Wetland	56.09	16.72	56.92	2.43

HUR+FR25%

Land Class	Aboveground Carbon	Belowground Carbon	Soil Organic Carbon	Dead Organic Carbon
Open Water	20.00	8.56	48.60	2.16
Developed (Open Space)	24.31	9.48	34.82	1.67
Developed (Urban Land)	18.71	8.61	30.70	1.34
Barren Land	13.02	6.40	33.64	1.33
Forestland	45.32	14.78	56.42	2.33
Shrub	45.05	14.57	55.17	2.33
Cropland and Pasture	10.85	4.04	26.42	1.23
Wetland	56.09	16.72	56.92	2.43

HUR+CFR

Land Class	Aboveground Carbon	Belowground Carbon	Soil Organic Carbon	Dead Organic Carbon
Open Water	20.00	8.56	48.60	2.16
Developed (Open Space)	24.31	9.48	34.82	1.67
Developed (Urban Land)	18.71	8.61	30.70	1.34
Barren Land	13.02	6.40	33.64	1.33
Forestland	45.85	15.09	57.10	2.38
Shrub	48.63	15.20	56.93	2.29
Cropland and Pasture	11.20	4.14	27.29	1.26
Wetland	56.09	16.72	56.92	2.43

CHAPTER 5

CONCLUSION

My dissertation on the sustainability of forestry resources at the nexus of changing land use and climate in the Gulf Coast of Panhandle Florida sheds light on the intricate relationship between extreme weather events and ecological factors. The findings of my research underscore the urgency of addressing ecologically critical issues to ensure the long-term sustainability of forestry resources in the region.

Chapter 2 reveals that using vegetation based indices with satellite imageries helps to identify potential hotspots of canopy loss after a major hurricane event. My findings demonstrate the effectiveness of applying optimized hotspot analysis and optimized outlier analysis to identify groups of changes in the urban green canopy that are connected to water content enrichment following Hurricane Michael. Estimating the changes in forest canopy after a major hurricane event can inform us of the ecological imbalances in forest health. Moreover, adding hotspots of canopy loss in the analysis explains more ecologically critical forests in a given geographic location. Hence, understanding the spatiotemporal variation in hazard occurrence is one of many things that can help identify the areas where mitigation projects are most necessary.

Chapter 3 concludes with statistical evidence of aboveground carbon reduction in different physiological parameters of forests after a catastrophic hurricane swept out. My study found that ‘stand type’, ‘height’, ‘physiographic classes’, and hurricane ‘affected status’ of the FIA plots are statistically significant factors while evaluating aboveground carbon change. Again, these factors are distributed in sapling, stump, bole and top of each FIA sampled plot. The rate of aboveground carbon change in foliage is observed to be higher than that of trees, and foliage carbon is a major source of energy and nutrients for many organisms in ecosystems. Therefore, adding foliage carbon to the analysis provides a new avenue to see the carbon dynamics after a major hurricane.

Due to its natural beauty and prospect of ocean side real estate, Gulf Coast historically attracts tourists and business. Urban expansion is expected, and it continuously grows regardless of how hurricanes react in built environments. Chapter 4 suggests urban expansion and forestland will increase at the end of 2050 despite the fact of increased frequency and intensity of catastrophic hurricane in the Gulf Coast. I evaluated the landowner's perspective on forestland conservation and fed the probability of forestland conservation in the land use prediction model. As more hurricanes come, more landowners conserve their croplands and existing forestlands to forestlands. These changes are well associated with the future scenarios of conservation easements in the Gulf Coast. Correspondingly, more carbon will be stored in the conservation easements and the rate of carbon sequestration will go higher than the rate of baseline. We try to evaluate future land use not only to bring environmental sustainability but also to raise awareness among the stakeholders about the significance of ecosystem services amid the increasing impact of hurricanes and other extreme weather events.

My research has revealed that the Gulf Coast of Panhandle Florida faces substantial challenges in preserving its forestry resources and ecosystem services. With increasing urbanization and shifting land use patterns, the delicate balance between human development and the natural environment has been disrupted. Moreover, the impacts of climate change are becoming more evident, affecting forest health and productivity. These dual challenges threaten the sustainability of forestry resources, which are not only vital for economic activities but also crucial for maintaining and enhancing the flow of ecosystem services. To address these challenges, it is imperative that stakeholder groups, including government bodies, landowners, conservation organizations, and local communities, collaborate to implement sustainable forestry management practices. This should involve the protection and restoration of critical forest ecosystems, as well as the development of resilient forestry strategies that can adapt to changing climatic conditions. Additionally, the integration of scientific research and traditional knowledge can play a significant role in identifying the most effective solutions.

REFERENCES

Abd El-Hamid, H.T., Hafiz, M.A., 2022. Modeling of carbon sequestration with land use and land cover in the northeastern part of the Nile Delta, Egypt. Arabian Journal of Geosciences 15, 1–12. https://doi.org/10.1007/s12517-022-10462-2

Abdul-Hamid, H., Mohamad-Ismail, F.N., Mohamed, J., Samdin, Z., Abiri, R., Tuan-Ibrahim, T.M., Mohammad, L.S., Jalil, A.M., Naji, H.R., 2022. Allometric Equation for Aboveground Biomass Estimation of Mixed Mature Mangrove Forest. Forests 13, 1–18. https://doi.org/10.3390/f13020325

Ades, M., Adler, R., Aldred, F., Allan, R.P., Anderson, J., Anneville, O., Aono, Y., Argüez, A., Arosio, C., Augustine, J.A., Azorin-Molina, C., Barichivich, J., Basu, A., Beck, H.E., Bellouin, N., Benedetti, A., Blagrave, K., Blenkinsop, S., Bock, O., Bodin, X., Bosilovich, M.G., Boucher, O., Bove, G., Buechler, D., Buehler, S.A., Carrea, L., Chang, K.L., Christiansen, H.H., Christy, J.R., Chung, E.S., Ciasto, L.M., Coldewey-Egbers, M., Cooper, O.R., Cornes, R.C., Covey, C., Cropper, T., Crotwell, M., Cusicanqui, D., Davis, S.M., de Jeu, R.A.M., Degenstein, D., Delaloye, R., Donat, M.G., Dorigo, W.A., Dunn, R.J.H., Durre, I., Dutton, G.S., Duveiller, G., Elkins, J.W., Estilow, T.W., Fedaeff, N., Fereday, D., Fioletov, V.E., Flemming, J., Foster, M.J., Frith, S.M., Froidevaux, L., Füllekrug, M., Garforth, J., Garg, J., Gentry, M., Gobron, N., Goodman, S., Gou, Q., Granin, N., Guglielmin, M., Hahn, S., Haimberger, L., Hall, B.D., Harris, I., Hemming, D.L., Hirschi, M., Ho, S.P., Holzworth, R., Hrbáček, F., Hubert, D., Hulsman, P., Hurst, D.F., Inness, A., Isaksen, K., John, V.O., Jones, P.D., Junod, R., Kääb, A., Kaiser, J.W., Kaufmann, V., Kellerer-Pirklbauer, A., Kent, E.C., Kidd, R., Kim, H., Kipling, Z., Koppa, A., L'Abée-Lund, J.H., Lan, X., Lantz, K.O., Lavers, D., Loeb, N.G., Loyola, D., Madelon, R., Malmquist, H.J., Marszelewski, W., Mayer, M., McCabe, M.F., McVicar, T.R., Mears, C.A., Menzel, A., Merchant, C.J., Miller, J.B., Miralles, D.G., Montzka, S.A., Morice, C., Mösinger, L., Mühle, J., Nicolas, J.P., Noetzli, J., Nõges, T., Noll, B., O'Keefe, J., Osborn, T.J., Park, T., Pellet, C., Pelto, M.S., Perkins-Kirkpatrick, S.E., Phillips, C., Po-Chedley, S., Polvani, L., Preimesberger, W., Price, C., Pulkkanen, M., Rains, D.G., Randel, W.J., Rémy, S., Ricciardulli, L., Richardson, A.D., Robinson, D.A., Rodell, M., Rodríguez-Fernández, N.J., Rosenlof, K.H., Roth, C., Rozanov, A., Rutishäuser, T., Sánchez-Lugo, A., Sawaengphokhai, P., Schenzinger, V., Schlegel, R.W., Schneider, U., Sharma, S., Shi, L., Simmons, A.J., Siso, C., Smith, S.L., Soden, B.J., Sofieva, V., Sparks, T.H., Stackhouse, P.W., Stauffer, R., Steinbrecht, W., Steiner, A.K., Stewart, K., Stradiotti, P., Streletskiy, D.A., Telg, H., Thackeray, S.J., Thibert, E., Todt, M., Tokuda, D., Tourpali, K., Tye, M.R., Van Der, A.R., van der Schalie, R., van der Schrier, G., van der Vliet, M., van der Werf, G.R., van Vliet, A., Vernier, J.P., Vimont, I.J., Virts, K., Vivero, S., Vömel, H., Vose, R.S., Wang, R.H.J., Weber, M., Wiese, D., Wild, J.D., Willett, K.M., Williams, E., Wong, T., Woolway, R.I., Yin, X., Yuan, Y., Zhao, L., Zhou, X., Ziemke, J.R., Ziese, M., Zotta, R.M., Allen, J., Camper, A., Hammer, G., Love-Brotak, S.E., Misch, D.J., Ohlmann, L., Riddle, D.B., Veasey, S.W., 2022. GLOBAL CLIMATE. Bull Am Meteorol Soc 103, S11–S142. https://doi.org/10.1175/BAMS-D-22-0092.1

Alabama Forestry Commission, 2022. Assessing and Managing Storm-Damaged Timber - Alabama Cooperative Extension System [WWW Document]. URL https://www.aces.edu/blog/topics/forestry/assessing-and-managing-storm-damaged-timber/ (accessed 10.10.23).

Amazon, 2015. USGS Landsat - Registry of Open Data on AWS [WWW Document]. URL https://registry.opendata.aws/usgs-landsat/ (accessed 8.8.22).

Anselin, L., 1995. Local Indicators of Spatial Association—LISA. Geogr Anal 27, 93–115. https://doi.org/10.1111/j.1538-4632.1995.tb00338.x

Aosier, B., Kaneko, M., Takada, M., 2007. Evaluation of the forest damage by typhoon using remote sensing technique. International Geoscience and Remote Sensing Symposium (IGARSS) 3022–3026. https://doi.org/10.1109/IGARSS.2007.4423481

Arco, J.E., Ortiz, A., Ramírez, J., Martínez-Murcia, F.J., Zhang, Y.D., Górriz, J.M., 2022. Uncertainty-driven ensembles of multi-scale deep architectures for image classification. Information Fusion 89, 53–65. https://doi.org/10.1016/j.inffus.2022.08.010

Arneth, A., Sitch, S., Pongratz, J., Stocker, B.D., Ciais, P., Poulter, B., Bayer, A.D., Bondeau, A., Calle, L., Chini, L.P., Gasser, T., Fader, M., Friedlingstein, P., Kato, E., Li, W., Lindeskog, M., Nabel, J.E.M.S., Pugh, T.A.M., Robertson, E., Viovy, N., Yue, C., Zaehle, S., 2017. Historical carbon dioxide emissions caused by land-use changes are possibly larger than assumed. Nat Geosci 10, 79–84. https://doi.org/10.1038/ngeo2882

Auret, L., Aldrich, C., 2012. Interpretation of nonlinear relationships between process variables by use of random forests. Miner Eng 35, 27–42. https://doi.org/10.1016/j.mineng.2012.05.008

Ayala-Silva, T., Twumasi, Y.A., 2004. Hurricane Georges and vegetation change in Puerto Rico using AVHRR satellite data. Int J Remote Sens 25, 1629–1640. https://doi.org/10.1080/01431160310001595037

Barbato, C.T., Strong, A.L., 2017. Farmer perspectives on carbon markets incentivizing agricultural soil carbon sequestration. NPJ Climate Action 2. https://doi.org/10.1038/s44168-023-00055-4

Beach, R.H., Sills, E.O., Liu, T.-M., Pattanayak, S., 2010. Advances in Threat Assessment and Their Application to Forest and Rangeland Management The Influence of Forest Management on Vulnerability of Forests to Severe Weather. Advances in Threat Assessment and Their Application to Forest and Rangeland Management PNW-GTR-80, 185–206.

Benedetti, J.K., Brown, M.B., 1978. Strategies for the Selection of Log-Linear Models. International Biometric Society 34, 680–686.

Blake, E.S., Rappaport, E.N., Jarrell, J.D., Landsea, C.W., 2005. The deadliest, costliest, and most intense united states tropical cyclones from 1851 to 2004 (and other frequently requested hurricane facts). Florida.

Blennow, K., Sallnäs, O., 2004. WINDA - A system of models for assessing the probability of wind damage to forest stands within a landscape. Ecol Modell 175, 87–99. https://doi.org/10.1016/j.ecolmodel.2003.10.009

Brandeis, T., Turner, J., Baeza Castro, A., Brown, M., Lambert, S., 2022. Assessing forest resource damage following natural disasters using national forest inventory plots. https://doi.org/10.2737/SRS-RP-65

Breiman, L., 2001. Random Forests. Machine Learning, 45, 5–32. Kluwer Academic Publishers. The Netherlands

Buotte, P.C., Law, B.E., Ripple, W.J., Berner, L.T., 2020. Carbon sequestration and biodiversity co-benefits of preserving forests in the western United States. Ecological Applications 30, 1–11. https://doi.org/10.1002/eap.2039

Burnham, K.P., Anderson, D.R., 2004. Multimodel inference: Understanding AIC and BIC in model selection. Sociol Methods Res 33, 261–304. https://doi.org/10.1177/0049124104268644

Castañeda-Moya, E., Rivera-Monroy, V.H., Chambers, R.M., Zhao, X., Lamb-Wotton, L., Gorsky, A., Gaiser, E.E., Troxler, T.G., Kominoski, J.S., Hiatt, M., 2020a. Hurricanes fertilize mangrove forests in

the Gulf of Mexico (Florida Everglades, USA). Proc Natl Acad Sci U S A 117, 4831–4841. https://doi.org/10.1073/pnas.1908597117

Chambers, J.Q., Fisher, J.I., Zeng, H., Chapman, E.L., Baker, D.B., Hurtt, G.C., 2007. Hurricane Katrina's carbon footprint on U.S. Gulf Coast forests. Science (1979) 318, 1107. https://doi.org/10.1126/science.1148913

Chan, D., Vecchi, G.A., Yang, W., Huybers, P., 2021. Improved simulation of 19th-and 20th-century North Atlantic hurricane frequency after correcting historical sea surface temperatures. Sci Adv 7. https://doi.org/10.1126/SCIADV.ABG6931

Chen, B., Huang, B., Xu, B., 2017. Multi-source remotely sensed data fusion for improving land cover classification. ISPRS Journal of Photogrammetry and Remote Sensing 124, 27–39. https://doi.org/10.1016/j.isprsjprs.2016.12.008

Chevalier, H., Brokaw, N.V.L., Ward, S.E., Zimmerman, J.K., Shiels, A.B., Bithorn, J., Matta Carmona, S., 2022b. Aboveground carbon responses to experimental and natural hurricane impacts in a subtropical wet forest in Puerto Rico. Ecosphere 13. https://doi.org/10.1002/ECS2.4041

Claeskens, G., Jansen, M., 2015. Model Selection and Model Averaging. International Encyclopedia of the Social & Behavioral Sciences: Second Edition 647–652. https://doi.org/10.1016/B978-0-08-097086-8.42057-X

Clerici, N., Rubiano, K., Abd-Elrahman, A., Hoestettler, J.M.P., Escobedo, F.J., 2016. Estimating aboveground biomass and carbon stocks in periurban Andean secondary forests using very high resolution imagery. Forests 7. https://doi.org/10.3390/f7070138

Cochran, W.G., 1977. Sampling Techniques, 3rd Edition.

Cole, J., Nowak, D.J., Greenfield Jason Cole jasoncole, E.J., Nowak davidnowak, D.J., Greenfield, E.J., 2021. Potential Hurricane Wind Risk to US Rural and Urban Forests. J For 119, 393–406. https://doi.org/10.1093/jofore/fvab018

Columbia Public Health, 2019. False Discovery Rate | Columbia Public Health [WWW Document]. URL https://www.publichealth.columbia.edu/research/population-health-methods/false-discovery-rate (accessed 7.25.22).

Coulston, J.W., Wear, D.N., Vose, J.M., 2015. Complex forest dynamics indicate potential for slowing carbon accumulation in the southeastern United States. Sci Rep 5, 8002. https://doi.org/10.1038/srep08002

Delphin, S., Escobedo, F.J., Abd-Elrahman, A., Cropper, W., 2013. Mapping potential carbon and timber losses from hurricanes using a decision tree and ecosystem services driver model. J Environ Manage 129, 599–607. https://doi.org/10.1016/j.jenvman.2013.08.029

Dong, J., Xiao, X., Menarguez, M.A., Zhang, G., Qin, Y., Thau, D., Biradar, C., Moore, B., 2016. Mapping paddy rice planting area in northeastern Asia with Landsat 8 images, phenology-based algorithm and Google Earth Engine. Remote Sens Environ 185, 142–154. https://doi.org/10.1016/J.RSE.2016.02.016

Emanuel, K., 2021. Atlantic tropical cyclones downscaled from climate reanalyses show increasing activity over past 150 years. Nat Commun 12, 1–8. https://doi.org/10.1038/s41467-021-27364-8

EOS, 2019. Normalized Difference Water Index: NDWI Formula And Calculations [WWW Document]. URL https://eos.com/make-an-analysis/ndwi/ (accessed 4.19.22).

EPA, 2019. Coastal Wetlands Initiative: Gulf of Mexico Review (EPA-843-R-10-005D).

ESRI, 2022. Change Detection in Amazon Floodplains Using Landsat Time Series, ESRI Blog.

ESRI, 2019a. How Hot Spot Analysis (Getis-Ord Gi*) works—ArcGIS Pro | Documentation [WWW Document]. URL https://pro.arcgis.com/en/pro-app/2.8/tool-reference/spatial-statistics/h-how-hot-spot-analysis-getis-ord-gi-spatial-stati.htm (accessed 4.27.22).

ESRI, 2019b. What is a z-score? What is a p-value?—Help | ArcGIS Desktop [WWW Document]. URL https://desktop.arcgis.com/en/arcmap/10.5/tools/spatial-statistics-toolbox/what-is-a-z-score-what-is-a-p-value.htm (accessed 7.25.22).

ESRI, 2019c. How Cluster and Outlier Analysis (Anselin Local Moran's I) works—ArcGIS Pro | Documentation [WWW Document]. URL https://pro.arcgis.com/en/pro-app/2.8/tool-reference/spatial-statistics/h-how-cluster-and-outlier-analysis-anselin-local-m.htm (accessed 6.18.22).

Fabozzi, F.J., Focardi, S.M., Rachev, S.T., Arshanapalli, B.G., 2014b. Model Selection Criterion: AIC and BIC. The Basics of Financial Econometrics 41, 399–403. https://doi.org/10.1002/9781118856406.app5

Fahey, T.J., Woodbury, P.B., Battles, J.J., Goodale, C.L., Hamburg, S.P., Ollinger, S. V., Woodall, C.W., 2010. Forest carbon storage: Ecology, management, and policy. Front Ecol Environ 8, 245–252. https://doi.org/10.1890/080169

FEMA, 2018. Mitigation Best Practices | FEMA.gov [WWW Document]. URL https://www.fema.gov/emergency-managers/risk/hazard-mitigation-planning/best-practices (accessed 8.8.22).

Foga, S., Scaramuzza, P.L., Guo, S., Zhu, Z., Dilley, R.D., Beckmann, T., Schmidt, G.L., Dwyer, J.L., Joseph Hughes, M., Laue, B., 2017. Cloud detection algorithm comparison and validation for operational Landsat data products. Remote Sens Environ 194, 379–390. https://doi.org/10.1016/J.RSE.2017.03.026

Geidarov, P.S., 2017. Clearly defined architectures of neural networks and multilayer perceptron. Optical Memory and Neural Networks (Information Optics) 26, 62–76. https://doi.org/10.3103/S1060992X16040044

Getis, A., Ord, J.K., 1992. The Analysis of Spatial Association by Use of Distance Statistics. Geogr Anal 24, 189–206. https://doi.org/10.1111/j.1538-4632.1992.tb00261.x

GFDL, 2023. Global Warming and Hurricanes – Geophysical Fluid Dynamics Laboratory [WWW Document]. URL https://www.gfdl.noaa.gov/global-warming-and-hurricanes/ (accessed 11.16.23).

Giri, C., Pengra, B., Long, J., Loveland, T.R., 2013. Next generation of global land cover characterization, mapping, and monitoring. International Journal of Applied Earth Observation and Geoinformation 25, 30–37. https://doi.org/10.1016/J.JAG.2013.03.005

Google Earth Engine, 2019. Compositing and Mosaicking | Google Earth Engine | Google Developers [WWW Document]. URL https://developers.google.com/earth-engine/guides/ic_composite_mosaic (accessed 7.25.22).

Gorelick, N., Hancher, M., Dixon, M., Ilyushchenko, S., Thau, D., Moore, R., 2017. Google Earth Engine: Planetary-scale geospatial analysis for everyone. Remote Sens Environ 202, 18–27. https://doi.org/10.1016/J.RSE.2017.06.031

Grafius, D.R., Corstanje, R., Warren, P.H., Evans, K.L., Hancock, S., Harris, J.A., 2016. The impact of land use/land cover scale on modelling urban ecosystem services. Landsc Ecol 31, 1509–1522. https://doi.org/10.1007/s10980-015-0337-7

Guan, D.J., Li, H.F., Inohae, T., Su, W., Nagaie, T., Hokao, K., 2011. Modeling urban land use change by the integration of cellular automaton and Markov model. Ecol Modell 222, 3761–3772. https://doi.org/10.1016/J.ECOLMODEL.2011.09.009

Guo, L., Liu, R., Men, C., Wang, Q., Miao, Y., Shoaib, M., Wang, Y., Jiao, L., Zhang, Y., 2021. Multiscale spatiotemporal characteristics of landscape patterns, hotspots, and influencing factors for soil erosion. Science of the Total Environment 779, 146474. https://doi.org/10.1016/j.scitotenv.2021.146474

Hakim, W.L., Lee, S.K., Lee, C.W., 2021. Land Subsidence Monitoring in Semarang, Indonesia Through Optimized Hot Spot Analysis Based on Time-Series Insar Processing. International Geoscience and Remote Sensing Symposium (IGARSS) 3789–3792. https://doi.org/10.1109/IGARSS47720.2021.9554374

Halunga, A.G., Orme, C.D., Yamagata, T., 2017. A heteroskedasticity robust Breusch-Pagan test for Contemporaneous correlation in dynamic panel data models ☆. J Econom 198, 209–230. https://doi.org/10.1016/j.jeconom.2016.12.005

Hanewinkel, M., Kuhn, T., Bugmann, H., Lanz, A., Brang, P., 2014. Vulnerability of uneven-aged forests to storm damage. Forestry 87, 525–534. https://doi.org/10.1093/forestry/cpu008

Hansen, M.C., Potapov, P. V., Moore, R., Hancher, M., Turubanova, S.A., Tyukavina, A., Thau, D., Stehman, S. V., Goetz, S.J., Loveland, T.R., Kommareddy, A., Egorov, A., Chini, L., Justice, C.O., Townshend, J.R.G., 2013. High-resolution global maps of 21st-century forest cover change. Science (1979) 342, 850–853. https://doi.org/10.1126/SCIENCE.1244693/SUPPL_FILE/HANSEN.SM.PDF

Hanssen, F., Barton, D.N., Venter, Z.S., Nowell, M.S., Cimburova, Z., 2021. Utilizing LiDAR data to map tree canopy for urban ecosystem extent and condition accounts in Oslo. Ecol Indic 130, 108007. https://doi.org/10.1016/j.ecolind.2021.108007

Harris, N.L., Goldman, E., Gabris, C., Nordling, J., Minnemeyer, S., Ansari, S., Lippmann, M., Bennett, L., Raad, M., Hansen, M., Potapov, P., 2017. Using spatial statistics to identify emerging hot spots of forest loss. Environmental Research Letters 12. https://doi.org/10.1088/1748-9326/aa5a2f

Hauser, S., Meixler, M.S., Laba, M., 2015. Quantification of Impacts and Ecosystem Services Loss in New Jersey Coastal Wetlands Due to Hurricane Sandy Storm Surge. Wetlands 35, 1137–1148. https://doi.org/10.1007/S13157-015-0701-Z/FIGURES/6

He, C., Zhang, D., Huang, Q., Zhao, Y., 2016. Assessing the potential impacts of urban expansion on regional carbon storage by linking the LUSD-urban and InVEST models. Environmental Modelling & Software 75, 44–58. https://doi.org/10.1016/J.ENVSOFT.2015.09.015

Heinze, G., Wallisch, C., Dunkler, D., 2018. Variable selection – A review and recommendations for the practicing statistician. Biometrical Journal 60, 431–449. https://doi.org/10.1002/bimj.201700067

Henderson, J.D., Abt, R.C., Abt, K.L., Baker, J., Sheffield, R., 2022. Impacts of hurricanes on forest markets and economic welfare: The case of hurricane Michael. For Policy Econ 140, 102735. https://doi.org/10.1016/j.forpol.2022.102735

Homer, C., Dewitz, J., Jin, S., Xian, G., Costello, C., Danielson, P., Gass, L., Funk, M., Wickham, J., Stehman, S., Auch, R., Riitters, K., 2020. Conterminous United States land cover change patterns 2001–2016 from the 2016 National Land Cover Database. ISPRS Journal of Photogrammetry and Remote Sensing 162, 184–199. https://doi.org/10.1016/J.ISPRSJPRS.2020.02.019

Hoover, C.M., Smith, J.E., 2023. Aboveground live tree carbon stock and change in forests of conterminous United States: influence of stand age. Carbon Balance and Management 2023 18:1 18, 1–11. https://doi.org/10.1186/S13021-023-00227-Z

Houghton, R.A., House, J.I., Pongratz, J., Van Der Werf, G.R., Defries, R.S., Hansen, M.C., Le Quéré, C., Ramankutty, N., 2012. Carbon emissions from land use and land-cover change. Biogeosciences 9, 5125–5142. https://doi.org/10.5194/bg-9-5125-2012

Hsieh, T.L., Vecchi, G.A., Yang, W., Held, I.M., Garner, S.T., 2020. Large-scale control on the frequency of tropical cyclones and seeds: a consistent relationship across a hierarchy of global atmospheric models. Clim Dyn 55, 3177–3196. https://doi.org/10.1007/S00382-020-05446-5

Hung, M.C., Ridd, M.K., 2002. A subpixel classifier for urban land-cover mapping based on a maximum-likelihood approach and expert system rules. Photogramm Eng Remote Sensing 68, 1173–1180.

Hurvich, C.M., Tsai, C.L., 1989. Regression and time series model selection in small samples. Biometrika 76, 297–307. https://doi.org/10.1093/biomet/76.2.297

IPCC, 2023a. Summary for Policymakers: Synthesis Report., Climate Change 2023: Synthesis Report. Contribution of Working Groups I, II and III to the Sixth Assessment Report of the Intergovernmental Panel on Climate Change.

IPCC, 2023b. Climate Change Synthesis Report, Intergovernmental Panel on Climate Change.

IPCC, 2015. Climate Change 2014 Synthesis Report, Journal of Crystal Growth. Geneva. https://doi.org/10.1016/S0022-0248(00)00575-3

IPCC, 2014. Climate Change 2014: Synthesis Report. https://doi.org/10.1017/CBO9781139177245.003

Jehn, F.U., Kemp, L., Ilin, E., Funk, C., Wang, J.R., Breuer, L., 2022. Focus of the IPCC Assessment Reports Has Shifted to Lower Temperatures. Earths Future 10. https://doi.org/10.1029/2022EF002876

Jones, M.C., Bernhardt, C.E., Krauss, K.W., Noe, G.B., 2017. The Impact of Late Holocene Land Use Change, Climate Variability, and Sea Level Rise on Carbon Storage in Tidal Freshwater Wetlands on the Southeastern United States Coastal Plain. J Geophys Res Biogeosci 122, 3126–3141. https://doi.org/10.1002/2017JG004015

Joshi, A. V., 2023. Perceptron and Neural Networks. Machine Learning and Artificial Intelligence 57–72. https://doi.org/10.1007/978-3-031-12282-8_6

Karnauskas, M., Kelble, C.R., Regan, S., Quenée, C., Allee, R., Jepson, M., Freitag, A., Craig, J.K., Carollo, C., Barbero, L., 2017. ECOSYSTEM STATUS REPORT UPDATE FOR THE GULF OF MEXICO.

Kay, S., Rega, C., Moreno, G., den Herder, M., Palma, J.H.N., Borek, R., Crous-Duran, J., Freese, D., Giannitsopoulos, M., Graves, A., Jäger, M., Lamersdorf, N., Memedemin, D., Mosquera-Losada, R., Pantera, A., Paracchini, M.L., Paris, P., Roces-Díaz, J. V., Rolo, V., Rosati, A., Sandor, M., Smith, J., Szerencsits, E., Varga, A., Viaud, V., Wawer, R., Burgess, P.J., Herzog, F., 2019. Agroforestry creates carbon sinks whilst enhancing the environment in agricultural landscapes in Europe. Land use policy 83, 581–593. https://doi.org/10.1016/j.landusepol.2019.02.025

Kemp, L., Xu, C., Depledge, J., Ebi, K.L., Gibbins, G., Kohler, T.A., Rockstrom, J., Scheffer, M., Schellnhuber, H.J., Steffen, W., Lenton, T.M., 2022. Climate Endgame: Exploring catastrophic climate change scenarios. Proc Natl Acad Sci U S A 119, 1–9. https://doi.org/10.1073/pnas.2108146119

Kingdom, F.A.A., Prins, N., 2016. Model Comparisons. Psychophysics 247–307. https://doi.org/10.1016/B978-0-12-407156-8.00009-8

Kinnucan, H.W., 2016. Timber price dynamics after a natural disaster: Hurricane Hugo revisited. J For Econ 25, 115–129. https://doi.org/10.1016/j.jfe.2016.09.002

Köhl, M., Neupane, P.R., Lotfiomran, N., 2017. The impact of tree age on biomass growth and carbon accumulation capacity: A retrospective analysis using tree ring data of three tropical tree species grown in natural forests of Suriname. PLoS One 12, 1–17. https://doi.org/10.1371/journal.pone.0181187

Kuhn, A.L., Kominoski, J.S., Armitage, A.R., Charles, S.P., Pennings, S.C., Weaver, C.A., Maddox, T.R., 2021. Buried hurricane legacies: increased nutrient limitation and decreased root biomass in coastal wetlands. Ecosphere 12. https://doi.org/10.1002/ecs2.3674

Kumar, L., Mutanga, O., 2018. Google Earth Engine Applications Since Inception: Usage, Trends, and Potential. Remote Sensing 2018, Vol. 10, Page 1509 10, 1509. https://doi.org/10.3390/RS10101509

Lacerda, L.I. de A., da Silveira, J.A.R., Santos, C.A.G., da Silva, R.M., Silva, A.M., do Nascimento, T.V.M., Ribeiro, E.L., de Freitas, P.V.N., 2021. Urban forest loss using a GIS-based approach and instruments for integrated urban planning: A case study of João Pessoa, Brazil. Journal of Geographical Sciences 31, 1529–1553. https://doi.org/10.1007/s11442-021-1910-4

Lai, L., Huang, X., Yang, H., Chuai, X., Zhang, M., Zhong, T., Chen, Z., Chen, Y., Wang, X., Thompson, J.R., 2016. Carbon emissions from land-use change and management in China between 1990 and 2010. Sci Adv 2, 1–9. https://doi.org/10.1126/sciadv.1601063

Lam, N.S.N., Liu, K.B., Liang, W., Bianchette, T.A., Platt, W.J., 2011. Effects of Hurricanes on the Gulf Coast ecosystems: A remote sensing study of land cover change around Weeks Bay, Alabama. J Coast Res 1707–1711.

Landry, S.M., Koeser, A.K., Kane, B., Hilbert, D.R., McLean, D.C., Andreu, M., Staudhammer, C.L., 2021. Urban forest response to Hurricane Irma: The role of landscape characteristics and sociodemographic context. Urban For Urban Green 61, 127093. https://doi.org/10.1016/j.ufug.2021.127093

Lee, J., Weger, R.C., Sengupta, S.K., Welch, R.M., 1990. A Neural Network Approach to Cloud Classification. IEEE Transactions on Geoscience and Remote Sensing 28, 846–855. https://doi.org/10.1109/36.58972

Li, M., Zang, S., Zhang, B., Li, S., Wu, C., 2014. A review of remote sensing image classification techniques: The role of Spatio-contextual information. Eur J Remote Sens 47, 389–411. https://doi.org/10.5721/EuJRS20144723

Li, Q., Lu, L., Weng, Q., Xie, Y., Guo, H., 2016. Monitoring urban dynamics in the Southeast U.S.A. using time-series DMSP/OLS nightlight imagery. Remote Sens (Basel) 8, 13–15. https://doi.org/10.3390/rs8070578

Li, Y., Zhang, H., Xue, X., Jiang, Y., Shen, Q., 2018. Deep learning for remote sensing image classification: A survey. Wiley Interdiscip Rev Data Min Knowl Discov 8, 1–17. https://doi.org/10.1002/widm.1264

Liu, Y., Bi, J., Lv, J., Ma, Z., Wang, C., 2017. Spatial multi-scale relationships of ecosystem services: A case study using a geostatistical methodology. Sci Rep 7, 1–12. https://doi.org/10.1038/s41598-017-09863-1

Lu, X., Kicklighter, D.W., Melillo, J.M., Reilly, J.M., Xu, L., 2015. Land carbon sequestration within the conterminous United States: Regional- and state-level analyses. J Geophys Res Biogeosci 120, 379–98. https://doi.org/10.1002/2014jg002818

Lugo, A.E., 2008. Visible and invisible effects of hurricanes on forest ecosystems: An international review. Austral Ecol 33, 368–398. https://doi.org/10.1111/j.1442-9993.2008.01894.x

Lv, F., Deng, L., Zhang, Z., Wang, Z., Wu, Q., Qiao, J., 2022. Multiscale analysis of factors affecting food security in China, 1980–2017. Environmental Science and Pollution Research 29, 6511–6525. https://doi.org/10.1007/s11356-021-16125-1

Lyons, M.B., Keith, D.A., Phinn, S.R., Mason, T.J., Elith, J., 2018. A comparison of resampling methods for remote sensing classification and accuracy assessment. Remote Sens Environ 208, 145–153. https://doi.org/10.1016/j.rse.2018.02.026

Ma, W., Domke, G.M., D'Amato, A.W., Woodall, C.W., Walters, B.F., Deo, R.K., 2018. Using matrix models to estimate aboveground forest biomass dynamics in the eastern USA through various combinations of LiDAR, Landsat, and forest inventory data. Environmental Research Letters 13. https://doi.org/10.1088/1748-9326/aaeaa3

McNulty, S.G., 2002. Hurricane impacts on US forest carbon sequestration. Environmental Pollution 116, 17–24. https://doi.org/10.1016/S0269-7491(01)00242-1

Melson, S.L., Harmon, M.E., Fried, J.S., Domingo, J.B., 2011. Estimates of live-tree carbon stores in the Pacific Northwest are sensitive to model selection. Carbon Balance Manag 6, 1–16. https://doi.org/10.1186/1750-0680-6-2

Mendoza-González, G., Martínez, M.L., Lithgow, D., Pérez-Maqueo, O., Simonin, P., 2012. Land use change and its effects on the value of ecosystem services along the coast of the Gulf of Mexico. Ecological Economics 82, 23–32. https://doi.org/10.1016/J.ECOLECON.2012.07.018

Moody, R., Geron, N., Healy, M., Rogan, J., Martin, D., 2021. Modeling the spatial distribution of the current and future ecosystem services of urban tree planting in Chicopee and Fall River, Massachusetts. Urban For Urban Green 66, 127403. https://doi.org/10.1016/j.ufug.2021.127403

MRLC, 2023. Data | Multi-Resolution Land Characteristics (MRLC) Consortium [WWW Document]. URL https://www.mrlc.gov/data (accessed 9.28.23).

MRLC, 2017. Multi-Resolution Land Characteristics (MRLC) Consortium | Multi-Resolution Land Characteristics (MRLC) Consortium [WWW Document]. URL https://www.mrlc.gov/ (accessed 9.23.21).

Murdiyarso, D., Purbopuspito, J., Kauffman, J.B., Warren, M.W., Sasmito, S.D., Donato, D.C., Manuri, S., Krisnawati, H., Taberima, S., Kurnianto, S., 2015. The potential of Indonesian mangrove forests for global climate change mitigation. Nat Clim Chang 5, 1089–1092. https://doi.org/10.1038/nclimate2734

NASA, 2022. A Force of Nature: Hurricanes in a Changing Climate – Climate Change: Vital Signs of the Planet [WWW Document]. URL https://climate.nasa.gov/news/3184/a-force-of-nature-hurricanes-in-a-changing-climate/ (accessed 6.8.23).

NASA, 2021. NASA Earth Exchange | NASA [WWW Document]. URL https://www.nasa.gov/nex (accessed 8.8.22).

NASA, 2007a. Forests Damaged by Hurricane Katrina Become Major Carbon Source [WWW Document]. URL https://www.nasa.gov/mission_pages/hurricanes/archives/2007/katrina_carbon.html (accessed 3.27.23).

NASA, 2007b. Katrina Damage to Gulf Coast Forests [WWW Document]. URL https://earthobservatory.nasa.gov/images/8357/katrina-damage-to-gulf-coast-forests (accessed 8.5.22).

National Weather Service, 2018. Hurricane Michael 2018 [WWW Document]. URL https://www.weather.gov/tae/HurricaneMichael2018 (accessed 7.25.22).

National Weather Service, 2005. Hurricane Ivan - September 16, 2004 [WWW Document]. URL https://www.weather.gov/mob/ivan (accessed 4.3.23).

NCED, 2022. National Conservation Easement Database | NCED [WWW Document]. URL https://www.conservationeasement.us/ (accessed 9.10.23).

NCEI, 2022. Billion-Dollar Weather and Climate Disasters | National Centers for Environmental Information (NCEI) [WWW Document]. URL https://www.ncei.noaa.gov/access/billions/ (accessed 7.12.22).

Needham, H., Brown, D., Carter, L., 2012. Impacts and Adaptation Options in the Gulf Coast. Louisiana.

Negrón-Juárez, R., Baker, D.B., Zeng, H., Henkel, T.K., Chambers, J.Q., 2010. Assessing hurricane-induced tree mortality in U.S. Gulf Coast forest ecosystems. J Geophys Res Biogeosci 115. https://doi.org/10.1029/2009JG001221

Nelson, E., Sander, H., Hawthorne, P., Conte, M., Ennaanay, D., Wolny, S., Manson, S., Polasky, S., 2010. Projecting global land-use change and its effect on ecosystem service provision and biodiversity with simple models. PLoS One 5. https://doi.org/10.1371/journal.pone.0014327

NOAA, 2023. NOAA Releases Updated 2023 Atlantic Hurricane Season Outlook | NESDIS [WWW Document]. URL https://www.nesdis.noaa.gov/news/noaa-releases-updated-2023-atlantic-hurricane-season-outlook (accessed 10.5.23).

NOAA, 2022a. NOAA predicts above-normal 2022 Atlantic Hurricane Season | National Oceanic and Atmospheric Administration [WWW Document]. URL https://www.noaa.gov/news-release/noaa-predicts-above-normal-2022-atlantic-hurricane-season (accessed 7.11.22).

NOAA, 2022b. International Best Track Archive for Climate Stewardship (IBTrACS) [WWW Document]. URL https://www.ncei.noaa.gov/products/international-best-track-archive (accessed 6.9.23).

NOAA, 2022c. Land Cover Change [WWW Document]. URL https://coast.noaa.gov/states/fast-facts/land-cover-change.html (accessed 7.12.22).

NOAA, 2021a. HURDAT comparison table [WWW Document]. URL https://www.aoml.noaa.gov/hrd/hurdat/comparison_table.html (accessed 6.8.23).

NOAA, 2021b. International Best Track Archive for Climate Stewardship (IBTrACS) | National Centers for Environmental Information (NCEI) [WWW Document]. URL https://www.ncei.noaa.gov/products/international-best-track-archive (accessed 10.23.22).

NOAA, 2021c. Hurricane Costs [WWW Document]. URL https://coast.noaa.gov/states/fast-facts/hurricane-costs.html

NOAA, 2021d. Land Cover Change [WWW Document]. URL https://coast.noaa.gov/states/fast-facts/land-cover-change.html (accessed 10.3.21).

NOAA, 2020. Hurricanes in History [WWW Document]. URL https://www.nhc.noaa.gov/outreach/history/ (accessed 11.7.21).

NOAA, 2019. Carbon cycle | National Oceanic and Atmospheric Administration [WWW Document]. URL https://www.noaa.gov/education/resource-collections/climate/carbon-cycle (accessed 10.11.23).

NOAA, 2018. LAND USE CHANGE WETLANDS AND URBAN DEVELOPMENT [WWW Document]. URL https://www.aoml.noaa.gov/ocd/ocdweb/ESR_GOMIEA/lulc.html (accessed 9.21.21).

NOAA, 2017a. Gulf of Mexico Regional Land Cover Change Report.

NOAA, 2017b. C-CAP Land Cover Atlas [WWW Document]. URL https://coast.noaa.gov/digitalcoast/tools/lca.html (accessed 9.28.23).

NOAA, 2017c. Hurricanes | National Oceanic and Atmospheric Administration [WWW Document]. URL https://www.noaa.gov/education/resource-collections/weather-atmosphere/hurricanes (accessed 8.8.22).

NOAA, 2015. NOAA analysis reveals significant land cover changes in U.S. coastal regions | National Oceanic and Atmospheric Administration [WWW Document]. URL https://www.noaa.gov/media-release/noaa-analysis-reveals-significant-land-cover-changes-in-us-coastal-regions (accessed 10.24.22).

NOAA, 2005. Hurricane Katrina - August 2005 [WWW Document]. URL https://www.weather.gov/mob/katrina (accessed 9.21.21).

NRCS, 2020. Gridded Soil Survey Geographic (gSSURGO) Database | Natural Resources Conservation Service [WWW Document]. URL https://www.nrcs.usda.gov/resources/data-and-reports/gridded-soil-survey-geographic-gssurgo-database (accessed 10.8.23).

Ojha, S.K., Naka, K., Dimov, L.D., 2020. Assessment of disturbances across forest inventory plots in the southeastern united states for the period 1995-2018. Forest Science 66, 242–255. https://doi.org/10.1093/forsci/fxz072

Oliphant, A.J., Thenkabail, P.S., Teluguntla, P., Xiong, J., Gumma, M.K., Congalton, R.G., Yadav, K., 2019. Mapping cropland extent of Southeast and Northeast Asia using multi-year time-series Landsat 30-m data using a random forest classifier on the Google Earth Engine Cloud. International Journal of Applied Earth Observation and Geoinformation 81, 110–124. https://doi.org/10.1016/j.jag.2018.11.014

Olofsson, P., Foody, G.M., Herold, M., Stehman, S. V., Woodcock, C.E., Wulder, M.A., 2014. Good practices for estimating area and assessing accuracy of land change. Remote Sens Environ 148, 42–57. https://doi.org/10.1016/j.rse.2014.02.015

ORNL, 2020. Global Aboveground and Belowground Biomass Carbon Density Maps for the Year 2010 [WWW Document]. URL https://daac.ornl.gov/VEGETATION/guides/Global_Maps_C_Density_2010.html (accessed 10.8.23).

Osland, M.J., Griffith, K.T., Larriviere, J.C., Feher, L.C., Cahoon, D.R., Enwright, N.M., Oster, D.A., Tirpak, J.M., Woodrey, M.S., Collini, R.C., Baustian, J.J., Breithaupt, J.L., Cherry, J.A., Conrad, J.R., Cormier, N., Coronado-Molina, C.A., Donoghue, J.F., Graham, S.A., Harper, J.W., Hester, M.W., Howard, R.J., Krauss, K.W., Kroes, D.E., Lane, R.R., McKee, K.L., Mendelssohn, I.A., Middleton, B.A., Moon, J.A., Piazza, S.C., Rankin, N.M., Sklar, F.H., Steyer, G.D., Swanson, K.M., Swarzenski, C.M., Vervaeke, W.C., Willis, J.M., Wilson, K. Van, 2017. Assessing coastal wetland vulnerability to sea-level rise along the northern Gulf of Mexico coast: Gaps and opportunities for developing a coordinated regional sampling network. PLoS One 12, e0183431. https://doi.org/10.1371/JOURNAL.PONE.0183431

Panama City Beach, 2022. Area Information | City of Panama City Beach, FL [WWW Document]. URL https://www.pcbfl.gov/about-us/visitors/area-information (accessed 7.25.22).

Pape, D., Lewandrowski, J., Steele, R., Man, D., Riley-Gilbert, M., Moffroid, K., Kolansky, S., 2016. Managing agricultural land for greenhouse gas mitigation within the United States.

Pati, P.K., Kaushik, P., Khan, M.L., Khare, P.K., 2022. Allometric equations for biomass and carbon stock estimation of small diameter woody species from tropical dry deciduous forests: Support to REDD+. Trees, Forests and People 9, 100289. https://doi.org/10.1016/j.tfp.2022.100289

Pelletier, C., Valero, S., Inglada, J., Champion, N., Dedieu, G., 2016. Assessing the robustness of Random Forests to map land cover with high resolution satellite image time series over large areas. Remote Sens Environ 187, 156–168. https://doi.org/10.1016/j.rse.2016.10.010

Peltola, H., Kellomäki, S., Väisänen, H., Ikonen, V.P., 1999. A mechanistic model for assessing the risk of wind and snow damage to single trees and stands of Scots pine, Norway spruce, and birch. Canadian Journal of Forest Research 29, 647–661. https://doi.org/10.1139/x99-029

Peneva-Reed, E.I., Krauss, K.W., Bullock, E.L., Zhu, Z., Woltz, V.L., Drexler, J.Z., Conrad, J.R., Stehman, S. V., 2021a. Carbon stock losses and recovery observed for a mangrove ecosystem following a major hurricane in Southwest Florida. Estuar Coast Shelf Sci 248, 106750. https://doi.org/10.1016/j.ecss.2020.106750

Philpott, S.M., Lin, B.B., Jha, S., Brines, S.J., 2008. A multi-scale assessment of hurricane impacts on agricultural landscapes based on land use and topographic features. Agric Ecosyst Environ 128, 12–20. https://doi.org/10.1016/j.agee.2008.04.016

Piao, S., Huang, M., Liu, Z., Wang, X., Ciais, P., Canadell, J.G., Wang, K., Bastos, A., Friedlingstein, P., Houghton, R.A., Le Quéré, C., Liu, Y., Myneni, R.B., Peng, S., Pongratz, J., Sitch, S., Yan, T., Wang, Y., Zhu, Z., Wu, D., Wang, T., 2018. Lower land-use emissions responsible for increased net land carbon sink during the slow warming period. Nat Geosci 11, 739–743. https://doi.org/10.1038/s41561-018-0204-7

Pimple, U., Simonetti, D., Sitthi, A., Pungkul, S., Leadprathom, K., Skupek, H., Som-ard, J., Gond, V., Towprayoon, S., 2018. Google Earth Engine Based Three Decadal Landsat Imagery Analysis for Mapping of Mangrove Forests and Its Surroundings in the Trat Province of Thailand. Journal of Computer and Communications 06, 247–264. https://doi.org/10.4236/jcc.2018.61025

Platt, W.J., Doren, R.F., Armentano, T. V., 2000. Effects of Hurricane Andrew on stands of slash pine (Pinus elliottii var. densa) in the everglades region of south Florida (USA). Plant Ecol 146, 43–60. https://doi.org/10.1023/A:1009829319862

Ploton, P., Mortier, F., Réjou-Méchain, M., Barbier, N., Picard, N., Rossi, V., Dormann, C., Cornu, G., Viennois, G., Bayol, N., Lyapustin, A., Gourlet-Fleury, S., Pélissier, R., 2020. Spatial validation reveals poor predictive performance of large-scale ecological mapping models. Nat Commun 11, 1–11. https://doi.org/10.1038/s41467-020-18321-y

Polinko, A.D., Willis, J.L., Sharma, A., Guldin, J.M., 2022. Stand-level structural characteristics dictate hurricane resistance and resilience more than silvicultural regime in longleaf pine woodlands. For Ecol Manage 526, 120585. https://doi.org/10.1016/j.foreco.2022.120585

Potter, C., 2021. Changes in the vegetation of New Orleans from the disturbance impacts of Hurricane Katrina in 2005. Remote Sens Appl 24, 100611. https://doi.org/10.1016/j.rsase.2021.100611

Prestemon, J.P., Holmes, T.P., 2010. Economic impacts of hurricanes on forest owners, General Technical Report PNW-GTR-802.

Qu, L., Chen, Z., Li, M., Zhi, J., Wang, H., 2021. Accuracy Improvements to Pixel-Based and Object-Based LULC Classification with Auxiliary Datasets from Google Earth Engine. Remote Sens (Basel) 13, 453. https://doi.org/10.3390/rs13030453

Rai, R., Zhang, Y., Paudel, B., Li, S., Khanal, N.R., 2017. A synthesis of studies on land use and land cover dynamics during 1930–2015 in bangladesh. Sustainability (Switzerland) 9, 1–20. https://doi.org/10.3390/SU9101866

Ramsey Ill, E.W., Chappell, D.K., Baldwin, D.G., 1997. AVHRR lmagery Used to Identify Hurricane Damage in a Forested Wetland of Louisiana.

Rapp, J., Wang, D., Capen, D., Thompson, E., Lautzenheiser, T., 2005. Evaluating error in using the national vegetation classification system for ecological community mapping in Northern New England, USA. Natural Areas Journal 25, 46–54.

Rappaport, E.N., 2014. Fatalities in the united states from atlantic tropical cyclones: New data and interpretation. Bull Am Meteorol Soc 95, 341–346. https://doi.org/10.1175/BAMS-D-12-00074.1

Remmel, T.K., Perera, A.H., 2017. Mapping forest landscapes: Overview and a primer, Mapping Forest Landscape Patterns. https://doi.org/10.1007/978-1-4939-7331-6_1

Rimal, B., Zhang, L., Keshtkar, H., Haack, B.N., Rijal, S., Zhang, P., 2018. Land Use/Land Cover Dynamics and Modeling of Urban Land Expansion by the Integration of Cellular Automata and Markov Chain. ISPRS International Journal of Geo-Information 2018, Vol. 7, Page 154 7, 154. https://doi.org/10.3390/IJGI7040154

Rivera-Monroy, V.H., Danielson, T.M., Castañeda-Moya, E., Marx, B.D., Travieso, R., Zhao, X., Gaiser, E.E., Farfan, L.M., 2019. Long-term demography and stem productivity of Everglades mangrove forests (Florida, USA): Resistance to hurricane disturbance. For Ecol Manage 440, 79–91. https://doi.org/10.1016/j.foreco.2019.02.036

Rodriguez-Galiano, V.F., Ghimire, B., Rogan, J., Chica-Olmo, M., Rigol-Sanchez, J.P., 2012. An assessment of the effectiveness of a random forest classifier for land-cover classification. ISPRS Journal of Photogrammetry and Remote Sensing 67, 93–104. https://doi.org/10.1016/J.ISPRSJPRS.2011.11.002

Rouder, J.N., Engelhardt, C.R., McCabe, S., Morey, R.D., 2016. Model comparison in ANOVA. Psychon Bull Rev 23, 1779–1786. https://doi.org/10.3758/s13423-016-1026-5

Rstudio, 2022. Package “sandwich” Title Robust Covariance Matrix Estimators. https://doi.org/10.18637/jss.v095.i01

Rwanga, S.S., Ndambuki, J.M., 2017. Accuracy Assessment of Land Use/Land Cover Classification Using Remote Sensing and GIS. International Journal of Geosciences 8, 611–622. https://doi.org/10.4236/ijg.2017.84033

Ryan, M.G., Binkley, D., Fownes, J.H., 1997. Age-related decline in forest productivity: pattern and process. Adv Ecol Res 27, 213–62. https://doi.org/10.1016/s0065-2504(08)60009-4

Salcedo-Sanz, S., Ghamisi, P., Piles, M., Werner, M., Cuadra, L., Moreno-Martínez, A., Izquierdo-Verdiguier, E., Muñoz-Marí, J., Mosavi, A., Camps-Valls, G., 2020. Machine learning information fusion in Earth observation: A comprehensive review of methods, applications and data sources. Information Fusion 63, 256–272. https://doi.org/10.1016/j.inffus.2020.07.004

Schimel, J., Chadwick, O., 2013. What’s in a name? The importance of soil taxonomy for ecology and biogeochemistry. Front Ecol Environ 11, 405–406. https://doi.org/10.1890/13.WB.016

Schmidt, M., Hanewinkel, M., Kändler, G., Kublin, E., Kohnle, U., 2010. An inventory-based approach for modeling singletree storm damage - experiences with the winter storm of 1999 in southwestern Germany. Canadian Journal of Forest Research 40, 1636–1652. https://doi.org/10.1139/X10-099

Schmidt, M., Pringle, M., Devadas, R., Denham, R., Tindall, D., 2016. A framework for large-area mapping of past and present cropping activity using seasonal landsat images and time series metrics. Remote Sens (Basel) 8. https://doi.org/10.3390/rs8040312

Schulp, C.J.E., Nabuurs, G.J., Verburg, P.H., 2008. Future carbon sequestration in Europe-Effects of land use change. Agric Ecosyst Environ 127, 251–264. https://doi.org/10.1016/j.agee.2008.04.010

Sha, Z., Bai, Y., Xie, Y., Yu, M., Zhang, L., 2008. Using a hybrid fuzzy classifier (HFC) to map typical grassland vegetation in Xilin River Basin, Inner Mongolia, China. Int J Remote Sens 29, 2317–2337. https://doi.org/10.1080/01431160701408436

Sharma, A., Ojha, S.K., Dimov, L.D., Vogel, J.G., Nowak, J., 2021. Long-term effects of catastrophic wind on southern US coastal forests: Lessons from a major hurricane. PLoS One 16, e0243362. https://doi.org/10.1371/journal.pone.0243362

Shell, A.B., Ojha, S.K., Sharma, A., 2021. Region-wide characterization of structural diversity of the U.S. Outer Coastal Plain Mixed Forests Province. For Ecol Manage 488, 118979. https://doi.org/10.1016/J.FORECO.2021.118979

Sidhu, N., Pebesma, E., Câmara, G., 2018. Using Google Earth Engine to detect land cover change: Singapore as a use case Using Google Earth Engine to detect land cover change: Singapore as a use. Eur J Remote Sens 51, 486–500. https://doi.org/10.1080/22797254.2018.1451782

Spawn, S.A., Sullivan, C.C., Lark, T.J., Gibbs, H.K., 2020. Harmonized global maps of above and belowground biomass carbon density in the year 2010. Sci Data 7. https://doi.org/10.1038/S41597-020-0444-4

Stanford University, 2018. Carbon Storage and Sequestration — InVEST® documentation [WWW Document]. URL http://releases.naturalcapitalproject.org/invest-userguide/latest/en/carbonstorage.html (accessed 10.8.23).

Stanford University, 2016. Carbon Storage and Sequestration — InVEST® documentation [WWW Document]. URL http://releases.naturalcapitalproject.org/invest-userguide/latest/en/carbonstorage.html (accessed 11.19.23).

Stanturf, J.A., Goodrick, S.L., Outcalt, K.W., 2007. Disturbance and coastal forests: A strategic approach to forest management in hurricane impact zones. For Ecol Manage 250, 119–135. https://doi.org/10.1016/j.foreco.2007.03.015

Staudhammer, C., Escobedo, F., Lawrence, A., Duryea, M., Smith, P., Merritt, M., 2011. Rapid assessment of change and hurricane impacts to houston's Urban forest structure. Arboric Urban For 37, 60–66. https://doi.org/10.48044/jauf.2011.009

Staudhammer, C.L., Escobedo, F., Luley, C., Bond, J., 2009. Patterns of Urban Forest Debris from the 2004 and 2005 Florida Hurricane Seasons. Southern Journal of Applied Forestry 33, 193–196.

Stewart, S.R., 2011. Tropic cyclone report Hurricane Ivan 2-24 September 2004 3, 1–44.

Subiyanto, S., Amarrohman, F.J., Rahmah, A.N., 2021. Modeling changes in land use using the integration of MLP-NN, CA-Markov models and GIS for settlement development in Tembalang District. IOP Conf Ser Earth Environ Sci 731. https://doi.org/10.1088/1755-1315/731/1/012026

Talkkari, A., Peltola, H., Kellomäki, S., Strandman, H., 2000. Integration of component models from the tree, stand and regional levels to assess the risk of wind damage at forest margins. For Ecol Manage 135, 303–313. https://doi.org/10.1016/S0378-1127(00)00288-7

Taud, H., Mas, J.F., 2018a. Multilayer Perceptron (MLP) 451–455. https://doi.org/10.1007/978-3-319-60801-3_27

Taud, H., Mas, J.F., 2018b. Multilayer Perceptron (MLP) BT - Geomatic Approaches for Modeling Land Change Scenarios. Geoinformation and Cartography 451–455.

Taylor, B., Kirschenfeld, C., Turpin, R.K., Handley, L.R., 2002. Perdido Bay, USDA Forest Service.

Tech, G., 2005. Existing Vegetation Classification and Mapping Technical Guide Version 1.0 United States Department of Agriculture Forest Service Ecosystem Management Coordination Staff Existing Vegetation Classification and Mapping Technical Guide Version 1.0.

Thamo, T., Pannell, D.J., 2016. Challenges in developing effective policy for soil carbon sequestration: perspectives on additionality, leakage, and permanence. Climate Policy 16, 973–992. https://doi.org/10.1080/14693062.2015.1075372

The Atlantic, 2017. Why Does the Gulf Coast Have So Many Natural Disasters? - The Atlantic.

Tian, H., Chen, G., Zhang, C., Liu, M., Sun, G., Chappelka, A., Ren, W., Xu, X., Lu, C., Pan, S., Chen, H., Hui, D., McNulty, S., Lockaby, G., Vance, E., 2012. Century-Scale Responses of Ecosystem Carbon Storage and Flux to Multiple Environmental Changes in the Southern United States. Ecosystems 15, 674–694. https://doi.org/10.1007/s10021-012-9539-x

Tian, S., Zhang, X., Tian, J., Sun, Q., 2016. Random forest classification of wetland landcovers from multi-sensor data in the arid region of Xinjiang, China. Remote Sens (Basel) 8, 1–14. https://doi.org/10.3390/rs8110954

Tian, Y., Shu, M., Jia, Q., 2021. Artificial Neural Network 1–4. https://doi.org/10.1007/978-3-030-26050-7_44-1

Toru, T., Kibret, K., 2019. Carbon stock under major land use/land cover types of Hades sub-watershed, eastern Ethiopia. Carbon Balance Manag 14, 1–14. https://doi.org/10.1186/s13021-019-0122-z

Trautenmüller, J.W., Péllico Netto, S., Balbinot, R., Watzlawick, L.F., Dalla Corte, A.P., Sanquetta, C.R., Behling, A., 2021. Regression estimators for aboveground biomass and its constituent parts of trees in native southern Brazilian forests. Ecol Indic 130. https://doi.org/10.1016/j.ecolind.2021.108025

UNFCCC, 2015. The Paris Agreement | UNFCCC [WWW Document]. URL https://unfccc.int/process-and-meetings/the-paris-agreement (accessed 10.11.23).

US Census Beauru, 2020. U.S. Census Bureau QuickFacts: Pensacola city, Florida [WWW Document]. URL https://www.census.gov/quickfacts/fact/table/pensacolacityflorida/BZA210219 (accessed 3.13.22).

US EPA, 2022. Climate Change Indicators: Weather and Climate [WWW Document]. URL https://www.epa.gov/climate-indicators/weather-climate (accessed 6.8.23).

U.S. Global Change Research Program, 2018. Climate Science Special Report. U.S. Global Change Research Program 1, 1–470. https://doi.org/10.7930/J0J964J6

US Global Change Research Program, 2017. Climate Science Special Report: 4 th US National Climate Assessment, Volume I. https://doi.org/10.1142/9789811213953_0022

USDA, 2021. Wood handbook: wood as an engineering materia.

USDA, 2020. Forest Service unites around hurricane-damaged forests | US Forest Service [WWW Document]. URL https://www.fs.usda.gov/inside-fs/delivering-mission/sustain/forest-service-unites-around-hurricane-damaged-forests (accessed 8.4.22).

USDA, 2016. Forest Soil Carbon and Climate Change | Climate Change Resource Center [WWW Document]. URL https://www.fs.usda.gov/ccrc/topics/forest-soil-carbon (accessed 10.11.23).

USFS, 2018. The Forest Inventory and Analysis Database: Population Estimation User Guide. USDA Forest Service 2, 1026.

USFS, 2016. Forest Soil Carbon and Climate Change | Climate Change Resource Center [WWW Document]. URL https://www.fs.usda.gov/ccrc/topics/forest-soil-carbon (accessed 11.19.23).

USFS, 2015. The Forest Inventory and Analysis Database, USDA Forest Service.

USGS, 2022. PAD-US Data Overview | U.S. Geological Survey [WWW Document]. URL https://www.usgs.gov/programs/gap-analysis-project/science/pad-us-data-overview (accessed 9.10.23).

USGS, 2016. Landsat Enhanced Vegetation Index | U.S. Geological Survey [WWW Document]. URL https://www.usgs.gov/landsat-missions/landsat-enhanced-vegetation-index (accessed 4.19.22).

USGS, 2015. Landsat Commercial Cloud Data Access | U.S. Geological Survey [WWW Document]. URL https://www.usgs.gov/landsat-missions/landsat-commercial-cloud-data-access (accessed 8.8.22).

USGS, 2014. Google Powers Platform for Earth Science Data and Analysis | U.S. Geological Survey [WWW Document]. URL https://www.usgs.gov/landsat-missions/google-powers-platform-earth-science-data-and-analysis (accessed 8.8.22).

Valinger, E., Fridman, J., 2011. Factors affecting the probability of windthrow at stand level as a result of Gudrun winter storm in southern Sweden. For Ecol Manage 262, 398–403. https://doi.org/10.1016/j.foreco.2011.04.004

Van Coppenolle, R., Temmerman, S., 2020. Identifying global hotspots where coastal wetland conservation can contribute to nature-based mitigation of coastal flood risks. Glob Planet Change 187, 103125. https://doi.org/10.1016/J.GLOPLACHA.2020.103125

Vecchi, G.A., Swanson, K.L., Soden, B.J., 2008. Climate change: Whither hurricane activity? Science (1979) 322, 687–689. https://doi.org/10.1126/science.1164396

Vermote, E., Justice, C., Claverie, M., Franch, B., 2016. Preliminary analysis of the performance of the Landsat 8/OLI land surface reflectance product. Remote Sens Environ 185, 46–56. https://doi.org/10.1016/j.rse.2016.04.008

von Eye, A., Mun, E.Y., 2013. Log-Linear Modeling: Concepts, Interpretation, and Application. Log-Linear Modeling: Concepts, Interpretation, and Application. https://doi.org/10.1002/9781118391778

Vorster, A.G., Evangelista, P.H., Stovall, A.E.L., Ex, S., 2020. Variability and uncertainty in forest biomass estimates from the tree to landscape scale: The role of allometric equations. Carbon Balance Manag 15, 1–20. https://doi.org/10.1186/s13021-020-00143-6

Wang, F., D'Sa, E.J., 2010. Potential of MODIS EVI in identifying hurricane disturbance to coastal vegetation in the Northern Gulf of Mexico. Remote Sens (Basel) 2, 1–18. https://doi.org/10.3390/rs2010001

Wang, F., Sun, Y., Jia, W., Zhu, W., Li, D., Zhang, X., Tang, Y., Guo, H., 2023. Development of Estimation Models for Individual Tree Aboveground Biomass Based on TLS-Derived Parameters. Forests 14. https://doi.org/10.3390/f14020351

Wang, R., Kalin, L., Kuang, W., Tian, H., 2014. Individual and combined effects of land use/cover and climate change on Wolf Bay watershed streamflow in southern Alabama. Hydrol Process 28, 5530–5546. https://doi.org/10.1002/hyp.10057

Waske, B., Braun, M., 2009. Classifier ensembles for land cover mapping using multitemporal SAR imagery. ISPRS Journal of Photogrammetry and Remote Sensing 64, 450–457. https://doi.org/10.1016/j.isprsjprs.2009.01.003

Weiskopf, S.R., Rubenstein, M.A., Crozier, L.G., Gaichas, S., Griffis, R., Halofsky, J.E., Hyde, K.J.W., Morelli, T.L., Morisette, J.T., Muñoz, R.C., Pershing, A.J., Peterson, D.L., Poudel, R., Staudinger, M.D., Sutton-Grier, A.E., Thompson, L., Vose, J., Weltzin, J.F., Whyte, K.P., 2020. Climate change effects on biodiversity, ecosystems, ecosystem services, and natural resource management in the United States. Science of the Total Environment 733. https://doi.org/10.1016/j.scitotenv.2020.137782

Wilson, E.H., Sader, S.A., 2002. Detection of forest harvest type using multiple dates of Landsat TM imagery. Remote Sens Environ 80, 385–396. https://doi.org/10.1016/S0034-4257(01)00318-2

Xi, F., Lin, G., Zhao, Y., Li, X., Chen, Z., Cao, C., 2023a. Land Use Optimization and Carbon Storage Estimation in the Yellow River Basin, China. Sustainability 2023, Vol. 15, Page 11278 15, 11278. https://doi.org/10.3390/SU151411278

Xi, W., Peet, R.K., Decoster, J.K., Urban, D.L., 2008a. Tree damage risk factors associated with large, infrequent wind disturbances of Carolina forests. Forestry 81, 317–334. https://doi.org/10.1093/forestry/cpn020

Xiao, Yang, Ouyang, Z., Xu, W., Xiao, Yi, Zheng, H., Xian, C., 2016. Optimizing hotspot areas for ecological planning and management based on biodiversity and ecosystem services. Chin Geogr Sci 26, 256–269. https://doi.org/10.1007/s11769-016-0803-4

Yang, B.Y., 2005. Can the strengths of AIC and BIC be shared? A conflict between model indentification and regression estimation. Biometrika 92, 937–950.

You, M., Filippi, A.M., Güneralp, I., Güneralp, B., 2017. What is the direction of land change? A new approach to land-change analysis. Remote Sens (Basel) 9, 1–18. https://doi.org/10.3390/rs9080850

Zaehle, S., Bondeau, A., Carter, T.R., Cramer, W., Erhard, M., Prentice, I.C., Reginster, I., Rounsevell, M.D.A., Sitch, S., Smith, B., Smith, P.C., Sykes, M., 2007. Projected changes in terrestrial carbon storage in Europe under climate and land-use change, 1990-2100. Ecosystems 10, 380–401. https://doi.org/10.1007/s10021-007-9028-9

Zampieri, N.E., Pau, S., Okamoto, D.K., 2020. The impact of Hurricane Michael on longleaf pine habitats in Florida. Sci Rep 10, 1–11. https://doi.org/10.1038/s41598-020-65436-9

Zeileis, A., 2006. Object-oriented computation of sandwich estimators. J Stat Softw 16, 1–16. https://doi.org/10.18637/JSS.V016.I09

Zeileis, A., 2004. Econometric computing with HC and HAC covariance matrix estimators. J Stat Softw 11, 1–17. https://doi.org/10.18637/JSS.V011.I10

Zeileis, A., Köll, S., Graham, N., 2020. Various versatile variances: An object-oriented implementation of clustered covariances in r. J Stat Softw 95, 1–36. https://doi.org/10.18637/JSS.V095.I01

Zeng, H., Chambers, J.Q., Negrón-Juárez, R.I., Hurtt, G.C., Baker, D.B., Powell, M.D., 2009. Impacts of tropical cyclones on U.S. forest tree mortality and carbon flux from 1851 to 2000. Proc Natl Acad Sci U S A 106, 7888–7892. https://doi.org/10.1073/PNAS.0808914106

Zhang, K., Thapa, B., Ross, M., Gann, D., 2016. Remote sensing of seasonal changes and disturbances in mangrove forest: A case study from South Florida. Ecosphere 7, 1–23. https://doi.org/10.1002/ecs2.1366

Zhou, Y., Hu, Q., Wang, Y., 2018. Deep super-class learning for long-tail distributed image classification. Pattern Recognit 80, 118–128. https://doi.org/10.1016/j.patcog.2018.03.003

Zhu, G., Qiu, D., Zhang, Z., Sang, L., Liu, Y., Wang, L., Zhao, K., Ma, H., Xu, Y., Wan, Q., 2021. Land-use changes lead to a decrease in carbon storage in arid region, China. Ecol Indic 127, 107770. https://doi.org/10.1016/j.ecolind.2021.107770

Zhu, Z., Wang, S., Woodcock, C.E., 2015. Improvement and expansion of the Fmask algorithm: Cloud, cloud shadow, and snow detection for Landsats 4-7, 8, and Sentinel 2 images. Remote Sens Environ 159, 269–277. https://doi.org/10.1016/J.RSE.2014.12.014

Zhu, Z., Woodcock, C.E., 2012. Object-based cloud and cloud shadow detection in Landsat imagery. Remote Sens Environ 118, 83–94. https://doi.org/10.1016/J.RSE.2011.10.028

Zurqani, H.A., Post, C.J., Mikhailova, E.A., Schlautman, M.A., Sharp, J.L., 2018. Geospatial analysis of land use change in the Savannah River Basin using Google Earth Engine. International Journal of Applied Earth Observation and Geoinformation 69, 175–185. https://doi.org/10.1016/j.jag.2017.12.006

APPENDIX-1

Google Earth Engine Code for Land use change analysis and vegetation indices analysis:

```
// Import the Perdido Bay Boundary and show it in console
var Panama City = ee.FeatureCollection("users/AsifulAlam/Panama City");
function getCols(tableMetadata) {
  print(tableMetadata.columns);
}
Panama City.limit(0).evaluate(getCols);
var trueColor = Panama City.select(['R', 'G', 'B']);
var trueColorVis = {
  min: 0.0,
  max: 255.0,
};
Map.addLayer(trueColor, trueColorVis, 'Panama City Boundary');
Map.setCenter(-86.1699, 30.3598, 8);

// Import the Cat#5 Hurricane and show it in console
var Cat_05_Hur = ee.FeatureCollection("projects/ee-asifuga21/assets/Category_5_HUR");
function getCols(tableMetadata) {
  print(tableMetadata.columns);
}
Cat_05_Hur.limit(0).evaluate(getCols);
var trueColor = Cat_05_Hur.select(['R']);
var trueColorVis = {
  min: 0.0,
  max: 255.0,
};
Map.addLayer(trueColor, trueColorVis, 'Category 5 Hurricane');
//Map.setCenter(-87.67782, 30.55895, 8);

//////////////////////////////////////////////////////////////////////////////////////
// LULC-2018 (Lansat-08)
//Import the refernce image NAIP
var naip = ee.ImageCollection('USDA/NAIP/DOQQ')
                .filterBounds(Panama City)
                .filter(ee.Filter.date('2017-06-01', '2018-08-30'));
var trueColor = naip.select(['R', 'G', 'B']);
var trueColorVis = {
  min: 0.0,
  max: 255.0,
};
Map.addLayer(trueColor, trueColorVis, 'NAIP');

// Import the Digital Elevation Model (DEM) layer
var DEM = ee.Image('USGS/SRTMGL1_003').clip(Panama City);
// Create the slope layer
var Slope = ee.Terrain.slope(DEM).rename('Slope');

var reference_data =
Open_Water.merge(Crops_Pasture).merge(Mixed_Forest).merge(Evergreen_Forest).merge(Developed_HighMediumLow).merg
e(Developed_OpenSpace).merge(Grasslands_Shrub).merge(Barren_Land).merge(Wetlands);
var reference_data = reference_data.randomColumn('random', 0);

// buffer the reference data by 30 meters (each point will be buffring by 30*30 m)
var buf_ref_data = reference_data.map(function(feature) {
```

```
  return feature.buffer(30).bounds(); });
Map.addLayer(buf_ref_data,{palette:'de9e4e'},'buf_ref_data');
Export.table.toAsset({
  collection: buf_ref_data,
  description:'buf_ref_data_30m',
  assetId: 'Buffer_30m',
});

// Apply the band names
var inBands = ['B2', 'B3', 'B4', 'B5', 'B6', 'B7', 'B10'];
var outBands = ['B2', 'B3', 'B4', 'B5', 'B6', 'B7', 'B10', 'NDVI','NDBI','NDWI'];

// Import the Landsat 8 TOA image collection.
var landsat_2018 = ee.ImageCollection('LANDSAT/LC08/C01/T1_TOA');
var image = ee.Image(
  landsat_2018.filterBounds(Panama City)
    .filterDate('2018-01-01', '2018-09-30')
    .filter(ee.Filter.eq('WRS_PATH', 19))
    .filter(ee.Filter.eq('WRS_ROW', 39))
    .sort('CLOUD_COVER')
    .first()
);
var visualization = {
  bands: ['B4', 'B3', 'B2'],
  min: 0.0,
  max: 0.3,
};

Map.setCenter(-86.1699, 30.3598, 8);
Map.addLayer(image, visualization, 'Landsat_2018');

// Apply the cloud mask function
var qa = image.select('cfmask');
var cloudMask = qa.bitwiseAnd(1<<5).eq(0)
  .and(qa.bitwiseAnd(1<<3).eq(0));
var masked = image.updateMask(cloudMask).clip(Panama City);

// Compute the Normalized Difference Vegetation Index (NDVI), Normalized Difference Built-up Index (NDBI) and Normalized
Difference Water Index (NDWI).
var Blue = image.select('B2');
var Green = image.select('B3');
var Red = image.select('B4');
var NIR = image.select('B5');
var SWIR_1 = image.select('B6');
var SWIR_2 = image.select('B7');
var TIR = image.select('B10');

var ndvi = NIR.subtract(Red).divide(NIR.add(Red)).rename('NDVI');
var ndbi = Blue.subtract(TIR).divide(Blue.add(TIR)).rename('NDBI');
var ndwi = NIR.subtract(SWIR_1).divide(NIR.add(SWIR_1)).rename('NDWI');

//var ndvi = image.normalizedDifference(['B5', 'B4']).rename('NDVI');
var addNDVI = function(image) {
  var ndvi = image.normalizedDifference(['B5', 'B4']).rename('NDVI');
  return image.addBands(ndvi);
};
//var ndbi = image.normalizedDifference(['B6', 'B5']).rename('NDBI');
var addNDBI = function(image) {
  var ndbi = image.normalizedDifference(['B2', 'B10']).rename('NDBI');
  return image.addBands(ndbi);
};
//var ndwi = image.normalizedDifference(['B5', 'B6']).rename('NDWI');
```

```
var addNDWI = function(image) {
  var ndwi = image.normalizedDifference(['B5', 'B6']).rename('NDWI');
  return image.addBands(ndwi);
};

// Test the addNDVI function on a single image.
var ndvi = addNDVI(image).select('NDVI');
var ndwi = addNDWI(image).select('NDWI');
var withIndices = landsat_2018.select(inBands).map(addNDVI).map(addNDBI).map(addNDWI);

//Map.addLayer(withIndices, {  min: 0.0, max: 0.3, bands: ['B4', 'B3', 'B2'],}, 'Indices_Band');

// Define and calculate the median bands and the other index statistics
var band_median = withIndices.select(inBands).median();
var ndvimax = withIndices.select('NDVI').reduce(ee.Reducer.max()).rename("NDVI_MAX");
var ndvimean = withIndices.select('NDVI').reduce(ee.Reducer.mean()).rename("NDVI");
var ndvistd = withIndices.select('NDVI').reduce(ee.Reducer.stdDev()).float().rename("NDVI_STD");
var ndwimax = withIndices.select('NDWI').reduce(ee.Reducer.max()).rename("NDWI_MAX");
var ndwimean = withIndices.select('NDWI').reduce(ee.Reducer.mean()).rename("NDWI");
var ndwistd = withIndices.select('NDWI').reduce(ee.Reducer.stdDev()).float().rename("NDWI_STD");
//Add the index statistics to the median bands and clip the dataset with the ROI
var compclip =
band_median.addBands(DEM).addBands(Slope).addBands(ndvimax).addBands(ndvimean).addBands(ndvistd).addBands(ndbim
ax).addBands(ndbimean).addBands(ndbistd).addBands(ndwimax).addBands(ndwimean).addBands(ndwistd).clip(Panama City);
print("Composition", compclip);

//Select and extract the images with the desideres bands defined as outBands
var final_bands= compclip.select(outBands);
print("Bands of the final image", final_bands);

//Map.addLayer(final_bands, {  min: 0.0, max: 0.3, bands: ['B4', 'B3', 'B2'],}, 'CI_RGB_2018');
//Map.addLayer(final_bands, {  min: 0.0, max: 0.3, bands: ['B5', 'B4', 'B3'],}, 'CI_CIR_2018');

//Export the image to an Earth Engine asset
Export.image.toAsset({
  image: final_bands,
  region: Panama City,
  description: 'CI_2018',
  scale: 30
});

// Divide the Reference data into Training (70%) and Testing (30%)
var Ref_Data = image.sampleRegions(buf_ref_data, ['LULC', 'random'], 30);
var training = Ref_Data.filter(ee.Filter.lte('random', 0.7));
var testing = Ref_Data.filter(ee.Filter.gt('random', 0.7));

// Applying Random Forest (RF) algorithm with 500 trees and train the classifier.
var trained = ee.Classifier.smileRandomForest(500).train(training, 'LULC',image.bandNames());
// Classify the image.
var classified_2018 = image.classify(trained);

var igbpPalette = [
  '1272d6', // Open_Water (0)
  'd3e013', // Crops_Pasture (1)
  '37d84b', // Mixed_Forest (2)
  '068015', // Evergreen_Forest (3)
  'da1111', // Developed_HighMediumLow (4)
  'de9e4e', // Developed_OpenSpace (5)
  '93c028', // Grassland_Shrub (6)
  'b78811', // Barren_land (7)
  '05d4de', // Wetlands (8)
];
```

```
// Map.addLayer(final_bands.clip(table), {bands: ['B3', 'B2', 'B1'], max: 0.4}, 'landsat');
Map.addLayer(classified_2018.clip(Panama City), {palette: igbpPalette, min: 0, max: 8}, 'LULC_2018');
Export.image.toDrive({
  image: classified_2018,
  region: Panama City,
  description: 'LULC_SAB_2018',
  scale: 30
});

// Accuracy assessment
// Get a confusion matrix representing resubstitution accuracy.
var trainAccuracy = trained.confusionMatrix();
print('Resubstitution error matrix 2018: ', trainAccuracy);
print('Training overall accuracy 2018: ', trainAccuracy.accuracy());

// Get a confusion matrix representing expected accuracy.
var Validated = testing.classify(trained);
var testAccuracy = Validated.errorMatrix('LULC', 'classification');
// Export error matrix
var exportAccuracy = ee.Feature(null, {matrix: testAccuracy.array()})
Export.table.toDrive({
  collection: ee.FeatureCollection(exportAccuracy),
  description: 'Error_matrix',
  fileFormat: 'CSV'
});
print('Validation error matrix 2018: ', testAccuracy);
print('Validation overall accuracy 2018: ', testAccuracy.accuracy());
print('Validation consumer accuracy 2018: ', testAccuracy.consumersAccuracy());
print('Validation producer accuracy 2018: ', testAccuracy.producersAccuracy());
print('Kappa Coefficient 2018: ', testAccuracy.kappa());

//F1 score
var CA = testAccuracy.consumersAccuracy().project([1]);
var PA = testAccuracy.producersAccuracy().project([0]);
var F1 = (CA.multiply(PA).multiply(2.0)).divide(CA.add(PA));
print("F1 score 2018:",F1);

//Calculate and print the areas
var areas = ee.Image.pixelArea().divide(1000 * 1000).addBands(classified_2018)
    .reduceRegion({reducer: ee.Reducer.sum().group({
    groupField: 1, groupName:'Code',}),
    geometry: Panama City,scale: 30,bestEffort:true,
    maxPixels: 1e9,tileScale: 16,});
print('Classification areas (km2)',  areas);
```

APPENDIX-2

R code for Log-linear model

```
#Set up the working directory#
setwd("D://FIA_Data")

#=========================================================================#
#Access the database from the local disk
perdido_data_2001_2007 <- read.xlsx("Perdido_Carbon_Analysis_v2.xlsx", sheet = 'Perdido_Carbon_Analysis_01_07_P') #set the location
colnames(perdido_data_2001_2007) #to see the column names in the dataset

perdido_data_2001_2007 <- read.xlsx("Perdido_Carbon_Analysis_v2.xlsx", sheet = 'PLOT_TimeSeries') #set the location
colnames(perdido_data_2001_2007) #to see the column names in the dataset

#+++++++++++++++++++++++++++++++++++++++++++++++++++++++++++++++++++++++++++++++#
#Run a multiple linear regression model for 2001-2007 period
perdido_lm_2001_2007_WF <- lm(log(CARBON_AG_WT_Foliage) ~
as.character(INVYR)+HT+STDSZ_NAME+AFFETED_STATUS+FLD_AGE+ELEV+PHYSCL_NAME+STAND_TYPE, data
= perdido_data_2001_2007)
summary(perdido_lm_2001_2007_WF)
ggcoef_model(perdido_lm_2001_2007_WF, facet_row = NULL)
par(mfrow=c(2,2)) # init 4 charts in 1 panel
plot(perdido_lm_2001_2007_WF)
coeftest(perdido_lm_2001_2007_WF, confint = TRUE, ci.width = .3, vcov = vcovHC(perdido_lm_2001_2007_WF, type =
"HC0"))

perdido_coef_WF <- coeftest(perdido_lm_2001_2007_WF, confint = TRUE, ci.width = .3, vcov =
vcovHC(perdido_lm_2001_2007_WF, type = "HC0"))
perdido_coef_WF
BIC(perdido_coef_WF)
ggcoef_model(perdido_coef_WF, facet_row = NULL)+  xlab("estimate for tree and foliage")
par(mfrow=c(2,2)) # init 4 charts in 1 panel
plot(perdido_coef_WF)
ggcoef(perdido_coef_WF, color = "blue", vline_color = "red", vline_linetype =  "solid", size =3 , shape = 18)

#Model for ANOVA test (with foliage)
perdido_lm_2001_2007_WF_m2 <- lm(log(CARBON_AG_WT_Foliage) ~
as.character(INVYR)+STDSZ_NAME+AFFETED_STATUS+FLD_AGE++ELEV+PHYSCL_NAME+STAND_TYPE, data =
perdido_data_2001_2007)
summary(perdido_lm_2001_2007_WF_m2)
coeftest(perdido_lm_2001_2007_WF_m2, confint = TRUE, ci.width = .3, vcov = vcovHC(perdido_lm_2001_2007_WF, type =
"HC0"))
perdido_lm_2001_2007_WF_int <- lm(log(CARBON_AG_WT_Foliage) ~
as.character(INVYR)+STDSZ_NAME+AFFETED_STATUS+HT*FLD_AGE++ELEV+PHYSCL_NAME+STAND_TYPE,
data = perdido_data_2001_2007)
summary(perdido_lm_2001_2007_WF_int)
coeftest(perdido_lm_2001_2007_WF_int, confint = TRUE, ci.width = .3, vcov = vcovHC(perdido_lm_2001_2007_WF, type =
"HC0"))
perdido_lm_2001_2007_WF_blc <- lm(log(CARBON_AG_WT_Foliage) ~
as.character(INVYR)+STDSZ_NAME+AFFETED_STATUS+HT+FLD_AGE++ELEV+PHYSCL_NAME+STAND_TYPE+B
ASAL_AREA, data = perdido_data_2001_2007)
summary(perdido_lm_2001_2007_WF_blc)
coeftest(perdido_lm_2001_2007_WF_blc, confint = TRUE, ci.width = .3, vcov = vcovHC(perdido_lm_2001_2007_WF, type =
"HC0"))
```

```
model.set <- list("Model 1" = perdido_lm_2001_2007_WF, "Model 2" = perdido_lm_2001_2007_WF_m2, "Model 3" =
perdido_lm_2001_2007_WF_int, "Model 4" = perdido_lm_2001_2007_WF_blc)
ggcoef_compare(model.set, type = "faceted")+ xlab("estimate for tree and foliage")
model.names <- c("Original", "Dropping", "Interaction", "Blocking")
anova(perdido_lm_2001_2007_WF, perdido_lm_2001_2007_WF_m2, perdido_lm_2001_2007_WF_int,
perdido_lm_2001_2007_WF_blc)
aictab(model.set, modnames = model.names)
bictab(model.set, modnames = model.names)

lmtest::bptest(perdido_lm_2001_2007_WF)  # Breusch-Pagan test
perdido_box <- caret::BoxCoxTrans(perdido_data_2001_2007$CARBON_AG_WT_Foliage)
print(perdido_box)

perdido_data_2001_2007 <- cbind(perdido_data_2001_2007, box_new =
predict(perdido_box,perdido_data_2001_2007$CARBON_AG_WT_Foliage))
head(perdido_data_2001_2007)
perdido_lm_2001_2007_WF_het <- lm(log(box_new) ~
as.character(INVYR)+HT+STDSZ_NAME+AFFETED_STATUS+FLD_AGE++ELEV+PHYSCL_NAME+STAND_TYPE,
data = perdido_data_2001_2007)
bptest(perdido_lm_2001_2007_WF_het)
par(mfrow=c(2,2)) # init 4 charts in 1 panel
plot(perdido_lm_2001_2007_WF_het)

# Look at relationship between fitted values and residuals with foliage and trees
ggplot(perdido_lm_2001_2007_WF, aes(x = .fitted, y = .resid)) +
  geom_point(color = "black", size = 2) +
  geom_smooth(method = "lm", color = "red")+
  xlab("Fitted Values")+
  ylab("Residuals")+
  scale_x_continuous(labels = number_format(accuracy = 0.1))


#+++++++++++++++++++++++++++++++++++++++++++++++++++++++++++++++++++++++++++++++++++++++++++++#

#Run a multiple linear regression model for 2001-2007 period for foliage only
perdido_lm_2001_2007_Fol <- lm(log(Foliage) ~
as.character(INVYR)+HT+STDSZ_NAME+AFFETED_STATUS+FLD_AGE++ELEV+PHYSCL_NAME+STAND_TYPE,
data = perdido_data_2001_2007)
summary(perdido_lm_2001_2007_Fol)
ggcoef(perdido_lm_2001_2007_Fol, color = "red", size =4 , shape = 20)
par(mfrow=c(2,2)) # init 4 charts in 1 panel
plot(perdido_lm_2001_2007_Fol)

# Robust standard errors t test with lm() function
perdido_coef_Fol <- coeftest(perdido_lm_2001_2007_Fol, confint = TRUE, ci.width = .3, vcov =
vcovHC(perdido_lm_2001_2007_Fol, type = "HC0"))
perdido_coef_Fol
par(mfrow=c(2,2)) # init 4 charts in 1 panel
plot(perdido_coef_Fol)
ggcoef_model(perdido_coef_Fol, facet_row = NULL)+  xlab("estimate for foliage only")
ggcoef(perdido_coef_Fol, color = "blue", vline_color = "red", vline_linetype =  "solid", size =3 , shape = 18)

#Model for ANOVA test (Foliage)
perdido_lm_2001_2007_Fol_m2 <- lm(log(Foliage) ~
as.character(INVYR)+STDSZ_NAME+AFFETED_STATUS+FLD_AGE++ELEV+PHYSCL_NAME+STAND_TYPE, data =
perdido_data_2001_2007)
summary(perdido_lm_2001_2007_Fol_m2)
coeftest(perdido_lm_2001_2007_Fol_m2, confint = TRUE, ci.width = .3, vcov = vcovHC(perdido_lm_2001_2007_Fol, type =
"HC0"))
```

```
perdido_lm_2001_2007_Fol_int <- lm(log(Foliage) ~
as.character(INVYR)+STDSZ_NAME+AFFETED_STATUS+HT*FLD_AGE++ELEV+PHYSCL_NAME+STAND_TYPE,
data = perdido_data_2001_2007)
summary(perdido_lm_2001_2007_Fol_int)
coeftest(perdido_lm_2001_2007_Fol_int, confint = TRUE, ci.width = .3, vcov = vcovHC(perdido_lm_2001_2007_Fol, type =
"HC0"))
perdido_lm_2001_2007_Fol_blc <- lm(log(Foliage) ~
as.character(INVYR)+STDSZ_NAME+AFFETED_STATUS+HT+FLD_AGE++ELEV+PHYSCL_NAME+STAND_TYPE+B
ASAL_AREA, data = perdido_data_2001_2007)
summary(perdido_lm_2001_2007_Fol_blc)
coeftest(perdido_lm_2001_2007_Fol_blc, confint = TRUE, ci.width = .3, vcov = vcovHC(perdido_lm_2001_2007_Fol, type =
"HC0"))

model.set <- list("Model 1" = perdido_lm_2001_2007_Fol, "Model 2" = perdido_lm_2001_2007_Fol_m2, "Model 3" =
perdido_lm_2001_2007_Fol_int, "Model 4" = perdido_lm_2001_2007_Fol_blc)
ggcoef_compare(model.set, type = "faceted")+ xlab("estimate for foliage only")
anova(perdido_lm_2001_2007_Fol, perdido_lm_2001_2007_Fol_m2, perdido_lm_2001_2007_Fol_int,
perdido_lm_2001_2007_Fol_blc)
model.names <- c("Original", "Dropping", "Interaction", "Blocking")
aictab(model.set, modnames = model.names)
bictab(model.set, modnames = model.names)

lmtest::bptest(perdido_lm_2001_2007_Fol)  # Breusch-Pagan test
perdido_box <- caret::BoxCoxTrans(perdido_data_2001_2007$Foliage)
print(perdido_box)

perdido_data_2001_2007 <- cbind(perdido_data_2001_2007, box_new =
predict(perdido_box,perdido_data_2001_2007$CARBON_AG_WO_Foliage))
head(perdido_data_2001_2007)
perdido_lm_2001_2007_Fol_het <- lm(log(box_new) ~
as.character(INVYR)+HT+STDSZ_NAME+AFFETED_STATUS+FLD_AGE++ELEV+PHYSCL_NAME+STAND_TYPE,
data = perdido_data_2001_2007)
bptest(perdido_lm_2001_2007_Fol_het)
par(mfrow=c(2,2)) # init 4 charts in 1 panel
plot(perdido_lm_2001_2007_Fol_het)

# Look at relationship between fitted values and residuals with foliage
ggplot(perdido_lm_2001_2007_Fol, aes(x = .fitted, y = .resid)) +
  geom_point(color = "black", size = 2) +
  geom_smooth(method = "lm", color = "red")+
  xlab("Fitted Values")+
  ylab("Residuals")+
  scale_x_continuous(labels = number_format(accuracy = 0.1))
```